Regulation of GLUT4 Translocation in Adipocytes: The Role of SNARE Proteins and Caveolae

Holly Taylor

MBiomedSci

Thesis submitted in fulfilment of the requirements for the Degree of Doctor of Philosophy

2023

Strathclyde Institute of Pharmacy and Biomedical Sciences

University of Strathclyde

Author's Declaration

This thesis is the result of the author's original research. It has been composed by the author and has not been previously submitted for examination which has led to the award of a degree.

Signed: *H Taylor*

Date: 24th April 2023

Abstract

Background

Following a meal, insulin stimulates the translocation of the glucose transporter GLUT4 to the plasma membrane (PM) of fat and muscle cells, resulting in increased glucose uptake. This process is impaired in individuals with type 2 diabetes and insulin resistance. Fusion of GLUT4 storage vesicles (GSVs) with the PM requires the formation of a SNARE complex containing the t-SNAREs Syntaxin4 and SNAP23, and the v-SNARE VAMP2, along with the regulatory SM-protein Munc18c. Previous work has shown that insulin-stimulated phosphorylation of Sx4 and Munc18c increases SNARE complex formation and subsequent GSV fusion with the PM. In adipocytes, bulb-shaped membrane microdomains known as caveolae play a key role in insulin action in adipocytes.

Methods

Caveolae isolation, immunoblotting methods (including with phospho-specific antibodies), glucose transport assays, and co-localisation experiments using immunofluorescence microscopy and Proximity Ligation Assays in 3T3-L1 adipocytes were used to examine the role of Sx4 phosphorylation in GLUT4 trafficking and to investigate caveolae as a potential site of SNARE protein phosphorylation and SNARE complex formation. siRNA knockdown in 3T3-L1 adipocytes and immunoblotting experiments with primary mouse fat

lysates were used to explore the role of the caveolae component EHD2 in GLUT4 trafficking and glucose transport.

Results

SNARE proteins were found to be enriched in caveolae-enriched cell fractions. Sx4 was found to co-localise and closely interact with the insulin receptor and the caveolae component Caveolin1. Knockdown of EHD2 in 3T3-L1 adipocytes resulted in reduced expression of key glucose transport proteins, reduced maximum glucose transport, and loss of the insulin stimulated increase in interactions between SNARE proteins. Loss of EHD2 in mice resulted in a reduced fold-change in insulin-stimulated Sx4 phosphorylation.

Conclusions

These data argue for an important role for caveolae in insulin stimulated glucose uptake, suggesting they act as a focal point for the intersection of the signalling and trafficking machinery in cultured adipocytes.

COVID-19 Pandemic Impact Statement

The laboratory work for this thesis took place from October 2019 to October 2022, and thus was severely impacted by the COVID-19 pandemic and related lockdowns and restrictions. From March 2020 to August 2020, I had no lab access due to the first national lockdown in Scotland. From August 2020 to May 2021, I had only part time access to the lab of around 3 days per week due to strict social distancing requirements limiting the number of people who could be in the lab at once. Out of hours lab access during evenings and weekends was also heavily restricted during this time. The work presented in Chapter 4 of this thesis on generating new 3T3-L1 stable cell lanes was particularly disrupted by loss of full-time lab access, as transfection, selection, and expansion of 3T3-L1 cell lines is a lengthy process taking many weeks, and often relying on out-of-hours lab access.

However, during the time that lab access was restricted, I was able to focus on reading and reviewing literature in depth, which I feel is particularly highlighted by my review of the literature on the role of caveolae in insulin action and GLUT4 trafficking presented in Section 1.5.

I am grateful to my funders, Diabetes UK, for granting me a 3-month stipend extension to help catch up on some of the time lost to the COVID-19 pandemic.

Table of Contents

List of Tables

List of Figures

Acknowledgements

My thanks go to Diabetes UK for funding this research, and to everyone at SIBPS who made it possible. I would especially like to thank my supervisor, Prof. Gwyn Gould for your limitless support, encouragement, and enthusiasm over what has been a challenging few years to be a PhD student.

Thank you to everyone on HW5, particularly to Shaun and Laura for all your help in the lab, and to Angéline, Justin and Rod for being a fantastic team. And of course, to all the physicists and biologists in the student office for all of the help, advice, and silliness over the last three years. A special thank you to Jordan- it would have been boring without you, and to Tanith- I couldn't have done it without you.

Thank you to Sarah, Matt, and Adam, for making me laugh every week for the past three years. Thank you, Chris, for your endless love, patience, and encouragement, and for always believing I could do it.

Finally, thank you to all of my family, but especially to Mum and Dad, for your lifelong love and support- we've come a long way from "booky"!

List of Abbreviations

Cav – caveolin

EHD2 – Eps15 homology domain–containing 2

ER – endoplasmic reticulum

GLUT4 – glucose transporter 4

GSV – GLUT4 storage vesicle

HDM – high density microsome

IF – immunofluorescence

IR – insulin receptor

IRAP – insulin-regulated aminopeptidase

IRS – insulin receptor substrate

IRV – insulin responsive vesicle

KD – knock down

KO – knock out

LDM – low density microsome

LRP1 – low-density lipoprotein receptor-related protein-1

MudPIT – multidimensional protein identification technology

PDK – phosphoinositide-dependent kinase

PI3K – phosphatidylinositol 3-kinase

PIP_3 – phosphatidylinositol trisphosphate

PLA – proximity ligation assay

PM – plasma membrane

PPARγ – peroxisome proliferator-activated receptor-gamma

SM – Sec1 Munc18

SNAP - soluble N-ethylmaleimide-sensitive factor attachment protein

SNARE – soluble N-ethylmaleimide-sensitive factor attachment protein receptors

Sx – Syntaxin

TGN – trans Golgi network

VAMP – vesicle-associated membrane protein

WT – wildtype

Chapter 1

Introduction

1 Introduction

1.1 Insulin and type 2 diabetes

Insulin-regulated control of glucose uptake into muscle and fat tissue is vital for health. Following a meal, insulin is released into the blood from the pancreas where it binds to the insulin receptor on the surface of many cell types, which triggers a signalling cascade resulting in a wide variety of metabolic effects. In fat and muscle cells, insulin stimulates the translocation of the insulin-responsive glucose transporter GLUT4 (sometimes known as SLC2A4) to the cell surface, which allows glucose to enter these cells from the blood. This process is impaired in individuals with type 2 diabetes and insulin resistance (Zierath et al. 1996; Gonzalez et al. 2011; S. X. Tan et al. 2015). Reduced clearance of glucose from the blood is a hallmark clinical feature of type 2 diabetes and insulin resistance, although the exact causes of these conditions are unclear (Klip, McGraw, and James 2019). As of 2019, 4.7 million people in the UK had been diagnosed with diabetes, with around 90% of those people having type 2 diabetes (Diabetes UK 2019). People with uncontrolled diabetes can suffer serious foot, eye and kidney complications, as well as being at a higher risk of developing cardiovascular disease (Diabetes UK 2019). It is therefore vitally important that the mechanisms of glucose transport, are better understood as this will lead to improved therapies and screening tools for these conditions.

1.2 Insulin signalling

1.2.1 The insulin receptor and its substrates

The insulin receptor (IR) is a disulphide-linked homodimer, which each of the two monomers consisting of an alpha (α-) subunit towards the N-terminal and a beta (β-) subunit towards the C terminal. The α-subunits sit at the cell surface and bind insulin, while the β-subunits contain the transmembrane domain and the intracellular tyrosine kinase domains which have multiple tyrosine autophosphorylation sites (Lawrence 2021). Binding of insulin to its receptor alters the conformation of IR. This activates this IR's tyrosine kinase activity, resulting in autophosphorylation of the receptor, which triggers the intracellular insulin signalling pathways (Ebina et al. 1985; Kasuga et al. 1982). IR is vital for health; mice lacking insulin receptors develop early postnatal diabetes as their tissues cannot respond to insulin, and thus have short lifespans (Kitamura, Kahn, and Accili 2003).

Activation of IR by insulin binding allows the recruitment of the insulin receptor substrate (IRS) family of proteins, particularly IRS-1 and IRS-2, which are activated by tyrosine phosphorylation (Lavan, Lane, and Lienhard 1997). IRS-1 and IRS-2 are crucial for insulin stimulated glucose transport; mice lacking IRS-1 and IRS-2 demonstrate impaired insulin stimulated glucose transport into both fat and muscle (Araki, Kahn, and Shichiri 1994).

Following activation by IR, IRS proteins bind phosphatidylinositol 3-kinase (PI3K), which acts as a docking protein to bind other signal-transducing molecules and providing a link between the IR tyrosine kinase and downstream enzymes affecting growth and metabolism (X. J. Sun et al. 1991). Following binding by IRS, PI3K generates phosphatidylinositol trisphosphate (PIP_3) at the plasma membrane, which is required to activate AKT. PIP_3 recruits the phosphoinositide-dependent kinase (PDK), which directly phosphorylates the Thr308 residue of AKT. A second phosphorylation of AKT, at the Ser473 residue, is carried out by mTOR complex 2 (mTORC2) (Haeusler, McGraw, and Accili 2018). Phosphorylation of both of these residues is required for maximal activation of the AKT (Manning and Toker 2017).

1.2.2 The Role of AKT

AKT is an insulin-activated serine/threonine kinase which links transduction of the insulin signal from IR to downstream effects such as GLUT4 trafficking and glucose uptake, glycogen synthesis, protein and lipid synthesis, and gene expression (Kohn, Kovacina, and Roth 1995). AKT has over 100 reported substrates, which allow for this diverse range of downstream effects (Manning and Toker 2017).

There are three isoforms of AKT, which have some isoform-specific effects (Manning and Toker 2017). There is evidence to suggest that AKT2 is the

most important isoform for glucose homeostasis, whereas AKT1 is more important for growth and AKT3 for brain development. Mice lacking AKT2 show impaired glucose homeostasis, whereas mice lacking AKT1 or AKT3 do not (Gonzalez and McGraw 2009). Furthermore, AKT2 has been shown to be specifically capable of promoting GLUT4 translocation to the cell surface because it is enriched in the plasma membrane of insulin-stimulated adipocytes, but AKT1 is not (Gonzalez and McGraw 2009). More recent work found that the catalytic activity of either AKT1 or AKT2 alone was sufficient to maintain GLUT4 transport (Kajno, McGraw, and Gonzalez 2015), but this study did find that AKT1 is specifically required for adipogenesis, confirming that isoform specificity is needed for some AKT functions.

Although there are a wide variety of downstream signalling effects of insulin signalling and AKT activation, their effect on GLUT4 trafficking will be explored here in depth. Part of the insulin signalling pathway responsible for GLUT4 translocation to the plasma membrane, and subsequently, glucose uptake, is shown below in Figure 1.1.

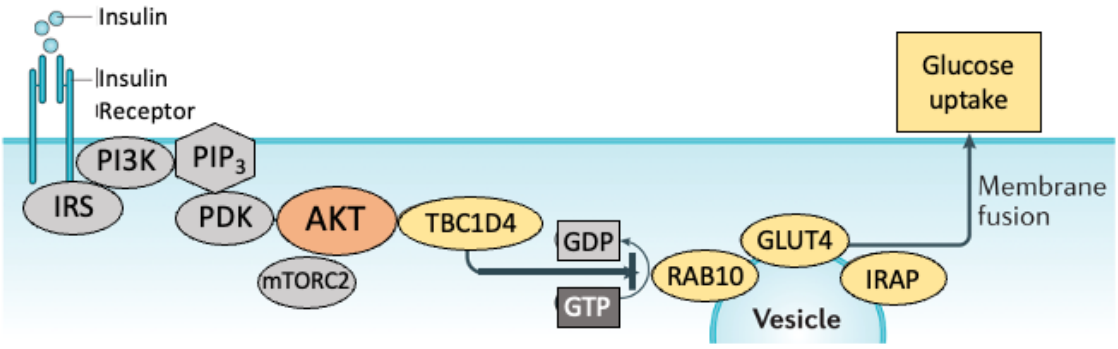

Figure 1.1 The insulin signalling pathway.
Components of the insulin signalling pathway involved glucose uptake. Proteins specifically involved in GLUT4 translocation are highlighted in yellow. Proteins touching or connected by arrows indicates interaction. Adapted from Figure 5b of Haeusler et al., 2018.

1.3 GLUT4

1.3.1 Introduction to GLUT4

Uptake of glucose in to fat and muscle cells was one of the first known actions of insulin, and was originally studied in primary rat adipocytes, where insulin stimulated glucose uptake was observed to be ten times higher than that of unstimulated, or basal, cells (Cushman and Wardzala 1980). Insulin exerts this control over glucose uptake by controlling the density of GLUT4 facilitative glucose transporters in the plasma membrane. In unstimulated cells, GLUT4 is sequestered intracellularly in GLUT4 storage vesicles (GSVs), sometimes referred to as insulin responsive vesicles (IRVs), that cluster near the trans-Golgi network (TGN) and the perinuclear endocytic recycling compartment but can also be found throughout the cytosol. Upon insulin stimulation these GSVs are trafficked to, dock and then fuse with the plasma membrane, where they facilitate increased glucose uptake into the cell. Upon cessation of the insulin signal, GLUT4 is retrieved by endocytosis and recycled back into GSVs (Klip, McGraw, and James 2019). Accordingly, plasma membrane levels of GLUT4 are increased in human muscle and fat cells in the postprandial state, when glucose uptake is high, and decreased in the fasted state when glucose uptake is low (Kahn 1994; Goodyear et al. 1996).

1.3.2 The GLUT4 trafficking itinerary in adipocytes

GLUT4 is localised to a number of intracellular compartments in adipocytes, including the plasma membrane, endosomes, TGN and other intracellular vesicles (Slot et al. 1991). Although the process by which GLUT4 navigates through the cell is not fully understood, a model has emerged for the trafficking itinerary of GLUT4 in adipocytes. Figure 1.2 summarises the current proposed model of the GLUT4 trafficking itinerary. Following endocytosis of GLUT4, which occurs via clathrin, cholesterol, and lipid raft dependent mechanisms (Blot and McGraw 2006; Ros-Baró et al. 2001; Shigematsu et al. 2003), GLUT4 is rapidly trafficked through the endosomal system from the plasma membrane. GLUT4 then enters a slower recycling pathway between recycling endosomes and a subsection of the TGN that specifically contains the SNARE proteins syntaxin6 (Sx6) and syntaxin16 (Sx16), from which GLUT4 is packaged into GSVs (Shewan et al. 2003; Proctor et al. 2006; Bryant and Gould 2011). It is from the GSVs that GLUT4 is translocated to the PM in response to insulin.

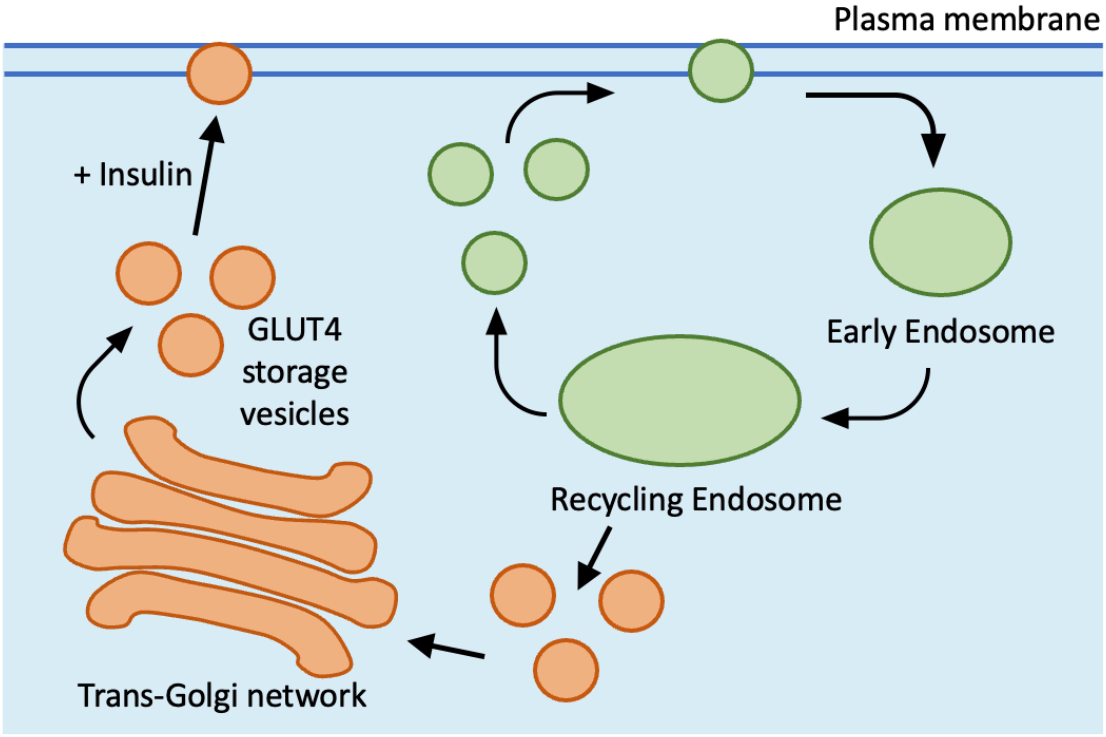

Figure 1.2 A model of the GLUT4 trafficking itinerary.
All membranes shown contain GLUT4. Compartments shown in green represent the rapid trafficking cycle, while compartments shown in orange represent the slower recycling pathway from which the insulin responsive GLUT4 storage vesicles are produced.

Since GLUT4 is trafficked through the endosomal and TGN compartments, the membrane transport machinery required for those pathways is required for GLUT4 transport to the plasma membrane, as well as the machinery specific to GSV exocytosis. Sortilin and retromer have been shown to mediate retrograde transport of GLUT4 in 3T3-L1 adipocytes (Pan et al. 2017), while in human cell lines CHC22 clathrin mediates membrane traffic from the ER-Golgi intermediate compartment that contributes to GSV

biogenesis (Camus et al. 2019). However, a full picture of the machinery required for the formation of GSVs has not yet been elucidated.

GLUT4 is not the only protein present in GSVs. The insulin-regulated aminopeptidase (IRAP) is a component of the GSV and is translocated to the cell surface along with GLUT4, but it does not appear to play a role in glucose homeostasis (Keller, Davis, and Clairmont 2002). The low-density lipoprotein receptor-related protein-1 (LRP1) is also found in GSVs, and its depletion did reduce GLUT4 expression and glucose transport (Jedrychowski et al. 2010). GSVs are also enriched in RAB10 (Yu Chen et al. 2012) and a number of vesicle-associated membrane proteins (VAMPs) (Sadler, Bryant, and Gould 2015).

1.3.3 Insulin signalling and GLUT4 translocation

Insulin signalling is known to regulate GLUT4 translocation at several steps downstream of AKT activation, with different effectors controlling different aspects of GLUT4 trafficking. One of the best described AKT substrates required for GLUT4 translocation is TBC1D4 (also known as AS160), a RAB GTPase activating protein (RAB GAP). TBC1D4 is required for both full intracellular retention of GLUT4 under basal conditions and GLUT4 translocation to the plasma membrane under insulin-stimulated conditions (Eguez et al. 2005; Sano et al. 2003). In basal conditions a RAB GAP would increase the GTPase activity of its target RAB proteins, thus switching them

from their active GTP-bound state to their inactive GDP-bound state. However, following insulin stimulation, AKT phosphorylation of TBC1D4 appears to inactivate this GAP activity, resulting in the activation of the RAB proteins targeted by TBC1D4 (Sano et al. 2003).

AKT phosphorylation of TBC1D4 catalyses its binding to 14-3-3 protein, and it has been suggested that this binding may also inhibit TBC1D4's GAP activity (Ramm et al. 2006). Moreover, TBC1D4 binds to GSV cargo, including IRAP and LRP1, and this interaction is reduced in response to insulin stimulation and therefore may also play a role in regulating TBC1D4's GAP activity (Stöckli et al. 2008). TBC1D4 has an N-terminal phospho-tyrosine binding domain that regulates its association with the plasma membrane, suggesting that TBC1D4 exerts its control over GLUT4 translocation at the plasma membrane (Tan et al. 2012). Indeed, phosphorylated TBC1D4 was found to be enriched at the plasma membrane (Ng et al. 2010) and it has been suggested that TBC1D4 may contribute to docking of GSVs at the plasma membrane prior to their fusion (Klip, McGraw, and James 2019). Ultimately, through a combination of the mechanisms described here, AKT phosphorylation of TBC1D4 leads to the activation of its target RABs.

In muscle cells, the primary RAB targets of TBC1D4 that promote insulin-stimulated translocation of GLUT4 to the plasma membrane are RAB8a and

RAB14 (Ishikura, Bilan, and Klip 2007; Y. Sun et al. 2014), whereas in adipocytes, RAB10 fills this role (Sano et al. 2007). GSVs are enriched in RAB10, which has been shown to facilitate translocation of these vesicles to the plasma membrane independently of endosomes, which are enriched in other RABs (Yu Chen et al. 2012). Additionally, with its effector SEC16a, it has been demonstrated that RAB10 promotes insulin-stimulated movement of GLUT4 from a TGN compartment, and plays a role in the biogenesis of the GSVs (Bruno et al. 2016). Loss of RAB10 in adipocytes decreases insulin stimulated GLUT4 translocation and glucose uptake by half (Vazirani et al. 2016), which shows that while RAB10-dependant signalling is important for insulin stimulated GLUT4 translocation, distinct RAB10-independent insulin signalling pathways must also contribute to GLUT4 translocation to the plasma membrane- particularly at the stage of GSV fusion with the plasma membrane.

1.4 The role of SNARE proteins in GLUT4 translocation

1.4.1 The SNARE machinery of GLUT4 translocation

Fusion of GSVs with the plasma membrane, like all membrane fusion events in the cell, requires the assembly of membrane-bridging complexes formed of members of the soluble N-ethylmaleimide-sensitive factor attachment protein receptors (SNARE) protein family. SNAREs are defined by an evolutionarily conserved alpha-helical 60-70 residue “SNARE motif”, and most SNAREs also contain a carboxy-terminal transmembrane domain close to the SNARE motif that serves to anchor the protein to its associated membrane (Baker and Hughson 2016).

SNAREs associated with vesicles are generally referred to as v-SNAREs, whereas SNARES on target membranes such as the plasma membrane are known as t-SNAREs (Südhof and Rothman 2009). In order to facilitate membrane fusion, four SNARE motifs from the SNARE proteins on two membranes must come together to form an energetically favourable four-helix bundle known as the trans-SNARE complex (Baker and Hughson 2016). The energy produced by the formation of this complex drives membrane fusion. This process is depicted in Figure 1.3. SNAREs are the minimal machinery required to achieve membrane fusion (Weber et al. 1998).

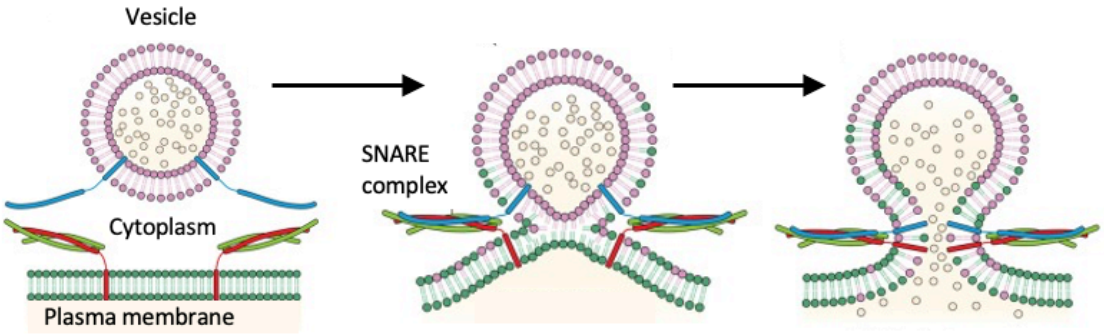

Figure 1.3 The SNARE membrane fusion machinery
The process by which SNARE proteins drive membrane fusion, shown from left to right. v-SNAREs are shown in blue, t-SNAREs are shown in red and green. Four SNARE motifs come together to form a SNARE complex, which provides the energy required to drive membrane fusion. Figure adapted from Kweon, Kong, and Shin 2017.

SNARE proteins can also be defined by the residue they contribute to the "zero layer" of the SNARE complex (a hydrophilic region at the longitudinal midpoint of the complex), as well as their position within the four-helix bundle. R-SNAREs contribute an Arg residue to the zero layer, whereas Q_a-, Q_b- and Q_c-SNAREs each contribute a Gln residue (Fasshauer et al. 1998). For the most part, v-SNAREs and t-SNARES can be defined as R-SNAREs and Q-SNAREs respectively (Baker and Hughson 2016).

Without a high level of regulation, uncontrolled membrane fusion facilitated by SNAREs would damage the internal architecture of the cell. Therefore, only specific combinations of SNAREs located on specific membranes are able to form a functional trans-SNARE complex, ensuring that vesicles can

only fuse with the appropriate target membrane (McNew et al. 2000). This concept is known as the SNARE hypothesis.

The t-SNAREs required for the fusion of GSVs with the plasma membrane are Syntaxin4 (Sx4) and SNAP23 (Bryant and Gould 2011) and the v-SNARE is VAMP2 (Sadler, Bryant, and Gould 2015). Sx4 and SNAP23 are sufficient for GSV tethering to the plasma membrane, while VAMP2 promotes fusion (Kawaguchi et al. 2010). Sx4/SNAP23/VAMP2 SNARE complex formation is highly regulated, and increases in response to insulin, driving insulin stimulated GSV fusion with the plasma membrane (Jaldin-Fincati et al. 2017).

1.4.2 Regulation of the GLUT4 translocation SNARE machinery

1.4.2.1 The structure and conformation of Syntaxins

Syntaxins, also known as Q_a-SNAREs, consist of a transmembrane domain at the C terminus, a SNARE domain adjacent to the C terminus and an N terminal domain known as the H_{abc} domain, linked to the SNARE domain by a flexible region of the protein (Bennett et al. 1993; Fernandez et al. 1998). Syntaxins can be regulated by the adoption of one of two distinct conformations: a closed conformation with the H_{abc} domain folded back onto the SNARE domain, thus preventing the formation of functional SNARE complexes, and an open conformation with the H_{abc} domain moved away from the SNARE domain, thus allowing SNARE complex formation (Dulubova et al. 1999).

1.4.2.2 Regulation by Munc18c

Syntaxins are regulated by the Sec1-Munc18 (SM) family of proteins (Jahn 2000). The SM protein that binds Sx4 under basal conditions is Munc18c (Bryant and Gould 2011), and this binding has an inhibitory effect on Sx4/SNAP23/VAMP2 SNARE complex formation (Brandie et al. 2008). Following insulin stimulation, Munc18c becomes phosphorylated on Y521, and this is likely done directly by the insulin receptor (Aran, Bryant, and Gould 2011). This phosphorylation causes Munc18c to dissociate from Sx4 (Kioumourtzoglou, Gould, and Bryant 2014), thus lifting its inhibitory effect on

SNARE complex formation. *In vitro* data has shown that Munc18c inhibits the formation of Sx4-containing SNARE complexes, whereas a phosphomimetic version of Munc18c was found to increase SNARE complex formation (Kioumourtzoglou, Gould, and Bryant 2014).

SM proteins can exert their regulation on syntaxins by switching them from the closed to open conformation (Struthers et al. 2009). There is some evidence that phosphorylation of Munc18c has this effect on Sx4, because *in vitro* experiments showed that the presence of phosphomimetic Munc18c increased the formation of Sx4-containing SNARE complexes, but it did not have this effect when WT Sx4 was replaced with an already permanently open Sx4 mutant (Kioumourtzoglou *et al*. 2014). Interestingly, another study showed that Munc18c blocked WT Sx4 from binding SNAP23, but did not block this binding when WT Sx4 was replaced with its “open” mutant (D’Andrea-Merrins et al. 2007). Taken together these studies show that both the phosphorylation of Munc18c and the opening of Sx4 lead to increase SNARE complex formation.

Munc18c expression has been found to be reduced in the adipose tissue of morbidly obese individuals and in that of mice fed a high-fat diet, potentially to compensate for issues with GSV fusion (Bakke et al. 2013; Garrido-Sanchez et al. 2013).

1.4.2.3 Regulation by Syntaxin4

A mass spectrometry study of changes in tyrosine phosphorylation following insulin stimulation in adipocytes found that Sx4 is phosphorylated on Y115 and Y251 following insulin stimulation (Schmelzle et al. 2006). In vitro studies have shown that the insulin receptor may also be responsible for directly phosphorylating Sx4, and that phosphorylation of Sx4 on these tyrosine residues resulted in a change in its conformation which was favourable for its ability to form SNARE complexes (Hannah Lucy Black 2016; Al Tobi 2018).

The regulatory effect of phosphorylation of Munc18c and Sx4 on insulin-stimulated SNARE complex formation is explored in greater detail in Section 3.1.3.

1.4.2.4 Other regulation of the SNARE machinery

Further insulin-dependent regulation of Sx4/SNAP23/VAMP2 SNARE complex formation in adipocytes is provided by Syntaxin4 interacting protein (Synip) (Min et al. 1999). Like Munc18c, Synip binds Sx4 under basal conditions, and this binding prevents the formation of Sx4-containing SNARE complexes, and thus preventing GSV fusion with the plasma membrane (Yu, Rathore, and Shen 2013). Synip is phosphorylated by AKT in response to insulin, and this allows its dissociation from Sx4, resulting in SNARE complex formation and GLUT4 translocation (Okada et al. 2007). The Syntaxin binding protein b-Tomosyn also plays a role in regulating Sx4-containing

SNARE complex assembly. It can bind Sx4 and SNAP23, and in doing so prevents SNARE complex formation. Overexpression of b-Tomosyn in 3T3-L1 adipocytes resulted in decreased insulin-stimulated GLUT4 translocation to the plasma membrane, providing further evidence for its inhibitory role in GSV fusion (Widberg et al. 2003).

In muscle cells, Sx4/SNAP23/VAMP2 SNARE complex formation is also regulated by changes in Ca^{2+} near the plasma membrane in response to insulin stimulation, via activation of Ca^{2+} sensitive proteins Doc2b, Tctex1d2 and E-Syt1 (reviewed in Jaldin-Fincati et al 2017).

1.5 The role of caveolae in insulin action and GLUT4 trafficking

1.5.1 Introduction to Caveolae

Caveolae are small, bulb-shaped plasma membrane invaginations that are present in most cell types, but are particularly abundant in adipocytes, endothelial cells and muscle – key insulin targets (Scherer et al. 1994). Adipocyte caveolae range from 25 to 150 nm in diameter and together make up around one third of the total adipocyte plasma membrane (Thorn et al. 2003). The structures are enriched in cholesterol and sphingolipids and are coated on their cytoplasmic side by a complex of caveolin and cavin proteins which allows them to provide a scaffolding for membrane proteins and act as signalling platforms within the cell (Lamaze et al. 2017). The caveolar coat consists of caveolins (Cav1-3) and cavins (Cavin1-4), while Pacsin2 is important for membrane bending and stabilizing caveolar invaginations, along with the ATPase EHD2, which is specifically localised at the neck region of caveolae. The structure of adipocyte caveolae is shown below in Figure 1.4. Caveolae have been proposed to play a role in metabolism and homeostasis across a range of cell types (Matthaeus and Taraska 2021). Caveolae and a number of caveolae-associated proteins have been implicated in insulin action and GLUT4 translocation to the plasma membrane. Here, the importance of caveolae for these functions in adipocytes is reviewed.

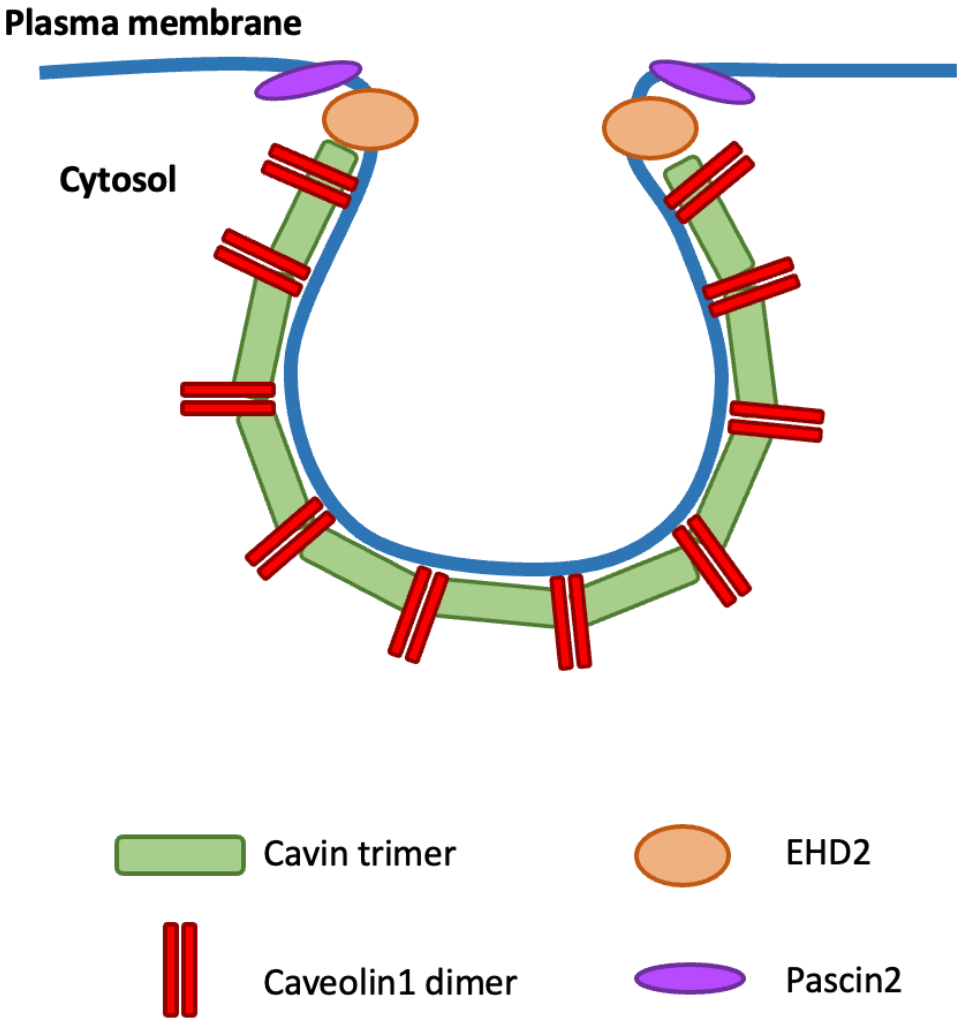

Figure 1.4 The structure of adipocyte caveolae.
Schematic cross-sectional diagram of adipocyte caveolae structure. The plasma membrane is shown in blue, along with cavins (green), Caveolin1 (red), EHD2 (orange) and Pascin2 (purple).

1.5.2 Does GLUT4 translocate to caveolae?

Whether GLUT4 translocates specifically to caveolae in response to insulin is a matter of some debate, with conflicting evidence for this localisation of GLUT4 presented in a number of studies.

Early studies of the insulin-stimulated translocation of GLUT4 to the plasma membrane in adipocytes using electron microscopy approaches found that GLUT4 did not localise to caveolae following insulin stimulated translocation to the plasma membrane (Robinson et al. 1992; Voldstedlund, Tranum-Jensen, and Vinten 1993). However, subsequent studies found that GLUT4 moved to a caveolae-enriched adipocyte cell fraction following insulin stimulation, indicating insulin stimulated translocation to caveolae (Scherer et al. 1994; Gustavsson, Parpal, and Strålfors 1996). Doubt is cast on these fractionation results, however, as later work on effectively isolating adipocyte caveolae found that the detergent-based fractionation methods used in these studies does not effectively separate caveolae from other lipid raft membrane domains (Pilch et al. 2007), and so the appearance of GLUT4 in these fractions does not guarantee that it localises to caveolae specifically or exclusively in the cell.

In a 2002 study, Karlsson et al used immunofluorescence microscopy, electron microscopy and biochemical isolation of caveolae from adipocytes to demonstrate that GLUT4 does translocate to caveolae in response to insulin.

The authors argued that the reason GLUT4 had not previously been observed in caveolae using electron microscopy was due to differences in methodology, and that they had optimised their fixing and staining procedure to produce adipocyte membranes with more intact caveolae (Karlsson et al. 2002). This evidence for GLUT4 translocation to caveolae is further supported by a study that found that TC10, which is required for GLUT4 translocation to the plasma membrane, was found to be enriched in caveolae (Watson et al. 2001).

Another study identified a number of caveolae subclasses in adipocytes and found that a lower-density subclass contained GLUT4 (Örtegren et al. 2006). This suggests that not all caveolae contain GLUT4 and may go some way towards explaining the discrepancies in results of studies investigating GLUT4 localisation at the plasma membrane. Further complicating this question was a 2007 study by Yuan et al that observed insulin-stimulated GLUT4 translocation to both caveolae and other lipid raft membrane domains in adipocytes, but by disrupting caveolae with Cav1 siRNA knockdown, found that caveolae were not required for GLUT4 translocation to the plasma membrane (Yuan et al. 2007).

Contrastingly, a study using TIRF microscopy to investigate the distribution of GLUT4 at the plasma membrane of rat adipocytes found no co-localisation between GLUT4 and caveolae (Stenkula et al. 2010). In a 2012 review of the

caveolae and insulin action, the authors suggested that TIRF microscopy may not be ideal for studying caveolae, as caveolae membranes may fall 50-100 nm away from the “flat” plasma membrane, so fluorescence from caveolae may be more difficult to detect (Strålfors 2012).

There have been few more recent studies probing the question of whether GLUT4 specifically translocates to adipocyte caveolae in response to insulin, with investigations into the wider role of caveolae in insulin action becoming more common. Taken together, the studies discussed here lean towards the conclusion that some GLUT4 does translocate to at least some caveolae in response to insulin in adipocytes. This is supported by further studies that found loss of Cav1(González-Muñoz et al. 2009) or Cavin1(Liu et al. 2008) from adipocytes increased GLUT4 degradation, showing that caveolae components are at least involved in GLUT4 stability. The question of whether GLUT4 translocates to caveolae has not yet been satisfactorily answered, and this topic demonstrates some of the challenges of studying adipocyte caveolae.

1.5.3 The role of caveolae in insulin action

One of the key pieces of evidence for a vital role of caveolae in insulin action in adipocytes is that the insulin receptor (IR) is localised to caveolae (Gustavsson et al. 1999), as is its effector IRS1 (Karlsson et al. 2004), along with a number of other proteins implicated in insulin signalling (Müller et al.

2001). Specifically, IR has been found to localise to the distinct neck region of caveolae (Foti et al. 2007). A study in rat primary adipocytes suggested that auto-phosphorylated IR is endocytosed via caveolae following insulin stimulation (Fagerholm et al. 2009). Another study demonstrated that IR disassociates from caveolae during inflammation-induced insulin resistance (Sekimoto et al. 2012), demonstrating the importance of caveolae as insulin signalling platforms.

When caveolae are disrupted, IRS phosphorylation, downstream insulin signalling and glucose transport are all reduced (Gustavsson et al. 1999; Parpal et al. 2001), and caveolae disruption has been shown to induce insulin resistance in adipocytes (Venugopal et al. 2004). Caveolae have also been demonstrated to play a critical role in ceramide signalling in adipocytes, providing negative regulation of insulin signalling (Blouin et al. 2010).

Another role of caveolae in insulin action was revealed in a recent study showing that caveolae are essential for the regulation of the exocytosis of high molecular weight adiponectin in response to insulin (Brännmark et al. 2020). Furthermore, another recent study into adipocyte differentiation found that human mesenchymal progenitor cells with elongated cilia suffered impaired adipogenic differentiation, and that this was due to inability to form caveolin-positive lipid rafts, a precursor to caveolae (Yamakawa et al. 2021). These poorly differentiated cells also suffered insulin resistance, showing the

importance of caveolae for not just insulin action, but adipocyte differentiation.

Alongside these studies highlighting the role of whole caveolae structures in insulin action in adipocytes, there is a wealth of data implicating caveolae components in insulin signalling.

1.5.4 The role of Caveolin1 in insulin action

Caveolin1 (Cav1) is a key structural and functional component of adipocyte caveolae. During adipocyte differentiation, Cav1 expression is significantly upregulated alongside GLUT4 and IR (Palacios-Ortega et al. 2014), suggesting that it is important for adipocyte function. One study identified a key role for Cav1 in insulin action using siRNA knockdown of Cav1 in 3T3-L1 adipocytes. Knockdown of Cav1 in these cells resulted in increased degradation of GLUT4 and IR, suggesting a role for Cav1 in maintaining the stability of key proteins involved in insulin signalling and glucose transport. Reduced levels of Cav1 in 3T3-L1 adipocytes was also linked to reduced IR activation, reduced insulin stimulated GLUT4 translocation to the plasma membrane, and lower rates of glucose uptake in response to insulin (González-Muñoz et al. 2009). Mice lacking Cav1 have much smaller fat pads than WT mice, show reduced adipocyte size, and suffer generalised adipose tissue pathology. Interestingly, the Cav1 knockout mice were resistant to developing diet-induced obesity, likely due to the reduction in

adipose tissue (Razani et al. 2002). Taken together, these studies on the effects of loss of Cav1 demonstrate a clear role for Cav1 in insulin signalling in adipocytes.

The role of Cav1 in insulin signalling has been proposed to be linked to its phosphorylation on Y14 by IR in response to activation by insulin stimulation (Kimura et al. 2002). In fact, Cav1 phosphorylation has been shown to be essential for insulin-stimulated glucose uptake in 3T3-L1 adipocytes that had been treated with an inflammatory factor to model low-grade adipose tissue inflammation found in obesity. In these cells, insulin sensitivity correlated with levels of active, phosphorylated Cav1 (Palacios-Ortega et al. 2015). Cav1 has also been implicated in the process of AKT activation by advanced glycation end products, the formation of which is accelerated by hyperglycaemia in diabetes (Yang et al. 2013). These studies show that Cav1 plays an important role in insulin signalling downstream of IR, particularly in adipocyte cell models mimicking the effects of obesity and diabetes. However, further studies will be required to identify downstream effectors of phosphorylated Cav1, particularly in healthy adipocytes.

Further evidence for the key role of Cav1 in insulin signalling, and more generally in adipocyte function, can be found in the effects of mutation to the human CAV1 gene. A number of these mutations have been identified and found to cause severe disease affecting adipose tissue. A homozygous

nonsense mutation in CAV1 (identified as p.Glu38X) resulted in the development of Berardinelli-Seip congenital lipodystrophy (BSCL), a disease characterized by near absence of adipose tissue, severe problems with lipid concentration in the blood, and insulin resistance (Kim et al. 2008). Another homozygous CAV1 mutation (identified as p.His79Glnfs*3) caused generalised lipodystrophy with reduced adipose tissue, and insulin resistance. Fibroblasts taken from these patients had no caveolae and were resistant to insulin (Karhan et al. 2021). The effects of these mutations in CAV1 demonstrate once again that the Cav1 protein is vital for healthy adipose tissue and insulin responsiveness.

1.5.5 Other caveolae-associated proteins involved in insulin action

1.5.5.1 Cavins

Cav1 is not the only caveolae associated protein to be implicated in insulin signalling and its downstream effects. Cavins, another set of proteins that contribute to the caveolar coat, are also involved in this process.
Loss of Cavin1 (also known as Polymerase I and transcript release factor/ PTRF) in mice resulted in a total loss of caveolae, and these mice had reduced adipose tissue and were resistant to insulin (Liu et al. 2008). Another study found that Cavin1 dissociates from adipocyte caveolae in response to insulin stimulation, and this process was shown to be important for mechanical protection of adipocytes during insulin-mediated lipid uptake

(Wang, Pilch, and Liu 2019). This demonstrates an important role for Cavin1 and caveolae in mediating insulin-induced cellular changes. Interestingly, another Cavin isoform, Cavin2, has been shown to bind IR and promote its stability in the cell, providing further evidence for the vital role caveolae play as a signalling platform for IR (Higuchi et al. 2022).

A number of studies have been carried out on the on the effects of hypoxia on adipocytes, as hypoxia is common in the adipose tissue of obese people and can lead to adipocyte dysfunction (Trayhurn 2013). Some of these studies found that hypoxia led to the loss of caveolae-associated proteins in adipocytes, particularly Cavins (Regazzetti et al. 2015; Varela-Guruceaga et al. 2020). This results in the loss of caveolae, along with disruption to insulin signalling and reduced GLUT4 translocation to the cell surface and glucose transport (Varela-Guruceaga et al. 2018). These hypoxia studies once again link caveolae components to insulin action in adipocytes.

1.5.5.2 PDE3B

The membrane bound cAMP degrading enzyme, phosphodiesterase 3B (PDE3B), is a key enzyme involved in insulin-stimulated lipogenesis, GLUT4 translocation, and glucose uptake in adipocytes (Zmuda-Trzebiatowska et al. 2006). A range of methods including subcellular fractionation using a sucrose gradient, and co-immunoprecipitation with Cav1, showed that PDE3B associates with caveolae in primary mouse and rat adipocytes (Nilsson et al.

2006). The appearance of a key enzyme of the insulin signalling pathway in caveolae once again demonstrates the importance of these membrane structures in insulin action.

1.5.5.3 SEPT11

SEPT11 is a cytoskeleton component found in adipocytes whose expression is upregulated during obesity. A study in human adipose tissue found that SEPT11 mRNA levels correlate with insulin resistance in subcutaneous adipose tissue. The authors also showed that SEPT11 associates with caveolae in human adipocytes, and specifically interacts with Cav1. SEPT11 silencing impaired both insulin signalling and insulin-induced lipid accumulation, demonstrating it to be another caveolae-associated protein with a key role in insulin action in adipocytes (Moreno-Castellanos et al. 2017).

1.5.5.4 NECC2

Another study found that the neuroendocrine long coiled-coil protein-2 (NECC2) was upregulated during adipocyte differentiation in 3T3-L1 cells. NECC2 was also shown to associate with caveolae and to co-immunoprecipitate with Cav1. Overexpression of NECC2 enhanced insulin induced AKT activation, while downregulation of NECC2 impaired AKT activation. NECC2 was also found to be upregulated in human adipose tissue from individuals with obesity and insulin resistance (Trávez et al. 2018). The

localisation and function of NECC2 in adipocytes illustrated in this study provides a link between caveolae and insulin signalling. Taken with the SEPT11 study described above, these data suggest that some caveolae components are upregulated in obesity and insulin resistance, suggesting a role for caveolae as a platform for compensatory regulation of insulin signalling in response to metabolic dysfunction in adipose tissue.

1.5.5.5 EHD2

The caveolae neck region associated ATPase EHD2 has also been shown to be upregulated during adipocyte differentiation, and knockdown of EHD2 impairs the adipocyte differentiation process, as well as affecting insulin sensitivity, lipid storage capacity, and lipolysis (Morén et al. 2019). EHD2 has also be implicated in caveolae stability, and, in contrast to SEPT11 and NECC2, is downregulated in obesity (Matthaeus et al. 2020). In Chapter 5, the role of EHD2 in insulin signalling, GLUT4 translocation and glucose transport will be examined in depth.

1.5.6 Caveolae conclusions

The studies discussed here paint a clear picture of the vital role caveolae and their associated proteins play in adipocyte insulin action. While the question of whether GLUT4 translocates to caveolae upon insulin stimulation remains to be satisfactorily answered, there is ample evidence that caveolae provide essential signalling platforms on which a great number of proteins involved in insulin signalling congregate. Of particular interest is the data showing up- or down-regulation of caveolae associated proteins in response to obesity and insulin resistance, as this suggests that caveolae and their various components could be key to better understanding the development of insulin resistance and type 2 diabetes.

1.6 Aims

Broadly, the aim of this thesis is to better understand the mechanisms linking signals from the insulin receptor to the SNARE membrane fusion machinery required for insulin stimulated GLUT4 translocation to the plasma membrane. Specifically, this work aims to examine the role of Syntaxin4, and Syntaxin4 phosphorylation by the insulin receptor, in insulin stimulated SNARE complex formation, GLUT4 trafficking and glucose uptake. Furthermore, caveolae will be investigated as a potential site of this SNARE protein phosphorylation and SNARE complex formation. Finally, this thesis aims to explore the role of caveolae, particularly the caveolae component EHD2, in GLUT4 trafficking and glucose transport.

Chapter 2

Materials and Methods

2 Materials and Methods

2.1 Materials

2.1.1 List of general suppliers

General laboratory kits, reagents, and plasticware were obtained from the following suppliers:

- Beckman Coulter, High Wycombe, UK
- BioRad Laboratories, Watford, UK
- Cell Signalling Technology Europe B.V., Leiden, Netherlands
- Fisher Scientific UK, Loughborough, Leicestershire, UK
- Merck UK, Poole, UK
- New England Biolabs, Hitchin, UK
- Stratech Scientific, Ely, UK
- Thermo Fisher Scientific UK, Cheshire, UK

2.1.2 Solutions

The following solutions were made with pure sterile water unless otherwise stated.

Phosphate buffered saline (PBS): 85 mM NaCl, 1.7 mM KCl, 5 mM Na_2HPO_4, 0.9 mM KH_2PO_4, pH 7.4

Phosphate buffered saline with Tween (PBST): 85 mM NaCl, 1.7 mM KCl, 5 mM Na_2HPO_4, 0.9 mM KH_2PO_4, 0.1% (v/v) Tween, pH 7.

Tris buffered saline (TBS): 20 mM Tris,150 mM NaCl, pH 7.4

Tris buffered saline with Tween (TBST): 20 mM Tris,150 mM NaCl, 0.1% (v/v) Tween, pH 7.4. (NB: for use in Proximity Ligation Assay wash steps, TBST with 0.05% (v/v) Tween was used)

Cell lysis buffer (also serves as immunoprecipitation buffer/ IP buffer): 50 mM Tris-HCl, 50 mM NaF, 1 mM $Na_4P_2O_7$, 1 mM EGTA, 1 mM EDTA, 1% (v/v) glycerol, 1% (v/v) Triton X-100, 0.5% (v/v) IGEPAL, 1 mM DTT, 1% (v/v) Sigma-Aldrich Phosphatase Inhibitor Cocktail Set II, plus Sigma-Aldrich complete mini EDTA-free protease inhibitor tablet, pH 7.4

Carbonate lysis buffer: 500 mM Na_2CO_3 1% (v/v) Sigma-Aldrich Phosphatase Inhibitor Cocktail Set II, plus Sigma-Aldrich complete mini EDTA-free protease inhibitor tablet, pH 11

MES buffered saline (MBS): 25 mM MES, 135mM NaCl, pH 6.5

4x Laemmli Sample Buffer (4x LSB): 4% (w/v) SDS, 20% (v/v) glycerol, 0.004 (w/v) bromophenol blue, 0.125 M Tris-HCl, 20 mM DTT, pH 6.8

HES buffer: 20mM HEPES, 1mM EDTA, 250mM sucrose, pH 7.4

HE buffer: 20mM HEPES, 1mM EDTA, pH 7.4

Acrylamide resolving gel: 75 mM Tris-HCl pH 8.8, 0.1 % (w/v) SDS, 8 to 12 % (v/v) acrylamide, 0.05 % (v/v) ammonium persulfate and 0.01 % (v/v) TEMED

Acrylamide stacking gel: 25 mM Tris-HCl pH 6.8, 0.1 % (w/v) SDS, 4 % (v/v) acrylamide, 0.05 % (v/v) Ammonium persulfate and 0.01 % (v/v) TEMED

SDS running buffer: 25 mM Tris, 190mM glycine, 0.1 % (w/v) SDS

Wet transfer buffer: 25 mM Tris, 190mM glycine, 20% ethanol (v/v)

Ponceau S: 0.2% (w/v) Ponceau S, 1% (v/v) acetic acid

Quench buffer: 85 mM NaCl, 1.7 mM KCl, 5 mM Na_2HPO_4, 0.9 mM KH_2PO_4, 50mM NH_4Cl, pH 7.4

Permeabilization buffer: 85 mM NaCl, 1.7 mM KCl, 5 mM Na_2HPO_4, 0.9 mM KH_2PO_4, 0.1% v/v Triton X-100, pH 7.4

Immunofluorescence buffer (IF buffer): 85 mM NaCl, 1.7 mM KCl, 5 mM Na_2HPO_4, 0.9 mM KH_2PO_4, 0.2% w/v fish skin gelatin, 0.1% v/v goat serum, pH 7.4

2.1.3 Cell lines

The 3T3-L1 cells used in this study are derived from mouse embryonic fibroblasts and were supplied by American Type Culture Collection (ATCC), Manassas, VA, USA.

The Syntaxin4 knockout 3T3-L1 cell line was generated by Dr Hannah Black and at the University of York on a joint grant held by Gwyn Gould and Nia Bryant and are described in the PhD theses of Hannah Black and Rachel Livingstone (Hannah Lucy Black 2016; Livingstone 2021).

2.1.4 Primary antibodies

Target	Species	Supplier	Catalogue number	RRID	Dilution for WB	Dilution for IF/PLA
AKT (pan)	Mouse	Cell Signalling Technology	2920	AB_1147620	1:1000	N/A
AKT phospho-S473	Rabbit	Cell Signalling Technology	4058	AB_331168	1:2000	N/A
Caveolin1	Rabbit	Abcam	ab2910	AB_303405	1:1000	1:500
EHD2	Rabbit	Abcam	ab154784	AB_2927498	1:1000	1:100
GAPDH	Mouse	Ambion	4300	AB_437392	1:80,000	N/A
GLUT4	Rabbit	Abcam	ab654	AB_305554	1:1000	N/A
Insulin Receptor β subunit	Mouse	Abcam	ab69508	AB_1209215	1:1000	1:100
Munc18c	Rabbit	Abcam	ab224625	N/A	1:1000	1:100
Munc18c	Mouse	Novus	H00006814-B01P	AB_2302682	N/A	1:100
Myc	Rabbit	Abcam	ab32	AB_303599	1:1000	N/A
Phospho-tyrosine	Rabbit	Abcam	ab179530	AB_2909401	1:1000	N/A
PPARγ	Rabbit	Abcam	ab209350	AB_2890099	1:1000	N/A
SNAP23	Rabbit	Synaptic Systems	111 203	AB_887787	1:1000	1:100
Syntaxin4	Rabbit	Synaptic Systems	110 042	AB_887853	1:1000	1:100
Syntaxin4	Mouse	Synaptic Systems	110 041	AB_11042324	1:1000	1:100
Syntaxin16	Rabbit	Abcam	ab134945	N/A	1:1000	N/A
Syntaxin16	Mouse	Proteintech	66775-1-Ig	AB_2882121	N/A	1:100
VAMP2	Mouse	Synaptic Systems	104 211	AB_887811	1:1000	1:100

Table 2.1 List of primary antibodies

List of primary antibodies used in this project, showing target protein, host species, supplier, supplier catalogue number, Research Resource Identifier (RRID) number where one was available, and dilution factor used for western blotting (WB) or immunofluorescent staining (IF) and proximity ligation assay (PLA), which used the same dilutions.

As well as the commercially available antibodies listed in Table 2.1, the following additional primary antibodies were used in this project:

- Anti-IRAP antibody was a generous gift from Susanna Keller, University of Virginia, USA.

- Antibodies against phosphorylated Syntaxin4 (anti-Sx4-Y115P and anti-Sx4-Y251P) were generated by Anatagene Inc., California and characterised by Mohammed Al-Tobi (Al Tobi 2018).

2.1.5 Secondary antibodies

Antibody	Supplier	RRID	Used for	Dilution Factor
IRDye 800CW Goat anti-Mouse IgG	LI-COR Biosciences	AB_621842	Western blotting	1:10,000
IRDye 800CW Goat anti-Rabbit IgG	LI-COR Biosciences	AB_621843	Western blotting	1:10,000
IRDye 680RD Goat anti-Mouse IgG	LI-COR Biosciences	AB_10956588	Western blotting	1:10,000
IRDye® 680RD Goat anti-Rabbit IgG	LI-COR Biosciences	AB_10956166	Western blotting	1:10,000
Alexa Fluor 647 goat anti-Rabbit IgG	Invitrogen	AB_2535812	Immunofluorescence	1:500
Alexa Fluor 647 goat anti-Mouse IgG	Invitrogen	AB_2535804	Immunofluorescence	1:500
Alexa Fluor 488 donkey anti-Rabbit IgG	Invitrogen	AB_2535792	Immunofluorescence	1:500
Alexa Fluor 488 donkey anti-Mouse IgG	Invitrogen	AB_141607	Immunofluorescence	1:500

Table 2.2 List of secondary antibodies

List of secondary antibodies used in this project, showing antibody name including host and target species, Research Resource Identifier (RRID) number, which technique the antibody was used for, and the dilution factor the antibody was routinely used at.

2.1.6 Plasmids

The plasmids used in Chapter 4 of this study were pcDNA3., a mammalian expression vector encoding Myc-tagged WT Syntaxin4 (Sx4), double phospho-mimetic Sx4 (Y115E, Y251E), or double phospho-resistant Sx4 (Y115F, Y251F), with a Kan/G418 resistance gene. The Myc tag was positioned between the N terminus and the H_{abc} domain of Sx4. These plasmids were generated by Hannah Black, University of York and Rachel Livingstone, University of Glasgow, under the supervision of Gwyn Gould and Nia Bryant and are described in the PhD thesis of both Hannah Black and Rachel Livingstone (Hannah Lucy Black 2016; Livingstone 2021). The original empty vector was supplied by GenScript, Piscataway, NJ, USA. The plasmid map of the original empty vector is shown in Appendix I.

2.1.7 RNA

The EHD2-targeting and control (sometimes referred to as scrambled) siRNA used in Chapter 5 of this thesis were as follows:

- EHD2 siRNA from ThermoFisher, catalogue number MSS281816
- Silencer Select Negative Control No. 1 siRNA from Invitrogen, catalogue number 4390844

2.1.8 Proximity Ligation Assay Kit

The proximity ligation assay reagent kit used in this study was the NaveniFlex MR kit from Navinci, Uppsala, Sweden (Product number: NF.MR.100).

2.2 Methods

2.2.1 Cell culture

2.2.1.1 Growth and maintenance of 3T3-L1 cells

3T3-L1 fibroblasts were cultured in 75 cm^2 cell culture flasks containing 12 mL growth media (10% new-born calf serum (NBCS) in DMEM (Gibco) supplemented with 5% glutamine), at 37°C in a humidified atmosphere of 10% CO_2. This media was replaced every 2 to 3 days. Cells were routinely passaged at 80% confluency using the following method: following removal of media, cells were washed with warm, sterile PBS and then incubated with 3 mL TrypLE Express enzyme (Gibco) at 37°C for 1 minute until all cells were detached from the cell culture flask. The TrypLE Express and cells were then diluted in an appropriate volume of 10% NBCS in DMEM for the number of plates required (10 mL per 10 cm dish, 12 mL per 12- or 6-well plate and 12 mL per 75 cm^2 flask). Cells were not generally maintained beyond passage number 13.

2.2.1.2 Differentiation of 3T3-L1 adipocytes

To differentiate 3T3-L1 fibroblasts into adipocytes, the cells were grown to 2 days post-confluency then fed with differentiation media (10% foetal bovine serum (FBS) in DMEM supplemented with 5% glutamine) containing 1 μM insulin, 5 μM troglitazone, 0.25 μM dexamethasone and 0.5 mM IBMX (day 0

feed). After 3 days the cells were fed with differentiation media containing 1 μM insulin and 5 μM troglitazone (day 3 feed). After a further 3 days the cells were fed with differentiation media only (day 6 feed). Cells were typically fixed or processed to produce cell lysates on day 10 of differentiation.

2.2.1.3 Transfection of 3T3-L1 cells with plasmids and generation of stable cell lines

3T3-L1 cells were transfected in 10 cm dishes at 60% confluency. 60 μL Lipofectamine 2000 (Invitrogen) and 24 μg plasmid DNA (plasmids described above in Section 2.1.6) were mixed with 3 mL Opti-MEM media (Gibco), vortexed, and then incubated at room temperature for 20 minutes. Cells were washed once with Opti-MEM alone before the Opti-MEM/Lipofectamine/DNA mixture was added dropwise. The cells were then incubated at 37°C for 4 hours, before being replaced with regular growth media for a further 24 hours. Cells were then transferred to growth media containing 0.7 mg/ml G418 (selection media), which was replaced every 2-3 days.

After 2 to 3 weeks growth with selection media, when visible colonies formed from single clones appeared, the media was aspirated and sterile steel cloning rings were placed over the colonies, secured with sterile grease. 200 μL TrypLE Express enzyme was added to the cloning rings for 1 minute, then the TrypLE and detached colony cells were transferred to 1 mL selection media in 12-well plates. Cells were grown in 12-well plates until they reached

80% confluency, at which point the cells were trypsinised as described in Section 2.2.1.1 and transferred to 6-well plates. The same procedure was followed to expand clone cell lines to 25 cm^2 and 75 cm^2 flasks sequentially to allow for validation of the cell lines.

2.2.1.4 siRNA knockdown of EHD2 in 3T3-L1 adipocytes

siRNA knockdown in 3T3-L1 adipocytes was performed as previously described (Duan et al. 2022). EHD2 or scrambled siRNA was added to 1.2 mL Opti-MEM to a final concentration of 40 nM with 48 µL TransIT-X2 transfection reagent (Mirus Bio). At 6 days post-differentiation, 3T3-L1 adipocytes grown on a 10cm dish were washed once with PBS, trypsinised with 2 mL TrypLE Express enzyme, resuspended in differentiation media and centrifuged at 200 x g for 5 min. The supernatant was removed, and pelleted cells were resuspended in 13.5 mL differentiation media. 900 μL cell suspension and 100 μL EHD2 or SCR siRNA/TransIT-X2/Opti-MEM mixture were reseeded onto each well of a 12 well plate. For use in Proximity Ligation Assays, these wells contained 13 mm glass coverslips. Cells were used in experiments 4 days following siRNA knockdown.

2.2.1.5 Insulin stimulation of 3T3-L1 adipocytes

All cells to be used in an experiment were incubated in serum-free DMEM for 2 hours prior to any insulin stimulation. Cells were incubated with 100 nM insulin for 5, 15 or 20 minutes as required. A subset of cells for each

experiment were not stimulated with insulin to provide a basal control. Following this process, all cells were immediately placed on ice and washed twice with ice cold PBS.

2.2.2 Preparation of 3T3-L1 lysates and sub-cellular fractions

All lysate preparation was carried out on ice and all spins were at 4°C unless otherwise stated. Protein concentration of lysate and cell fraction samples was routinely checked using Pierce BCA Protein Assay Kit (ThermoFisher), according to the manufacturer's instructions.

2.2.2.1 Production of whole cell lysates

3T3-L1 adipocytes were lysed 10 days post differentiation. Where 3T3-L1 fibroblast lysates were produced, the cells were at 80% confluency. 3T3-L1 adipocytes were serum starved, insulin stimulated and washed as described above in Section 2.2.1.5. Cells were then scraped into 2 ml per 10cm dish of ice-cold cell lysis buffer, keeping insulin stimulated and basal cells separate, before being passed through a 23G needle 10 times. Lysates were then centrifuged at 14,000rpm in a benchtop centrifuge for 5 minutes, and fat was removed from the top of the lysate by aspiration.

2.2.2.2 Isolation of caveolae-enriched cell fraction

3T3-L1 adipocytes were serum starved, insulin stimulated and washed as described above in Section 2.2.1.5. Cells were then scraped into 2 ml per

10cm dish of ice-cold carbonate lysis buffer. The cells were lysed by passing through a 23G needle 10 times.

500 μL lysate was added to 500 μL 85% sucrose in MBS in an ultracentrifuge tube, mixed and then left to stand on ice for 1 hour. This mixture was then overlaid with 750 μL 30% sucrose in MBS containing 250 mM Na_2CO_3, and then with 250 μL 5% sucrose in MBS containing 250 mM Na_2CO_3. The samples were then centrifuged at 100,000 x g for 18 hours at 4°C. Either 10x 200 μL fractions were taken from the top to the bottom of the centrifuge tube, or the top 400 μL caveolae-enriched fraction was taken from the top of the tube. Trichloroacetic acid (TCA) precipitation of these fractions was performed for further protein recovery.

Equal volumes of protein-containing solution and 20% w/v TCA were combined and left to stand for 1 hour before spinning at 14,000 rpm in a benchtop centrifuge at 4°C for 20 minutes. The supernatant was completely removed, and the pellet resuspended in 30 μL 0.1 M NaOH to neutralise any remaining TCA.

2.2.2.3 Isolation of plasma membranes and microsomes

3T3-L1 adipocytes were serum starved, insulin stimulated and washed as described above in Section 2.2.1.5. Cells were then scraped into 1 ml HES buffer and passed through a 23G needle 10 times. The resulting lysates were

spun at 8000 rpm for 20 minutes in a TLA 100.4 rotor. The supernatant was collected and transferred to clean 5 mL ultracentrifuge tubes and stored on ice. The pellet was resuspended in 1 mL HES buffer and layered over a sucrose cushion of HES buffer containing 1.12 M sucrose, before being spun at 25,000 rpm for 60 minutes in a TLS 55 rotor. Following this centrifugation step, the plasma membrane (PM) enriched fraction was collected from a layer just above the sucrose cushion with a pipette and transferred to a clean 5 mL ultracentrifuge tube, where the volume was adjusted to 5 mL with HE buffer. The diluted PM fraction was then spun at 60,000 rpm for 60 minutes in the TLA100.4 rotor. The resulting pellet was enriched in PM and was resuspended in 200 μL HES buffer.

The supernatant from the initial spin was then spun at 16,000 rpm for 20 minutes in the TLA 100.4 rotor. The resulting pellet was enriched in high density microsomes (HDMs) and was resuspended in 200 μL HES buffer. The supernatant was collected, transferred to clean ultra-centrifuge tubes, and spun at 60,000 rpm for 60 minutes in the TLA100.4 rotor. The resulting pellet was enriched in low density microsomes (LDMs) and was resuspended in 200 μL HES buffer.

2.2.2.4 Enrichment of GLUT4 storage vesicles by 16k fractionation

A 16K fractionation method was used to produce a crude GLUT4 storage vesicle (GSV) enriched fraction, as previously described (Sadler et al. 2016).

3T3-L1 adipocytes grown in 6-well plates were serum starved, insulin stimulated and washed as described above in Section 2.2.1.5. Cells in each well were then scraped into 200 μL ice cold PBS supplemented with 1% (v/v) Sigma-Aldrich Phosphatase Inhibitor Cocktail Set II and Sigma-Aldrich complete mini EDTA-free protease inhibitor tablet, before being passed through a 23G needle 10 times. The resulting lysates were spun at 1000 g for 10 minutes in a benchtop centrifuge. The resulting pellet was discarded, and the supernatant was transferred to clean tubes and spun at 16,000 g for 20 minutes. The resulting pellet from this spin was resuspended in 200 μL PBS. This pellet was enriched in plasma membranes. The supernatant from the 16,000 g spin was transferred to a clean ultracentrifuge tube and spun at 50,000 g for 1 hour. The resulting pellet was resuspended in 200 μL PBS. This pellet was enriched in GLUT4 storage vesicles (GSVs).

2.2.3 Analysis of proteins by western blotting

2.2.3.1 SDS-PAGE

Lysates or cell fractions produced as described above in Section 2.2.2 were combined at a 1:4 ratio with 4x LSB and heated to 95°C for 10 minutes in order to denature the proteins in the sample. Where GLUT4 levels were to be analysed by western blotting, samples were heated to 65°C only. The proteins in the cell lysates or cell fractions were resolved by sodium dodecyl sulfate polyacrylamide gel electrophoresis (SDS-PAGE) carried out using a

Bio-Rad Mini-PROTEAN Tetra cell gel apparatus (Bio-Rad Laboratories Ltd) according to the manufacturer's instructions. Precision Plus Protein Standards (Bio-Rad) were run alongside protein samples. Gels were prepared with 8 to 12 % (v/v) acrylamide resolving gel overlaid with a 4 % stacking gel. Gels were run in SDS running buffer at 100 V for approximately 2 hours.

2.2.3.2 Wet Transfer

Proteins were transferred from gels to nitrocellulose membrane using a Bio-Rad Mini Trans-Blot Cell according to the manufacturer's instructions. The transfer was run in wet transfer buffer at 200 mA for 2 hours. Transfer efficiency to the nitrocellulose membrane was routinely checked by brief staining with Ponceau S, followed by three 10-minute washes with TBST to remove the Ponceau stain.

2.2.3.3 Immunoblotting

Following protein transfer the membrane was blocked for 1 hour in 5% milk powder or Bovine Serum Albumin (BSA) in TBST. BSA was used in place of milk powder when using phospho-specific antibodies. Primary antibodies were diluted to the appropriate concentration (Table 2.1) in 1% BSA or milk in TBST and incubated with the membrane overnight at 4°C. Membranes were then washed three times for 10 minutes in TBST. Appropriate secondary antibodies (Table 2.2) were diluted 1:10,000 in 1% BSA or milk in TBST and

incubated with the membrane for 1 hour at room temperature. The membranes were again washed three times in TBST for 10 minutes.

2.2.3.4 Densitometry and statistics

The blots were visualised using a LI-COR scanner. Where n ≥3, protein of interest expression was quantified as follows. Background-subtracted densities of protein bands were calculated using ImageStudioLite software. Band density was then normalised to a GAPDH or other appropriate control band. If appropriate for a given experiment, as described in each figure legend, normalised density values were expressed as protein expression relative to a basal or WT control. Relative band density across at least 3 biological replicates were compared using T Test, one- or two-way ANOVA as appropriate, carried out using R Studio software.

2.2.4 Co-immunoprecipitation with anti-phosphotyrosine beads

Anti-phosphotyrosine antibody conjugated magnetic immunoprecipitation beads (Cell Signalling Technology, catalogue number 8095) were washed 3 times with 1 mL IP buffer using a magnetic tube rack to pellet the beads. 20 μL of the washed beads were added to 200 μL cell lysate or caveolae fraction, produced as described in Section 2.2.2. A proportion of the unprocessed lysate was set aside as the “start lysate”. The beads and lysate were incubated overnight at 4°C with rotation. The immunodepleted lysate was removed as set aside as the “end lysate”. The beads were washed 3

times with 1 mL IP buffer, before being resuspended in 20 μL 4x LSB. The beads were then heated to 95°C for 10 minutes, which released the captured proteins from the beads. The bead protein sample was then collected and subjected to immunoblot analysis (Section 2.2.3) alongside the start and end lysates. This process was repeated with the same start lysates and Protein A magnetic beads (Thermo Scientific, catalogue number 88845) as a control.

2.2.5 Immunofluorescence microscopy

2.2.5.1 Fixing and blocking

3T3-L1 cells were grown and insulin-stimulated on 13mm glass coverslips in 12-well plates as described in Section 2.2.1. Media was aspirated from wells and coverslips were washed three times with PBS followed by incubation with 1 mL 4 % (w/v) warm p-formaldehyde for 20 minutes. Cells were then washed three times with PBS and incubated with 1 mL quench buffer for 10 minutes followed by a further three washes with PBS. Cells were incubated with 1 mL permeabilization buffer for 5 minutes. Permeabilization buffer was aspirated, and cells were incubated in 1 mL IF buffer for at least 20 minutes to block non-specific sites.

2.2.5.2 Antibody staining for standard immunofluorescence

Primary antibodies were diluted to the appropriate concentration (Table 2.1) in IF buffer, and 50 μL of this antibody solution was pipetted onto a clean

Parafilm coated surface. Coverslips were removed from the wells, inverted, and placed onto the antibody solution using fine pointed tweezers. Coverslips were incubated with the primary antibody for 1 hour at room temperature. Coverslips were returned to the wells and washed three times with IF buffer. Appropriate secondary antibodies were prepared in the same manner as primary antibodies (Table 2.2), but coverslips were only incubated for 30 minutes. Coverslips were again returned to their wells and washed three times with IF buffer. During incubation with the primary and secondary antibodies, coverslips were covered to reduce evaporation and prevent photobleaching of secondary antibodies.

2.2.5.3 Proximity Ligation Assay

Proximity Ligation Assay (PLA) was performed on 3T3-L1 adipocytes that had been fixed and permeabilized as described above in Section 2.2.5.1 and was carried out using the NaveniFlex MR kit (Navinci, product number: NF.MR.100) according to the manufacturer's instructions. Briefly, cells were blocked to prevent non-specific binding of antibodies before being incubated with a pair of primary antibodies from mouse and rabbit host species respectively (see Table 2.1 for dilution factors). Cells were then incubated with a pair of anti-mouse and anti-rabbit Navenibodies, which are specifically designed secondary antibodies conjugated to an oligonucleotide. These antibodies were then subjected to a series of enzymatic reactions which, given the proteins targeted by the initial pair of primary antibodies were within

400 nM of one another, allowed the ligation and amplification of the oligonucleotide complex. This amplified complex could then be detected by application of the detection fluorophore to the cells. When the cells are imaged, this process results in the appearance of fluorescent dots marking incidences of colocalization between the two proteins targeted by the initial pair of primary antibodies. All incubations took place in a humidity chamber at 37°C and cells were washed 3 times with TBST between each step. All reaction volumes were 40 μL per 13mm coverslip.

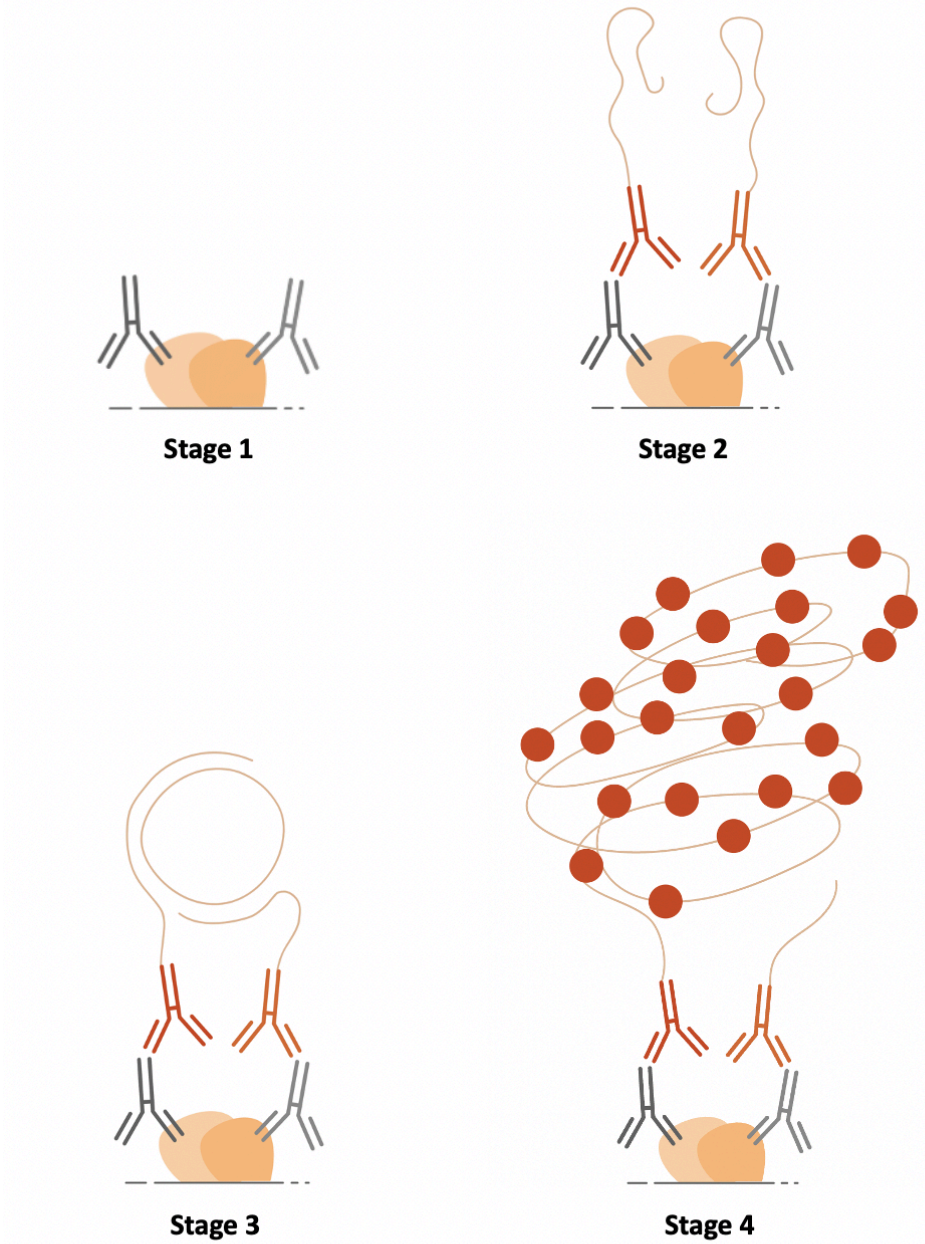

Figure 2.1 Protocol for Proximity Ligation Assays.
Diagram of the Proximity Ligation Assay (PLA) protocol steps, adapted from the kit manufacturer's website (navinci.se/technology, accessed 01/04/2023). Two proteins in close proximity are shown in orange. Step 1 shows primary antibody incubation. Step 2 shows incubation with specialised oligonucleotide-conjugated secondary antibodies. Step 3 shows the oligonucleotides forming a circle during the ligation step. Step 4 shows the result of the amplification and detection steps. Application of the detection fluorophore to the amplified DNA allows the two colocalised proteins to be detected with a fluorescent dot.

2.2.5.4 Staining of DNA

For cells that had undergone either standard IF or PLA, DNA was stained with 4',6-diamidino-2-phenylindol (DAPI). Following the procedures described above, cells were incubated with 1 μg/mL DAPI for 10 min.

2.2.5.5 Mounting coverslips on slides

A drop of Immu-Mount (Fisher Scientific) was applied to a glass microscope slide. Coverslips were carefully placed with cells facing down on the Immu-Mount, avoiding bubbles. The slides were covered and left to dry overnight.

2.2.5.6 Imaging and analysis

Cells were imaged using a Leica TCS SP8 confocal microscope system with a 63× oil immersion objective and using LASX software. All images were processed using ImageJ software. For standard IF, co-localisation was quantified with Pearsons and Manders coefficients, using the JACoP ("Just Another Co-localisation Plugin") Plugin for ImageJ (Bolte and Cordelières 2006). For PLA, signals were counted in ImageJ, using the protocol and parameters previously described by López-Cano et al (López-Cano, Fernández-Dueñas, and Ciruela 2019). Two-way ANOVA statistical tests were used to compare PLA signals between different conditions.

2.2.6 Glucose transport assay

Glucose transport assays described in Chapter 5; Section 5.2.2 were carried out by Gwyn Gould. The experimental design, cell culture work and subsequent data analysis for these experiments was performed by myself but handling of radioisotope was undertaken by Gwyn Gould as he is suitably trained.

Glucose uptake was measured by the uptake of 2-[^{3}H]-deoxy-glucose as previously described (Gould et al, 1988). 3T3-L1 adipocytes grown in 24 well plates and were incubated for 2 hours in serum-free DMEM prior to the start of this experiment. Cells were then transferred to a hot plate at 37°C and washed 3 times with 0.5 mL of Krebs-Ringer phosphate (KRP; 130 mM NaCl, 4.8 mM KCl, 5 mM NaH_2PO_4, 1.25 mM $MgSO_4$, 1.25 mM $CaCl_2$, pH 7.4) solution before being incubated in 237 μL of KRP. The cells were then stimulated with 100 nM insulin for 20 minutes. Glucose transport was initiated by the addition of 2-deoxy-glucose and 2-[^{3}H]-deoxyglucose at a final concentration of 50 μM and 0.5 μCi respectively for 5 minutes. The assay was terminated by removing the assay mixture from the cells and immersing the plates in 2 litres of ice-cold PBS. After air-drying the plates for 1 hour, 0.25 mL of 1% (v/v) Triton-X100 was added to the wells and incubated at room temperature for up to 24 hours. The samples were added to 5 ml of scintillation fluid and radioactivity levels were measured using a Beckman Multi-Purpose scintillation counter.

All measurements were done in triplicate and 10 μM cytochalasin-B (CB) was used in parallel otherwise identical incubations. CB is a non-competitive inhibitor of GLUTs and so allows estimation of the non-specific association of radioactivity with the cells (Bloch 1973). This value was subtracted from the counts recorded in the absence of CB to give the true uptake values.

2.2.7 Production of mouse primary adipocyte lysates

As a guest student in the lab of Karin Stenkula at the University of Lund, I carried out western blot analysis of Syntaxin4 and AKT phosphorylation in whole cell lysates prepared from inguinal fat of WT and ehd2-/- C57BL6/N mice (described in Matthaeus et al. 2020), which are presented in Chapter 5; Section 5.2.6. Mouse inguinal adipocyte cell lysates were kindly prepared for this project by Maria Lindahl, University of Lund, as described below. The experimental design, western blotting and subsequent data analysis for these experiments was performed by myself.

Mice were put on 2 weeks HFD (Research Diets D12492, 60% fat) adipocytes were prepared from inguinal fat on individual animals. Primary mouse adipocytes were isolated from inguinal fat tissue as described previously (Rodbell 1964). Briefly, fat tissue was placed in Krebs-Ringer Bicarbonate HEPES (KRBH) buffer (120 mM NaCl, 5 mM KCl, 2 mM $CaCl_2$, 1 mM $MgCl_2$, 25 mM $NaHCO_3$, 5.5 mM HEPES, and 1 mM D-glucose, pH 7.4) containing 200 nM adenosine and 3% (w/v) BSA and cut into fine pieces.

Collagenase type 1 (Worthington Biochem) was added to a final concentration of 1.5 mg/mL and the tissue pieces were digested in a shaking water bath at 37°C for approximately 1 hour. The cell suspension was filtered through a 400 μm nylon mesh and washed three times in KRBH buffer.

Isolated cells were suspended (20% (v/v) suspension) in KRBH buffer containing 200 nM adenosine and 3% (w/v) BSA and 1 mL of this suspension was used per incubation. 10 nM insulin was added to half of the samples, which were then incubated at 37°C, with shaking at 80 cycles per minute. After 5 minutes, samples were washed in KRBH without BSA and subsequently lysed in 200 μL lysis buffer (50 mM Tris/HCl, 1 mM EGTA, 1 mM EDTA, 1 mM Na_3VO_4, 10 mM sodium-β-glycerophosphate, 50 mM NaF, 5 mM $Na_4P_2O_7$, 0.27 M sucrose, 1% NP-40, 1 mM DTT, complete protease inhibitor cocktail, pH 7.5). Lysates were centrifuged at 13,000 g for 10 min at 4°C and the supernatant was collected. Samples were then subjected to immunoblot analysis as described in Section 2.2.3.

Chapter 3

Investigating Syntaxin4 Phosphorylation by the Insulin Receptor

3 Investigating Syntaxin4 Phosphorylation by the Insulin Receptor

3.1 Introduction

3.1.1 Syntaxin4 is part of the GLUT4 translocation SNARE machinery

As introduced in section 1.4, the combination of specific SNARE proteins into a SNARE complex provides the minimal machinery required for membrane fusion in the cell (Weber et al. 1998). Syntaxin4 (Sx4) is one of the t-SNAREs involved in the fusion of GLUT4 storage vesicles (GSVs) with the plasma membrane, along with SNAP23 (Bryant and Gould 2011; Kawaguchi et al. 2010), and the v-SNARE VAMP2 (Sadler, Bryant, and Gould 2015). Insulin stimulation has been shown to increase the number of Sx4-containing SNARE complexes in adipocytes (Kioumourtzoglou, Gould, and Bryant 2014). The SM protein that binds Sx4 and regulates Sx4/SNAP23/VAMP2 SNARE complex formation is Munc18c (Bryant and Gould 2011; Tamori et al. 1998; Brandie et al. 2008).

3.1.2 The two pools of Syntaxin4

Proximity ligation assays examining the pairwise interactions of Sx4, SNAP23, VAMP2 and Munc18c in adipocytes found that only the associations between VAMP2 and SNAP23, and those between SNAP23 and Munc18c increased in response to insulin (Kioumourtzoglou, Gould, and

Bryant 2014). Importantly, it was also demonstrated that these protein pairs did not directly interact. This led the authors to propose a model in which, under basal conditions, there are two pools of Sx4, one of which is associated with SNAP23, and the other is associated with VAMP2 and Munc18c, as shown in Figure 3.1.

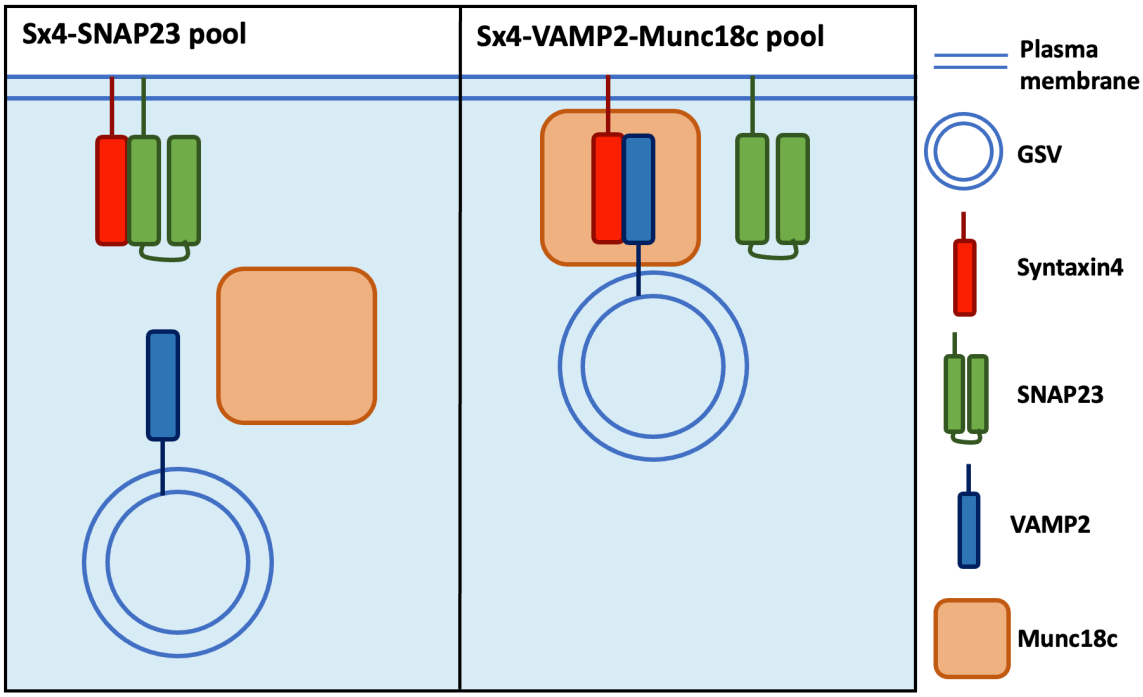

Figure 3.1 Sx4 pools under basal conditions.
In one pool, Sx4 is associated with the t-SNARE SNAP23 (left). In the other it is associated with the v-SNARE VAMP2 located on GLUT4 storage vesicles (GSV), and the SM protein Munc18c (right). Based on Kioumourtzoglou et al., 2014.

Using recombinant proteins, the same group also observed that a binary complex of the t-SNAREs Sx4 and SNAP23, when incubated with VAMP2 *in vitro*, had a higher rate of SNARE complex formation than that of the SNARE proteins without the pre-formed t-SNARE complex. Contrastingly, a Sx4-VAMP2-Munc18c complex was inhibitory to SNARE complex formation, suggesting that these two pools of Sx4 have separate functions. (Kioumourtzoglou, Gould, and Bryant 2014). The proposed model for these functions is as follows: the Sx4-SNAP23 (Figure 3.1, left) pool is required for constitutive recycling of GLUT4 through the plasma membrane under basal conditions, and the Sx4-VAMP2-Munc18c pool (Figure 3.1, right) is required for insulin-stimulated fusion of GSVs with the plasma membrane. This model is supported by studies demonstrating that a significant proportion of GSVs are held within 100 nm of the plasma membrane even under basal conditions (Yan et al. 2009; Stenkula et al. 2010).

3.1.3 Regulation of the Sx4/SNAP23/VAMP2 complex by phosphorylation

3.1.3.1 Regulation by Munc18c

Munc18c is of particular interest in insulin-stimulated GLUT4 translocation, because it has been demonstrated that, at least *in vitro*, the insulin receptor (IR) directly phosphorylates Munc18c on Y521 (Aran, Bryant, and Gould 2011). These experiments were performed using the recombinant cytosolic

insulin receptor kinase (CIRK), a protein consisting of the part of the beta subunit of the IR responsible for its tyrosine kinase activity (Kuhné et al. 1994). *In vivo*, tyrosine phosphorylation of Munc18c increases in response to insulin stimulation, but this effect is independent of PI3K activation (Jewell et al. 2011), giving weight to the argument that the IR directly phosphorylates Munc18c *in vivo*. This tyrosine phosphorylation of Munc18c has been shown to prevent its binding to Sx4, therefore lifting its inhibitory effect on SNARE complex formation (Aran, Bryant, and Gould 2011).

Munc18c is hypothesised to be the molecular switch that specifically activates the Sx4-VAMP2 pool to form SNARE complexes in response to insulin, as phosphorylation of Munc18c in response to insulin causes its dissociation from Sx4. Moreover, *in vitro*, Munc18c inhibits the formation of Sx4-containing SNARE complexes, whereas introduction of phospho-mimetic Munc18c increases SNARE complex formation (Kioumourtzoglou, Gould, and Bryant 2014). Furthermore, as discussed in Section 1.4.2.2, phosphorylation of Munc18c may allow the conformation change of Sx4 from its closed, inhibitory conformation to its open, active confirmation, allowing it to form functional SNARE complexes.

Munc18c is dephosphorylated by protein-tyrosine phosphatase 1B (PTP1B), and this allows Munc18c to reassociate with Sx4, which in turn inhibits glucose uptake (Bakke et al. 2013). Accordingly, mice either lacking PTP1B

or with PTP1B inhibition exhibit increased glucose uptake (Tamrakar, Maurya, and Rai 2014). Selective PTP1B inhibitors have been discussed as a potential therapy for type 2 diabetes and insulin resistance (Tamrakar, Maurya, and Rai 2014), highlighting the importance of Munc18c phosphorylation in insulin stimulated GLUT4 translocation.

3.1.3.2 Regulation by Syntaxin4

In a mass spectrometry analysis of tyrosine phosphorylation in 3T3-L1 adipocytes post-insulin stimulation, it was found that Sx4 is phosphorylated on Y115 and Y251 following insulin stimulation (Schmelzle et al. 2006). Currently unpublished work from Gould group has shown that, like Munc18c, Sx4 can be phosphorylated on Y115 and Y251 directly by CIRK *in vitro* (Gwyn Gould, personal communication). Following this, the effect of Sx4 phosphorylation on SNARE complex formation and GLUT4 translocation was investigated in the PhD thesis of Dr. Hannah Black. It was found that *in vitro*, phospho-mimetic Sx4 formed more SNARE complexes with SNAP23, VAMP2 and Munc18c than WT Sx4. Furthermore, the phospho-mimetic Sx4 formed more binary associations with SNAP23 and with VAMP2 than WT Sx4 did. It was also shown that overexpression of phospho-mimetic Sx4 in a HeLa cell model expressing a HA-GLUT4-GFP construct increased cell-surface GLUT4 under basal conditions.

In a limited proteolysis experiment, it was shown that the phospho-mimetic Sx4 was digested to a greater extent than the WT Sx4, and at a comparable rate to that of a Sx4 mutant which is in a permanently open conformation (Hannah Lucy Black 2016). Sx4 is more easily digested in its open conformation, so this this experiment suggests that phosphorylation of Sx4 may alter its conformation to the open form, in which it can more readily form SNARE complexes (Dulubova et al. 1999).

This idea is supported in the PhD thesis of Dr. Mohammed Al Tobi, who used a number of approaches to confirm that phosphorylation of Sx4 leads to a change in its conformation. Al Tobi also found that phospho-mimetic Sx4 could bind SNAP23 more tightly, providing further evidence that insulin-induced phosphorylation of Sx4 leads to increased SNARE complex formation (Al Tobi 2018).

Taken together, the data discussed in this section suggest a model in which, upon insulin stimulation, IR phosphorylates both Munc18c on Y521 and Sx4 on Y115 and Y251, and that these phosphorylation events alter the conformation of these two proteins in a way that allows increased SNARE complex formation, and thus increased fusion of GSVs with the plasma membrane (depicted in Figure 3.2), leading to increased GLUT4 at the plasma membrane and increased glucose transport.

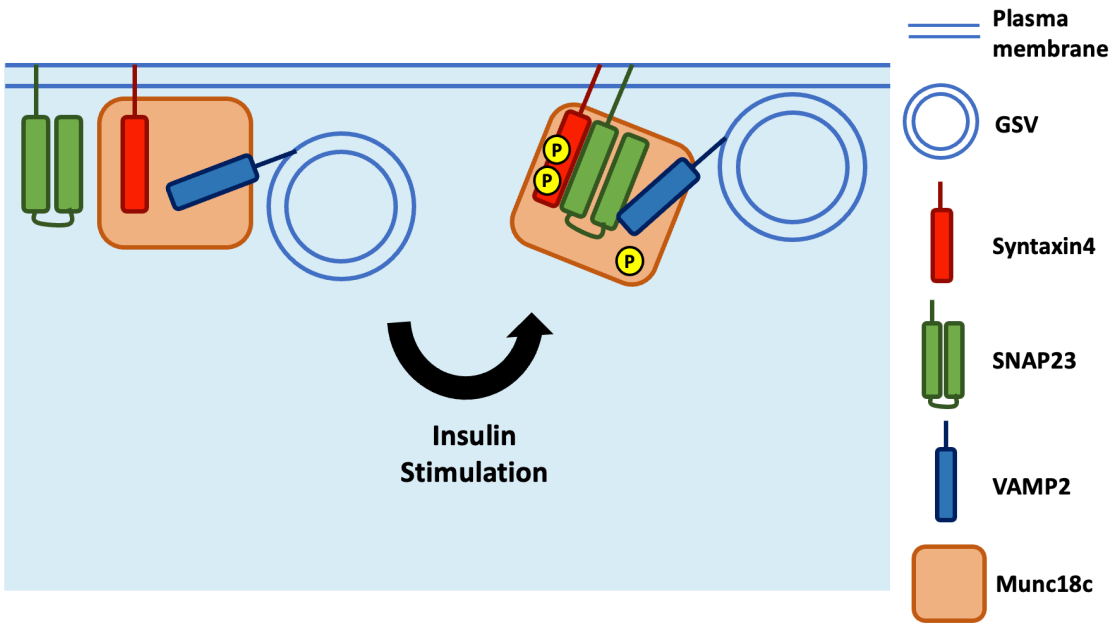

Figure 3.2 A model of the effect of insulin stimulation on SNARE complex formation required for GLUT4 storage vesicle fusion with the adipocyte plasma membrane.
Insulin stimulates the phosphorylation (yellow P) of Munc18c (orange) on Y521 and Sx4 (red) on Y115 and Y251, likely by the insulin receptor itself. This alters the conformation of these proteins, leading to increased SNARE complex formation, allowing increased fusion of GSVs with the plasma membrane, and ultimately increasing glucose transport into the cell.

3.1.4 Caveolae as a site for insulin receptor phosphorylation of SNARE proteins

Work using recombinant proteins has shown that CIRK can directly phosphorylate Sx4 and Munc18c *in vitro*. If IR phosphorylates these proteins *in vivo*, co-localisation of IR and the trafficking machinery in the plasma membrane of adipocytes would be expected. As discussed in section 1.5, caveolae are a plasma membrane microdomain abundant in adipocytes (Thorn et al. 2003), that act as signalling platforms and play a key role in insulin signalling. IR is abundant in caveolae, specifically in the neck region (Foti et al. 2007). Therefore, if IR directly phosphorylates Sx4 in the cell, it is a reasonable hypothesis that this interaction may occur in caveolae.

This chapter aims to investigate whether IR and Sx4 colocalise in adipocyte caveolae, and whether caveolae are the site of insulin stimulated Sx4 phosphorylation.

3.2 Results

3.2.1 Localisation of proteins to a caveolae-enriched fraction in adipocytes

In order to investigate Syntaxin4 (Sx4) phosphorylation in adipocyte caveolae, caveolae-enriched fractions were produced from 3T3-L1 adipocyte lysates. The lysates were subjected to a non-detergent-based caveolae isolation protocol using an alkaline lysis buffer and overnight ultracentrifugation in a 5-30-42% sucrose gradient (Callera, Bruder-Nascimento, and Touyz 2017) (described in Section 2.2.2.2). Samples were taken from across this gradient and subjected to immunoblot analysis to identify where the caveolae marker Caveolin1 (Cav1) was present, and thus where in the sucrose gradient caveolae were enriched. This revealed that caveolae were enriched in the fractions at the 5-30% sucrose interface (Figure 3.3, top panel). Similar results have been seen in other studies utilising this method for caveolae isolation (Trávez et al. 2018).

The insulin receptor (IR) is known to localise to caveolae (Foti et al. 2007). Here, IR beta subunit was enriched in the same fraction as Cav1 (Figure 3.3, second panel), further validating this fractionation approach. Interestingly, Sx4 was also enriched in this caveolae fraction (Figure 3.3, third panel), suggesting that both it and IR localise to caveolae. Furthermore, SNAP23, a binding partner of Sx4 during GLUT4 storage vesicle (GSV) fusion with the

plasma membrane, was found in this caveolae-enriched fraction, whereas the v-SNARE VAMP2 and regulatory SM protein Munc18c, also involved in this fusion process, were not (Figure 3.3, fourth to sixth panels). GLUT4 itself was enriched in the caveolae fraction (Figure 3.3, seventh panel). GAPDH, a housekeeping protein not associated with caveolae and usually serving as a loading control, acts here as a negative control for caveolae association, and thus is not enriched in the 5-30% sucrose interface fraction (Figure 3.3, bottom panel).

For subsequent experiments presented in this chapter, caveolae enriched fractions are taken from the 5-30% sucrose border of the sucrose gradient produced by this protocol.

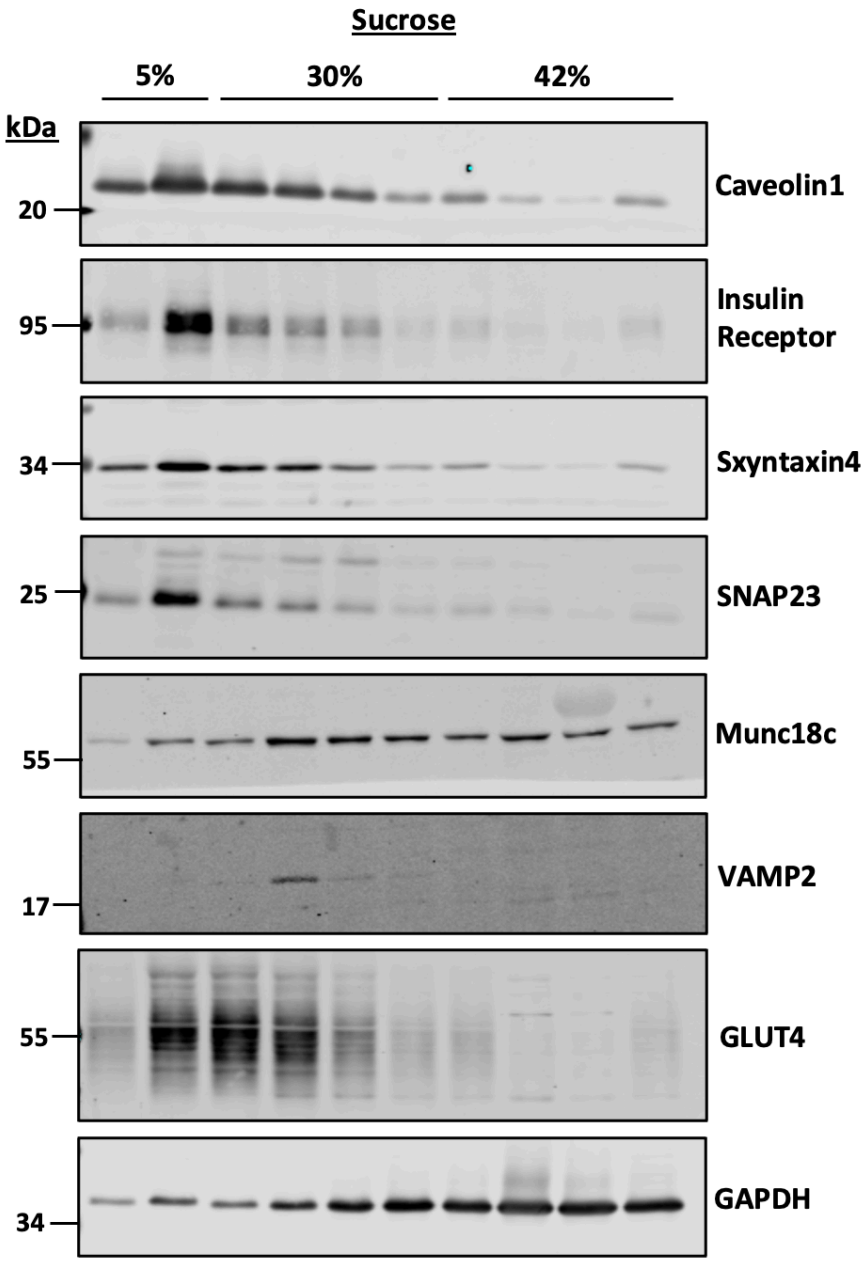

Figure 3.3 Protein localisation to a caveolae enriched fraction of 3T3-L1 adipocytes.

Caveolae-enriched membranes from basal 3T3-L1 adipocytes were isolated using a detergent-free method based on a discontinuous sucrose gradient (5-30-42% w/v). 10 fractions of equal volume were taken across this gradient and subjected to TCA protein precipitation. Representative western blots of these fractions are shown, probing for (top to bottom): the caveolae marker Caveolin1, Insulin Receptor beta subunit, Syntaxin4, SNAP23, Munc18c, VAMP2, GLUT4 and GAPDH. Blots are representative of n=2 independent experiments.

3.2.2 Investigating Synaxtin4 phosphorylation in 3T3-L1 adipocytes

Antibodies specific to Sx4 phosphorylated on Y115 and Y251, the residues previously shown to be phosphorylated in response to insulin (Schmelzle et al. 2006), were used on both whole cell lysates and caveolae-enriched fractions from 3T3-L1 adipocytes, either basal or following 20-minute 100 nM insulin stimulation, to determine whether Sx4 phosphorylation increases in response to insulin in these cells.

In Figure 3.4, western blots using these antibodies on whole cell lysates and caveolae fractions, as well as recombinant Sx4 controls, are shown. The western blots on the recombinant Sx4 controls are shown separately in Figure 3.4, panel A for clarity as well as included on the main blots in Figure 3.4 panel B. The recombinant Sx4 proteins are GST-tagged and are either WT or a phospho mimetic variant of Y115E or Y251E as indicated. These proteins had undergone *in vitro* phosphorylation by recombinant cytosolic insulin receptor kinase (CIRK), which consists of the part of the beta subunit of the IR responsible for its tyrosine kinase activity (Kuhné et al. 1994), and so should phosphorylated Sx4 on Y115 and Y251. As the replacement of the 115 and 251 tyrosine residues with glutamic acid residues in the phosphomimetic Sx4 proteins prevents CIRK phosphorylation of those residues, the recombinant Sx4 proteins are actually phosphorylated as follows: WT Sx4 on both Y115 and Y251; Sx4-Y115E on Y251; and Sx4-

Y251E on Y115. Therefore, the Sx4-Y115-P antibody is validated by detecting the WT and Y251E proteins (Figure 3.4, panel A, middle), and the Sx4-Y251-P antibody is validated by detecting the WT and Y115E proteins (Figure 3.4, panel A, bottom).

A

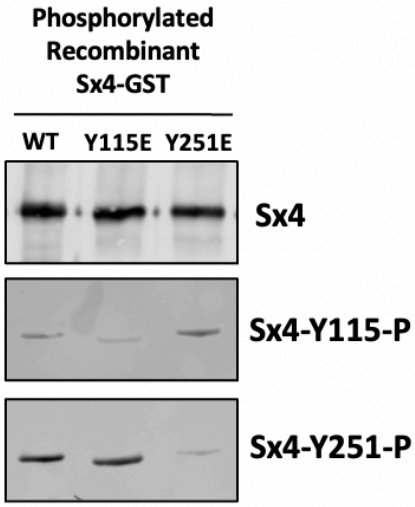
Phosphorylated
Recombinant
Sx4-GST
WT
Y115E
Y251E
Sx4
Sx4-Y115-P
Sx4-Y251-P

B

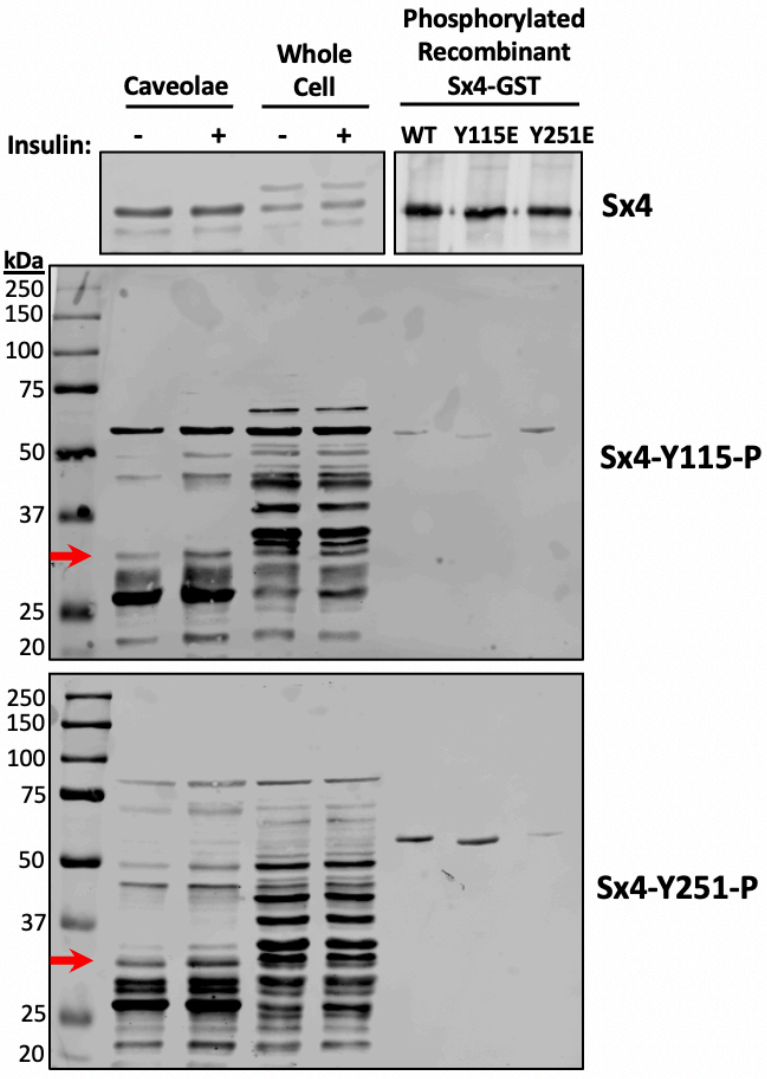
Caveolae
Whole
Cell
Phosphorylated
Recombinant
Sx4-GST
Insulin:
-
+
-
+
WT
Y115E
Y251E
Sx4
kDa
250
150
100
75
50
37
25
20
Sx4-Y115-P
Sx4-Y251-P

Figure 3.4 Validation of phospho-specific Syntaxin4 antibodies.
A) Representative western blots with total Syntaxin4 (Sx4), Sx4-Y115P and Sx4-Y251P antibodies in 200 ng CIRK-phosphorylated recombinant GST-tagged Sx4 proteins, either WT a phospho-mimetic versions: Sx4 Y115E or Sx4 Y251E.
B) Representative western blots of total Sx4, Sx4-Y115P and Sx4-Y251P in whole cell lysates or caveolae enriched cell fractions (isolated using a detergent-free method with a discontinuous sucrose gradient; fraction taken from 5-30% sucrose interface) from basal or insulin stimulated (100 nM for 20 minutes) 3T3-L1 adipocytes. 30 μg protein was loaded for each sample. The red arrows indicate the expected molecular weight of Sx4, 34kDa. Also included on these blots are the CIRK-phosphorylated recombinant GST-tagged Sx4 proteins separated for clarity in **A**. Blots are representative of at least 3 independent experiments. Quantification was not possible due to high background.

Unfortunately, both of the phospho-specific antibodies had a great deal of non-specific binding, particularly when used on whole cell lysates (Figure 3.4, panel B). In the caveolae fractions, some bands around the correct size for Sx4 (34 kDa, indicated with red arrows on Figure 3.4, panel) were seen in both the Sx4-Y115-P and Sx4-Y251-P blots, but there remained too much non-specific binding to determine which band was the true Sx4 band, let alone ascertain whether Sx4 phosphorylation increased in response to insulin.

Following this, immunoblotting with the Sx4 phospho-specific antibodies was optimised to reduce non-specific binding. The following conditions produced the best results, as shown in Figure 3.5: lowering antibody concentration to 1

in 2000, rather than the 1 in 1000 used for most antibodies, using 3% BSA rather than 5% milk powder solution for blocking, and increasing the duration of all wash steps to 20 minutes. Figure 3.5 shows blots for Sx4, Sx4 Y115-P, Sx4 Y251-P and Cav1 in caveolae and whole cell lysates, from both WT and Sx4 knockout (Sx4 KO) 3T3-L1 adipocytes, either basal or stimulated with 100 nM insulin for 20 minutes. Sx4 KO cells were included here as a negative control for Sx4 phosphorylation. The optimised protocol allowed bands of the correct size for Sx4 to be seen when using the Sx4 Y115-P and Sx4 Y251-P antibodies on WT cells that were not present in Sx4 KO cells. Notably, these bands could only be detected in the caveolae enriched fraction. However, the signal produced with these antibodies was not strong enough, nor consistent enough between repeats of this experiment to conclude whether or not phosphorylated Sx4 increases in caveolae in response to insulin.

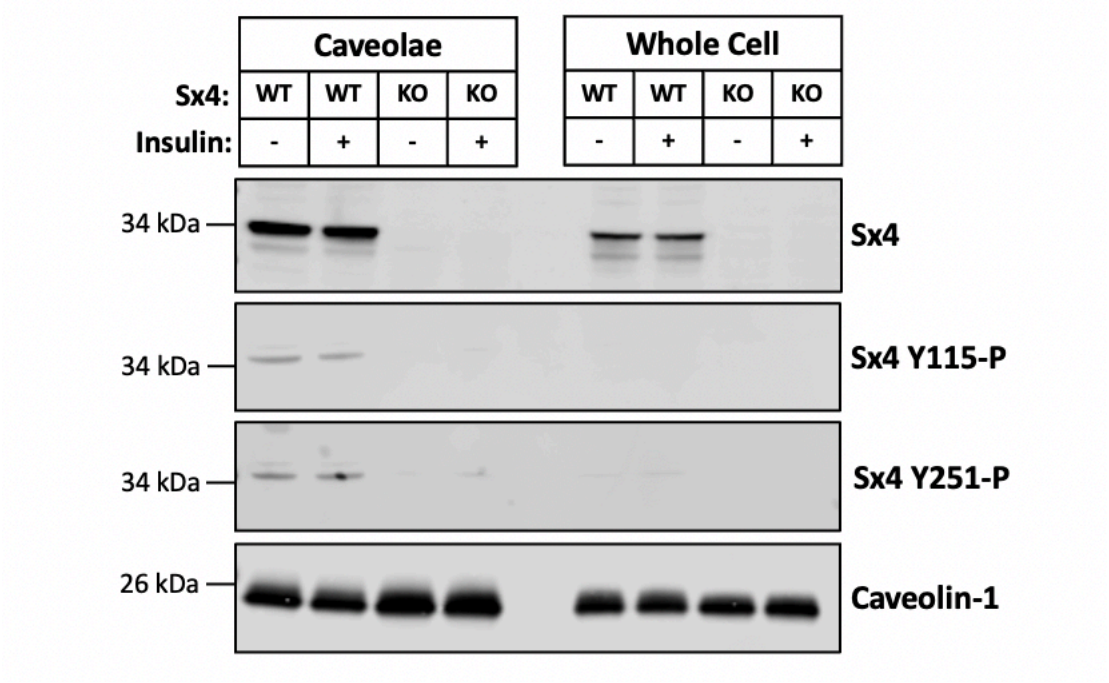

Figure 3.5 Phosphorylated Syntaxin4 in adipocyte caveolae.
Western blots of total Syntaxin4 (Sx4), Sx4-Y115P and Sx4-Y251P and Caveolin1 in whole cell lysates or caveolae enriched cell fractions (isolated using a detergent-free method with a discontinuous sucrose gradient; fraction taken from 5-30% sucrose interface) from basal or insulin stimulated (100 nM for 20 minutes) WT or Sx4 knockout (KO) 3T3-L1 adipocytes. 15 μg protein was loaded for each sample. Blots are representative of n=2 biological replicates.

With the phospho-specific antibodies proving insufficient tools to answer the question of whether Sx4 is phosphorylated in response to insulin in adipocytes, an immunoprecipitation experiment with anti-phospho-tyrosine beads was used to further investigate this question. In Figure 3.6, start lysate taken prior to incubation with any beads, end lysate taken after incubation with anti-phospho-tyrosine beads, and the proteins taken from the beads themselves, which should capture any tyrosine-phosphorylated proteins, were subjected to immunoblotting for IR, Sx4 and Cav1. End lysate and

bead-captured proteins from control Protein A beads were also included in these blots. The lysates were produced from both basal and insulin-stimulated WT 3T3-L1 adipocytes and were either from the whole cell, or from the caveolae enriched fraction.

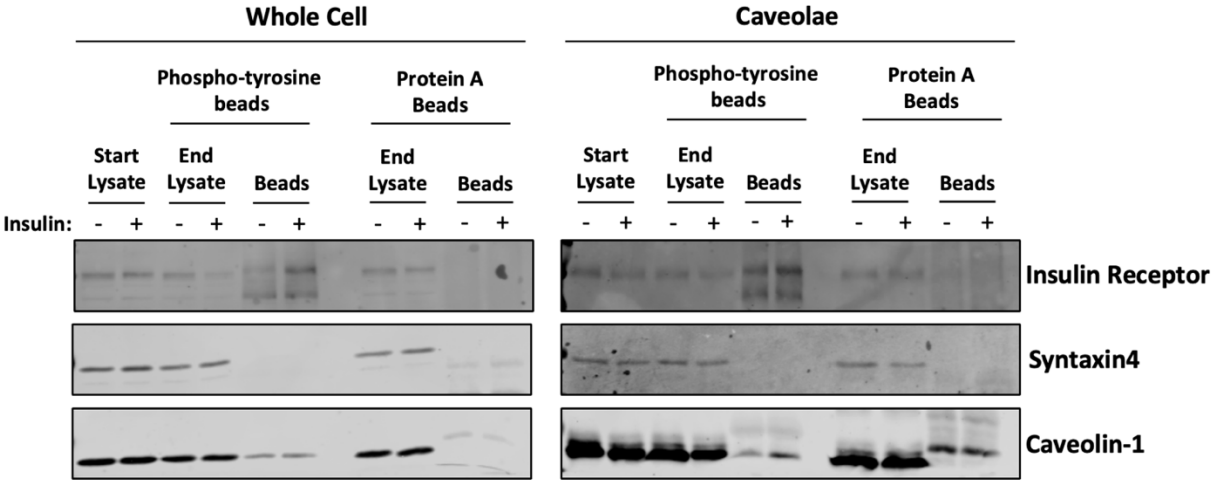

Figure 3.6 Immunoprecipitation with anti-phospho-tyrosine beads. Whole cell or caveolae enriched lysates (isolated using a detergent-free method with a discontinuous sucrose gradient; fraction taken from 5-30% sucrose interface) from basal or insulin stimulated (100 nM for 20 minutes) 3T3-L1 adipocytes were incubated overnight with anti-phospho-tyrosine beads or control protein A beads. Shown are representative western blots of the Insulin Receptor, Synaxtin4 and Caveolin1 in start lysates, immunodepleted end lysates and immunoprecipitated proteins from the beads. 15 μg protein was loaded for each sample. Blots are representative of n=2 independent experiments.

IR was captured by the phospho-tyrosine beads, more so in insulin stimulated cells. This can be seen by the drop in IR between the basal and insulin stimulated end lysates, and the rise in IR between the basal and insulin stimulated bead-captured fraction (Figure 3.6). This pattern is the same across whole cell and caveolae, and shows that, as expected, IR

becomes tyrosine-phosphorylated in response to insulin stimulation. Cav1 in whole cell lysates is also captured by the anti-phospho-tyrosine beads, confirming that at least a fraction of Cav1 is tyrosine phosphorylated (Lee et al. 2000). Interestingly, in caveolae, where Cav1 is concentrated, there is an insulin stimulated increase in the amount of Cav1 captured by the anti-phospho-tyrosine beads, showing an insulin stimulated rise in Cav1 phosphorylation, likely as a result of phosphorylation by IR (Kimura et al. 2002). No Sx4 was captured by the anti-phospho-tyrosine beads, meaning that no tyrosine phosphorylation of Sx4, insulin stimulated or otherwise, was detected in this experiment.

3.2.3 Co-Localisation of Syntaxin4 and the Insulin Receptor

The experiments presented thus far in this chapter have not been able to identify any insulin stimulated rise in Sx4 phosphorylation, despite previously published mass spectrometry data from 3T3-L1 adipocytes demonstrating this (Schmelzle et al. 2006). It is possible that this phosphorylation effect does occur, but in a small enough pool of Sx4 in the cell that it is difficult to detect with the immunoblotting-based methods used so far. To take a different approach, the co-localisation of Sx4 and IR were investigated, as in order for IR phosphorylate Sx4 directly, they must be in close proximity to one another. Both immunofluorescent microscopy-based co-localisation and proximity ligation assays have been used here to this end.

3.2.3.1 Validation of antibodies for use in co-localisation experiments

Both standard immunofluorescence and proximity ligation assays used here to study co-localisation rely on antibodies against Cav1 (Abcam, ab2910) and IR beta (Abcam, ab69508) and two antibodies against Sx4, one raised in rabbit (Synaptic Systems 110 042) and the other raised in mouse (Synaptic Systems 110 041) (Table 2.1). These antibodies were tested at a range of concentrations for both western blotting and single-antibody immunofluorescence, to ensure they produced minimal non-specific binding and localised as expected within the cell.

The Cav1 antibody (Figure 3.7, panel A) showed very little non-specific binding in immunoblotting, and specifically stained the plasma membrane of 3T3-L1 adipocytes, which was expected as caveolae make up a large proportion of the adipocyte cell surface (Thorn et al. 2003). The IR antibody also had little non-specific binding in immunoblotting, in immunofluorescence it stained the plasma membrane clearly as expected (Figure 3.7, panel B). This antibody also showed some staining of the nucleus, which is to be expected because it has recently been shown that IR beta subunit can associate with promotors in the nucleus (Hancock et al. 2019). Both antibodies against Sx4 also had minimal non-specific binding in western blotting. In immunofluorescence, the Sx4 antibodies did not stain the plasma membrane as clearly as Cav1 and IR, but concentrated Sx4 staining can be seen at the surface of most cells (Figure 3.7, panels C and D). The

antibodies show here could therefore all be taken forward for use in co-localisation experiments. All antibodies examined here worked well at a dilution of 1:100 for immunofluorescence, except Cav1, which could be used at 1:500.

A) Caveolin1

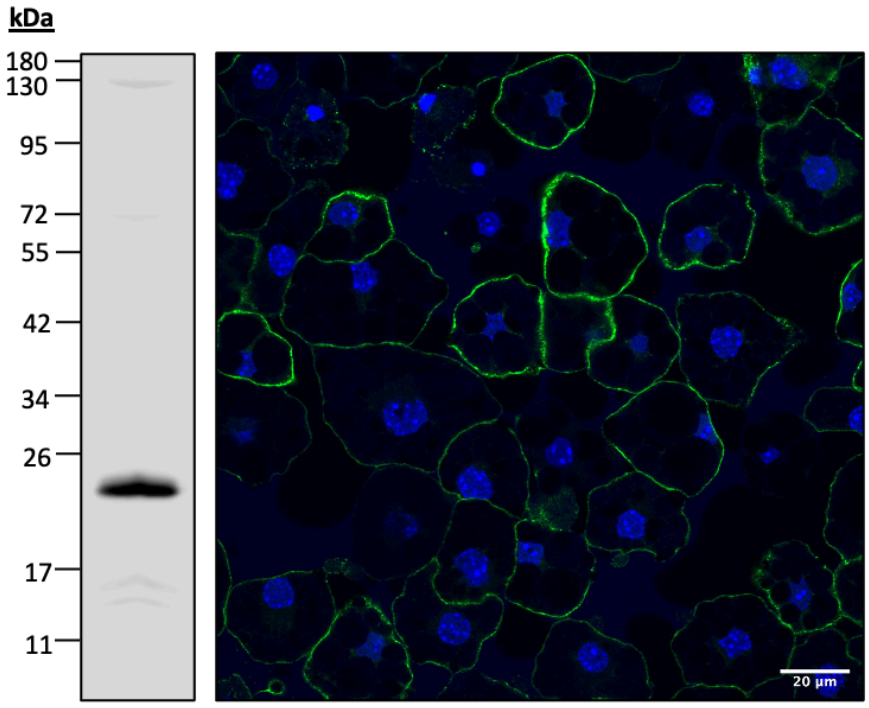

B) Insulin Receptor (Beta Subunit)

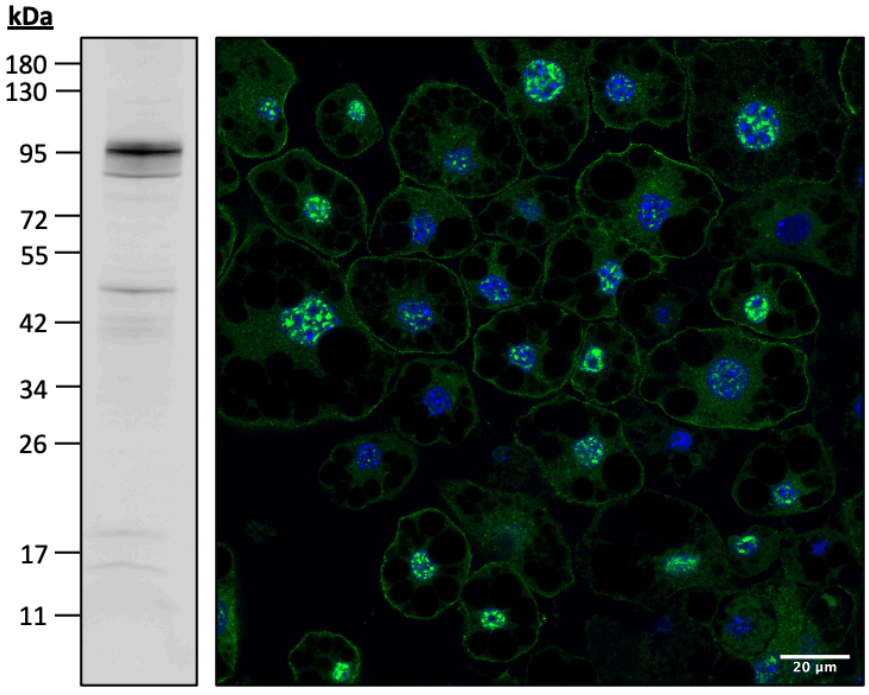

C) Syntaxin4 (Mouse)

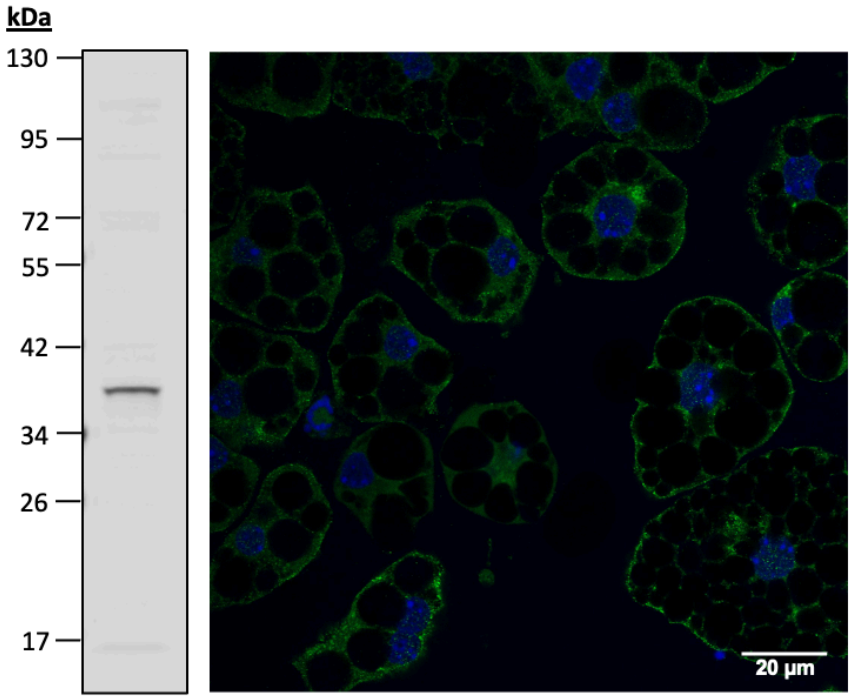

D) Syntaxin4 (Rabbit)

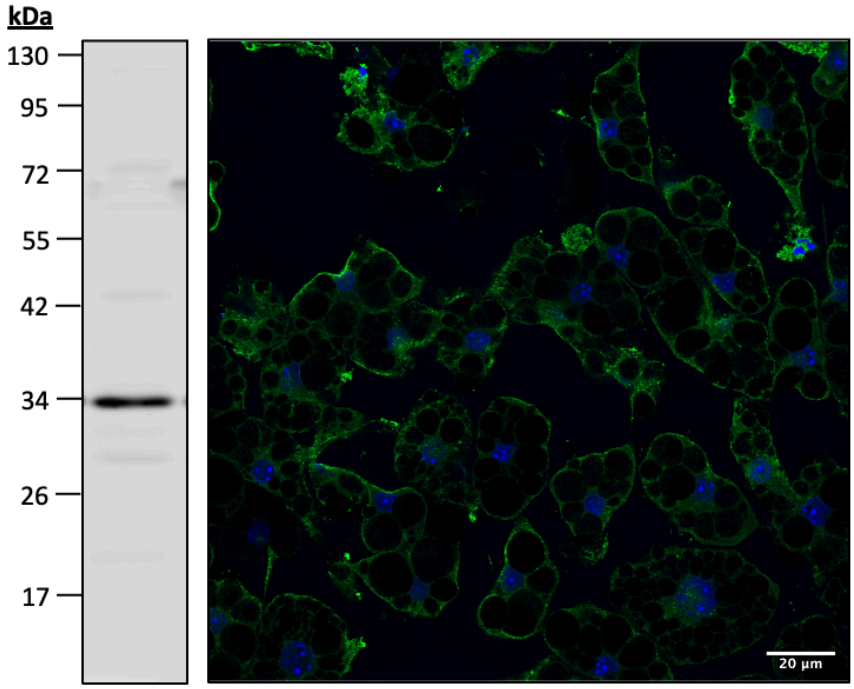

Figure 3.7 Validation of antibodies for co-localisation experiments. Right: 3T3-L1 adipocytes were fixed, quenched and permeabilised before non-specific binding sites were blocked. Cells were then incubated with the following antibodies: **(A)** Caveolin1 (Abcam, ab2910), **(B)** Insulin receptor beta subunit (Abcam, ab69508), **(C)** Syntaxin4 (raised in mouse, Synaptic Systems 110 041) and **(D)** Syntaxin4 (raised in rabbit, Synaptic Systems 110 042), followed by incubation with an appropriate Alexa Fluor 488 conjugated secondary antibody (green). DNA was stained with DAPI (blue). Staining was visualised using a Leica 8 TCS SP8 confocal microscope. Images were assembled in ImageJ. Scale bars are 20 μm. **Left:** 3T3-L1 cell lysates were prepared and subjected to SDS-PAGE and immunoblotting, probing for the same antibodies listed above for **(A)**-**(D)**.

3.2.3.2 Co-localisation using standard immunofluorescence microscopy

In Figure 3.8 panel A, immunofluorescence staining showed that the following pairs of proteins co-localise at the adipocyte plasma membrane: IR and Sx4 (Figure 3.8, panel A, top row); IR and Cav1 (Figure 3.8, panel A, middle row); Sx4 and Cav1 (Figure 3.8, panel A, bottom row).

Figure 3.8 panel B shows a table of Pearsons and Manders Coefficients calculated from images of 3T3-L1 adipocytes that were either untreated (Basal) or stimulated with 100 nM insulin for 20 minutes (Insulin) prior to fixing and staining with the pairs of antibodies previously mentioned. Each image contained on average 20 cells, and three biological replicates were carried out for each protein pair and insulin stimulation condition. The Pearsons coefficient is a measure of the linear relationship between the intensity of pixels in the green channel image and the intensity of those same pixels in the red channel image. This number can range from -1 to 1, with -1

representing a strong negative correlation, 1 representing a strong positive correlation and 0 representing no correlation. If intensity between pixels in both channels give a positive correlation and thus a positive Pearsons Coefficient, it suggests that the proteins stained for in those channels co-localise. The authors of the 2006 review “A guided tour into subcellular colocalization analysis in light microscopy”, who created the ImageJ plugin JACoP (“Just Another Co-localisation Plugin”) used for the analysis shown in Figure 3.8 panel B, recommend that conclusions about co-localisation can only be confidently drawn when Pearsons Coefficient is greater than 0.5. As this is the case for all protein pairs examined here (excluding the Cav1 and Sx4 pair images of insulin stimulated cells, which fall just short with an average Pearsons Coefficient of 0.487), it is likely that IR, Cav1 and Sx4 all co-localise in adipocytes.

Also included in Figure 3.8 panel B are the Manders Coefficients from the same images. Manders is an overlap coefficient representing how much the staining captured in one channel overlaps the staining captured in the other channel. Accordingly, there are two Manders coefficients for each protein pair, M1 and M2. M1 is the ratio of the intensities of pixels from the green image for which the intensity in the red channel is above zero, to the total intensity in the green channel. M2 is defined conversely for the red channel. Therefore, M1 is a good indicator of the proportion of the green signal

coincident with a signal in the red channel in relation its total intensity, and vice versa for M2.

For the IR and Sx4 pair, M1 represents the fraction of IR that overlaps with Sx4, and M2 is the fraction of Sx4 that overlaps with IR. M2 is on average higher for this pair, likely due to IR staining of the nucleus, where Sx4 is not present (Figure 3.8, panel A, top row). For the Cav1 and Sx4 pair, M1 is the fraction of Sx4 overlapping with Cav1, whereas M2 represents the fraction of Cav1 that overlaps Sx4. Once again, M2 was on average higher for this pair, likely because Cav1 very specifically stains the plasma membrane, whereas Sx4 also produced some staining inside the cell (Figure 3.8, panel A, bottom row). Finally, for the IR and Cav1 pair, M1 represents the fraction of IR that overlaps with Cav1 and M2 represents the fraction of Cav1 that overlaps with IR. Once again, M2 is lower for this pair, again most likely due to IR staining in the nucleus, where it does not co-localise with Cav1 or Sx4 as it does at the plasma membrane.

Importantly, across all pairs and for all coefficients measured here, no significant difference in co-localisation between basal and insulin stimulated cells was found. Insulin does not appear to affect the co-localisation of these proteins.

A

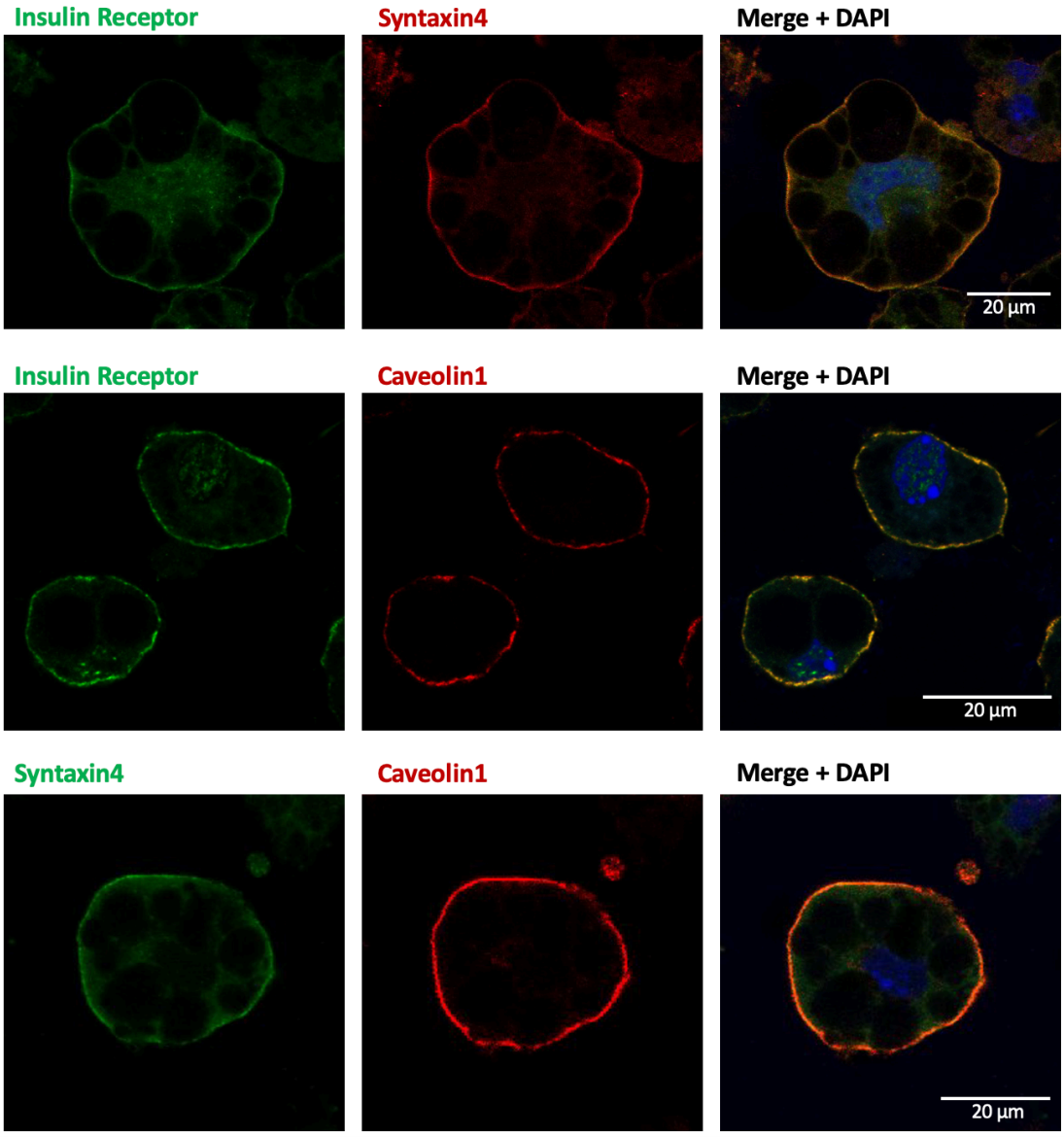
Insulin Receptor
Syntaxin4
Merge + DAPI
20 µm
Insulin Receptor
Caveolin1
Merge + DAPI
20 µm
Syntaxin4
Caveolin1
Merge + DAPI
20 µm

B

	IR + Sx4		Cav1 + Sx4		IR + Cav1	
	Basal	**Insulin**	**Basal**	**Insulin**	**Basal**	**Insulin**
Pearsons Coefficient	0.681	0.581	0.549	0.477	0.651	0.504
	0.620	0.702	0.546	0.414	0.559	0.520
	0.596	0.696	0.488	0.569	0.504	0.508
Average	**0.632**	**0.660**	**0.528**	**0.487**	**0.571**	**0.511**
Manders Coefficient (M1)	0.692	0.161	0.263	0.120	0.454	0.267
	0.298	0.406	0.252	0.125	0.326	0.245
	0.402	0.374	0.376	0.289	0.207	0.337
Average	**0.464**	**0.314**	**0.297**	**0.178**	**0.329**	**0.283**
Manders Coefficient (M2)	0.645	0.324	0.478	0.573	0.561	0.451
	0.724	0.554	0.596	0.281	0.571	0.590
	0.619	0.399	0.644	0.605	0.648	0.572
Average	**0.663**	**0.426**	**0.573**	**0.486**	**0.593**	**0.538**

Figure 3.8 Co-localisation of Insulin Receptor, Syntaxin4 and Caveolin1 using immunofluorescence microscopy.

(A) 3T3-L1 adipocytes were fixed, quenched and permeabilised before non-specific binding sites were blocked. Cells were then incubated with antibodies against the following protein pairs: (top row) Insulin receptor (IR) and Syntaxin4 (Sx4); (middle row) IR and Caveolin1 (Cav1); (bottom row) Sx4 and Cav1, followed by incubation with an appropriate Alexa Fluor 488 (green) or Alexa Fluor 647 (red) conjugated secondary antibodies. DNA was stained with DAPI (blue). Staining was visualised using a Leica 8 TCS SP8 confocal microscope, and images were assembled with ImageJ. Scale bars are 20 μm.

(B) Table of Pearsons and Manders Coefficients from images of basal and insulin stimulated (100 nM for 20 minutes) 3T3-L1 adipocytes produced as described above. Each image contained on average 20 cells and represents an independent biological replicate, of which n=3 were performed for each condition and protein pair. Analysis was carried out with ImageJ using the JACoP plugin. No significant change in either coefficient was found between basal and insulin stimulated cells.

3.2.3.3 Using Proximity Ligation Assays to measure co-localisation

Although standard immunofluorescence microscopy can give good insight into co-localisation, conclusions cannot be drawn about whether proteins that co-localise in the cell are directly interacting, due to the limitations of microscope resolution.

Proximity ligation assay (PLA) is a technique that allows pairwise protein-protein interactions to be visualised in the cell. Briefly, two proteins were detected with primary antibodies in fixed and permeabilised 3T3-L1 adipocytes. Specially designed secondary antibodies conjugated to an oligonucleotide detect those primary antibodies, and a series of reaction steps ligates and amplifies this DNA, allowing a fluorescent probe to detect and visualise the complex (Section 2.2.5.3, Figure 2.1). Ultimately, this means that if the proteins in question are less than 40 nm apart, and therefore closely interacting, they will be marked by a fluorescent dot (or "signal") in the cell when imaged with a confocal microscope.

In Figure 3.9 panel A, representative PLA images for Sx4 and IR (top left), IR and Cav1 (top right) and Cav1 and Sx4 (bottom left) are shown. For all of these pairs, a number of green dots in a ring-shape around the cell can be seen, showing that these proteins closely interact at the cell surface. A

representative image of a cell from a PLA control lacking primary antibodies is also shown (bottom right).

Figure 3.9 panel B shows the quantification of fold change in average PLA signal per cell following 20-minute 100 nM insulin stimulation for Sx4 and IR, and Cav1 and IR pairs. PLA signals for Sx4 and IR did not significantly change in response to insulin. However, PLA signals for Cav1 and IR in insulin stimulated cells decreased to 0.41-fold (+/-0.067 p=0.006) that in basal cells. This observation is interrogated further and discussed in chapter 5.

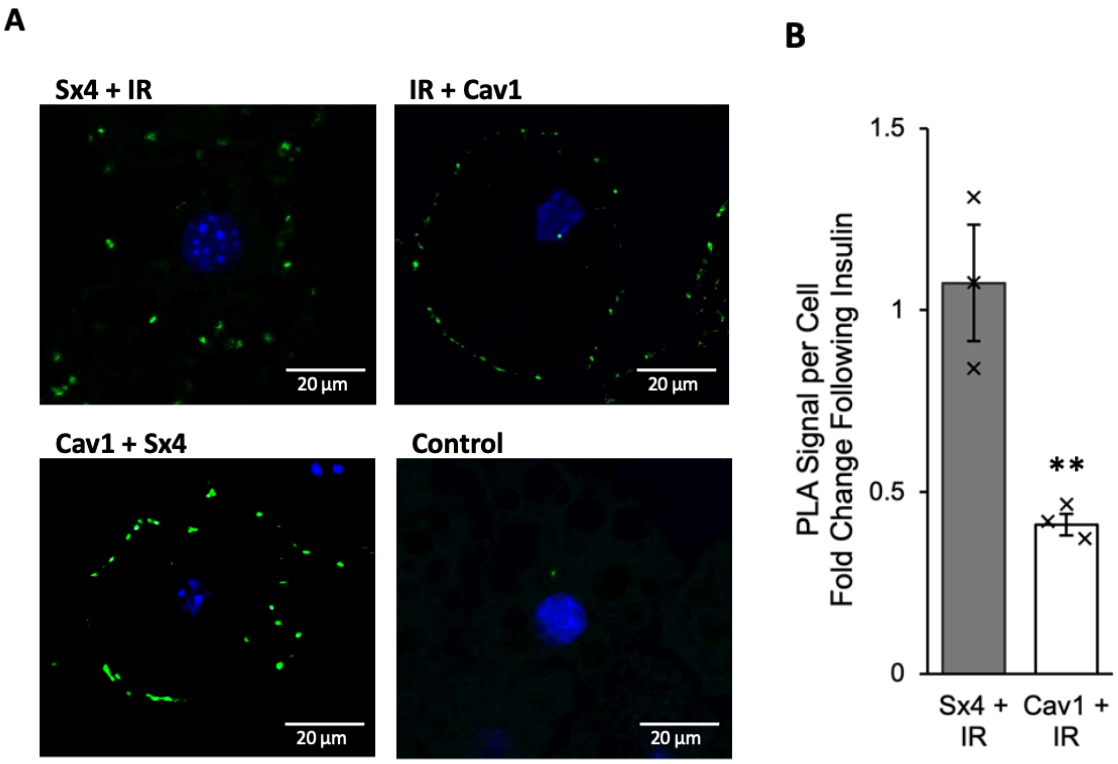

Figure 3.9 Co-localisation of Insulin Receptor, Syntaxin4 and Caveolin1 using Proximity Ligation Assay.

(A) Proximity Ligation Assay (PLA) was used to assess pairwise interactions of proteins in 3T3-L1 adipocytes. Representative images, with PLA signal in green and nuclei staining with DAPI in blue, are shown for the following protein pairs: Insulin receptor (IR) and Syntaxin4 (Sx4) (top left); IR and Caveolin1 (Cav1) (top right); Sx4 and Cav1 (bottom left). A PLA control lacking primary antibodies is also shown (bottom right).

(B) Quantification of fold change in PLA signal per cell for the IR and Sx4, and IR and Cav1 pairs in insulin stimulated (100 nM for 20 minutes) 3T3-L1 adipocytes compared to basal. Each x on the chart represents the mean number of PLA signals per cell in approximately 100 insulin-stimulated cells expressed as fold change from the mean number of PLA signals per cell in approximately 100 basal cells. Mean and SD of n = 3 independent experiments are shown. Quantification was performed in ImageJ and statistical analysis was with unpaired t-tests, ** p=0.006. Scale bars are 10 μm.

3.3 Discussion

3.3.1 SNARE proteins are localised in caveolae

This chapter aimed to investigate whether caveolae could be the site of insulin receptor (IR) phosphorylation of Syntaxin4 (Sx4) in adipocytes. This would make caveolae a key cellular compartment in which signals from IR meet the membrane trafficking machinery responsible for GLUT4 translocation to the plasma membrane. Therefore, first, caveolae enriched cell fractions from basal 3T3-L1 adipocytes were probed for a number of key proteins involved in this process, including IR, GLUT4 and the SNARE proteins involved in GLUT4 storage vesicle (GSV) fusion with the plasma membrane: Sx4, SNAP23 and VAMP2, as well as their regulatory SM protein, Munc18c (Figure 3.3). IR, GLUT4 and the t-SNARE proteins Sx4 and SNAP23 were all enriched in the same fraction as Caveolin1 (Cav1), and so are likely to be enriched in caveolae. Munc18c and the v-SNARE VAMP2 were not enriched in caveolae. Sx4 and SNAP23 are the membrane bound components of the GSV fusion SNARE complex (Kawaguchi et al. 2010), so the fact that they appear to be associated with caveolae in basal cells suggests that their insulin-stimulated complex formation with VAMP2 and subsequent GSV fusion with the plasma membrane may be linked to caveolae.

As discussed in section 1.5.2, there is conflicting evidence as to whether, and to what extent, GLUT4 localises to the caveolae. However, the GLUT4 panel in Figure 3.3 supports previous studies that found a proportion of GLUT4 localised to caveolae in basal adipocytes (reviewed in Stralfors 2012).

3.3.2 Investigating Syntaxin4 phosphorylation in caveolae

As demonstrated in Figure 3.4, using phospho-specific antibodies to detect Sx4-Y115P and Sx4-Y251P proved challenging. The phosphorylated recombinant protein controls in this figure show that these antibodies are capable of specifically recognising the phosphorylation of Y115 or Y251 residues in Sx4 in purified proteins. However, the antibodies suffered from a great deal of non-specific binding when used with whole cell lysates or caveolae enriched cell fractions.

Even following a great deal of optimisation to reduce non-specific binding, bands produced by these antibodies were weak and difficult to consistently reproduce. However, as shown in Figure 3.5, Sx4-Y115P and Sx4-Y251P could be more readily detected in caveolae enriched fractions. This is likely because, as shown in Figure 3.3, Sx4 is enriched in caveolae, but could also suggest that Sx4 is phosphorylated specifically in caveolae. No increase in phosphorylated Sx4 was observed in response to insulin, however the weak signal and non-specific binding issues with the phospho-specific antibodies

made these blots difficult to quantify, and thus difficult to draw conclusions from.

Immunoprecipitation with anti-phosphotyrosine beads was used as an alternative method to investigate whether Sx4 is phosphorylated on Y115 and Y251 in response to insulin in adipocytes (Figure 3.6). The effectiveness of the beads was validated as they pulled down both IR and Cav1 from the lysates, and both are known to be tyrosine-phosphorylated in adipocytes (Kimura et al. 2002). This immunoprecipitation method was shown to be able to detect changes in protein phosphorylation states in cells, as more IR was captured from lysates of insulin-stimulated cells than those from basal cells (Figure 3.6, top panels). The same is true of Cav1, specifically in the caveolae cell fraction where Cav1 is enriched (Figure 3.6, bottom right panel). However, in both whole cell and caveolae enriched lysates, no tyrosine phosphorylated Sx4 was pulled down.

The data presented so far in this chapter do not point to any insulin-stimulated phosphorylation of Sx4, in spite of previous mass spectrometry data showing that phosphorylation on Y115P and Y251P increased more than 3x within 5 minutes of insulin stimulation in 3T3-L1 adipocytes (Schmelzle et al. 2006). It is worth noting that this phosphorylation of Sx4 in response to insulin in adipocytes was also observed using mass spectrometry by Mohammed Al Tobi in his PhD research (Al Tobi 2018), so

the findings of Schmelzle et al. can be replicated. However, the fact that this phosphorylation cannot be detected by immunoblotting methods raises questions as to whether this phosphorylation effect is as pronounced as first suggested. Indeed, perhaps only a sub-population of cellular Sx4 is phosphorylated in response to insulin, possibly the insulin-responsive Sx4-VAMP2-Munc18c pool hypothesised by Kioumourtzoglou et al. and described in Section 3.1.2.1 and Figure 3.1 (right panel). Sx4 from this pool may be phosphorylated in response to insulin, but to levels that are not detectable using the immunoblotting-based methods employed here.

3.3.3 Syntaxin4 co-localises with Insulin Receptor and Caveolin1

Following difficulty detecting phosphorylated Sx4, co-localisation between Sx4, IR and Cav1 were investigated. This was a means to test the hypothesis that IR phosphorylates Sx4 directly, as the two proteins would have to be in close proximity for this to occur, and to test the hypothesis that this phosphorylation occurs in caveolae, as it would be expected that both proteins would co-localise with the caveolae component Cav1 if this were the case.

Standard immunofluorescence microscopy (Figure 3.8) showed that each pair of proteins (IR and Sx4, Sx4 and Cav1, and IR and Cav1) co-localised in 3T3-L1 adipocytes, with an average Pearsons coefficient of >0.5 across all combinations of proteins. There was not total co-localisation between each

pair of proteins, as shown by the Manders overlap coefficients (Figure 3.8, panel B, and described in depth in Section 3.2.3.2). This is because, as can be seen in Figure 3.8 panel A, co-localisation of each pair of proteins occurs primarily at the plasma membrane, but not elsewhere in the cell. These data are consistent with the hypothesis that IR, Sx4 and Cav1 colocalise in caveolae.

3.3.5 Syntaxin4 interacts with Insulin Receptor and Caveolin1

Limitations of the resolution of standard immunofluorescence microscopy mean that co-localisation of proteins, as demonstrated for Sx4, IR and Cav1 in Figure 3.8 does not necessarily imply that those proteins directly physically interact in the cell as would be required for phosphorylation. Proximity Ligation Assays (PLA) allows *in situ* detection of protein-protein interactions closer together than 40 nm, and so has been employed here to determine whether Sx4, IR and Cav1 closely interact in adipocytes.

Figure 3.9 panel A shows of PLA signals (green dots) localised to the plasma membrane, representing pairwise interactions between Sx4 and IR (top left), IR and Cav1 (top right) and Cav1 and Sx4 (bottom left). This represents the first *in vivo* evidence that Sx4 could be phosphorylated by IR, as this PLA data shows that two proteins closely interact. Both Sx4 and IR's close interactions with Cav1 further demonstrate that the two co-localise in caveolae.

PLA was also used to investigate whether the number of interactions between Sx4 and IR, and between IR and Cav1, change in response to insulin (Figure 3.9, panel B). Strikingly, PLA signals per cell for the IR and Cav1 decreased by half following insulin stimulation, demonstrating that interactions between these proteins are reduced in response to insulin. This effect is investigated and discussed further in Chapter 5 (see Sections 5.2.3 and 5.3.3.1), however it is interesting to note here that co-localisation between IR and Cav1 as measured by standard immunofluorescence microscopy did not change in response to insulin (Figure 3.8, panel B). This suggests that although interactions between IR and Cav1 decrease in response to insulin, this probably does not equate to IR completely disassociating from caveolae, as the pair still co-localise in insulin stimulated cells. Furthermore, this discrepancy further demonstrates the sensitivity of PLA over standard immunofluorescence microscopy.

There was no change in PLA signal per cell for Sx4 and IR in response to insulin. This shows that Sx4 and IR remain in close proximity regardless of insulin activation.

3.3.4 Conclusions

Although the findings from mass spectrometry data that Sx4 is phosphorylated on Y115 and Y251 in response to insulin could not be corroborated here, phosphorylated Sx4 has been observed in caveolae

(Figure 3.5) and Sx4 has been shown to closely interact with both IR and the caveolae component Cav1, lending weight to the hypothesis that IR phosphorylates Sx4 in adipocyte caveolae and suggesting that caveolae could be a key site where insulin signalling meets the GLUT4 trafficking machinery.

It would be of interest in future studies to repeat some of the experiments discussed here with a focus on Sx4's binding partner Munc18c. Of particular interest would be PLA between IR and Munc18c, as Munc18c is also tyrosine phosphorylated in response to insulin, on Y521 (Aran, Bryant, and Gould 2011), so uncovering whether IR and Munc18c are in close proximity in adipocytes could provide *in vivo* evidence that IR also directly phosphorylates Munc18c. PLA between Munc18c and Cav1 could also reveal whether this interaction might occur in caveolae, and would provide further evidence that caveolae provide a platform for interactions between the insulin receptor and SNARE trafficking machinery required for glucose transport.

Chapter 4

Characterisation of Syntaxin4 Knockout 3T3-L1 Adipocytes and Generation of Phospho-Syntaxin4 Cell Lines

4 Characterisation of Syntaxin4 Knockout 3T3-L1 Adipocytes and Generation of Phospho-Syntaxin4 Cell Lines

4.1 Introduction

4.1.1 Generation of Syntaxin4 knockout 3T3-L1 cell line

In order to study the role of Syntaxin4 (Sx4) in adipocyte biology, a Sx4 knockout (Sx4 KO) 3T3-L1 cell line was generated by Dr. Hannah Black, University of Glasgow, using CRISPR-Cas9 technology. This cell line was confirmed to be able to differentiate into adipocytes using the standard 3T3-L1 differentiation protocol (Section 2.2.1.2), both by examination of the morphological features of the cells (Hannah Lucy Black 2016), and by Oil Red O staining, which allows lipid droplets to be visualised (Al Tobi 2018).

Continuing from this work, the first aim of this chapter was to characterise how well Sx4 KO cells differentiate into adipocytes and, subsequently, to assess the insulin response in Sx4 KO adipocytes. As the Sx4 KO cells were to later be used to generate new cell lines for the purpose of studying Sx4 in adipocyte biology, it was important to demonstrate that these cells could differentiate successfully into insulin-responsive adipocytes. These experiments, shown in Figures 4.1, 4.2 and 4.3, form part of a larger study into the role of Sx4 in adipocyte biology, published as “Knockout of syntaxin-

4 in 3T3-L1 adipocytes reveals new insight into GLUT4 trafficking and adiponectin secretion" in 2022 (Black et al. 2022).

4.1.2 Generation of cell lines to study the effect of Syntaxin4 phosphorylation

As discussed in Section 3.1.2.2, Sx4 has been shown to be phosphorylated on Y115 and Y251 in response to insulin in 3T3-L1 adipocytes (Schmelzle et al. 2006). In vitro, CIRK, the recombinant insulin receptor kinase, can phosphorylate Sx4 on Y115 and Y251, and data presented in Chapter 3 demonstrates that Sx4 and the insulin receptor (IR) closely interact in the cell, suggesting that IR itself phosphorylates Sx4 following insulin stimulation. When phosphorylated on these residues, Sx4 changes conformation, and more readily forms SNARE complexes with its cognate SNAREs, SNAP23 and VAMP2, which are required for GSV fusion with the plasma membrane (Black 2016; Al Tobi 2018). A better understanding of the effect of Sx4 phosphorylation in adipocytes could provide greater insight into the mechanisms of insulin stimulated GLUT4 trafficking in these cells. Consequently, the second aim of this chapter was to generate 3T3-L1 cell lines that stably express either phospho-mimetic or phospho-resistant Sx4, with the goal of examining GLUT4 trafficking and glucose transport in these cells.

The work presented in this chapter took place in 2020 and 2021, and so was greatly disrupted by lockdowns and restrictions brought in during the COVID19 pandemic. The effect of the pandemic on this thesis are detailed in the COVID19 Impact Statement (page x.y) and will be touched on where relevant to this chapter in Section 4.2.

4.2 Results

4.2.1 Differentiation of Syntaxin4 knockout 3T3-L1 cells

Differentiation of Sx4 KO 3T3-L1 fibroblasts into adipocytes following the standard 10-day differentiation protocol described in Section 2.2.1.2 was assessed by immunoblot analysis of proteins known to increase during adipocyte differentiation: GLUT4; the transcription factor peroxisome proliferator-activated receptor-gamma (PPARγ); and the Insulin Receptor (IR) (Cristancho and Lazar 2011) in undifferentiated (fibroblast) and differentiated (adipocyte) WT and Sx4 KO lysates. Figure 4.1 panel A shows that IR, PPARγ and GLUT4 levels all increased following differentiation of both WT and Sx4 KO cells, though to a lesser extent in the Sx4 KO cells. Figure 4.1 panel B is taken from the PhD thesis of Dr Mohammed Al Tobi and shows Oil Red O lipid staining of WT and Sx4 KO 3T3-L1 adipocytes at day 11 post differentiation. This staining confirms that the Sx4 KO cells can develop into adipocytes.

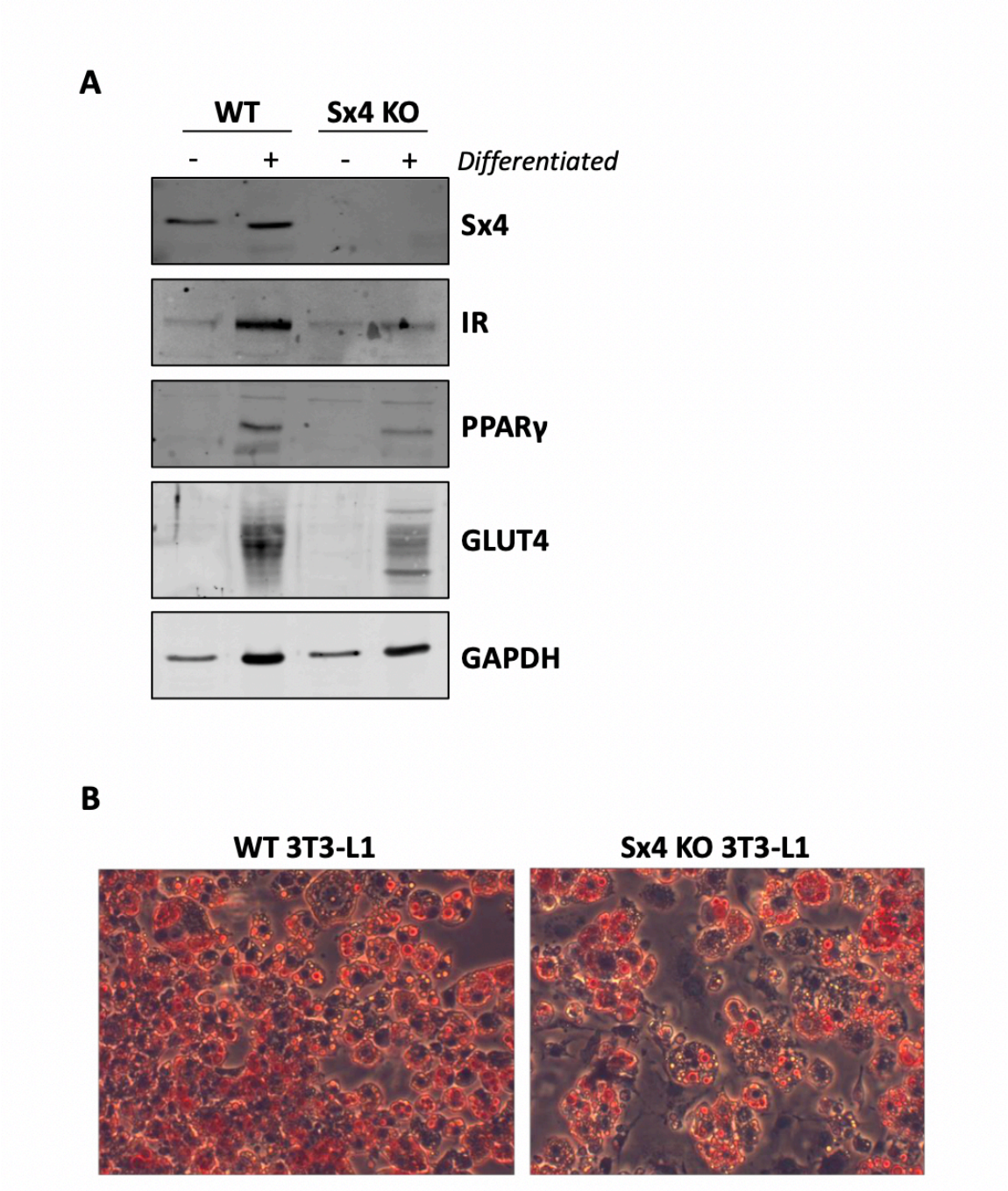

Figure 4.1 Syntaxin4 knockout 3T3-L1 cells can differentiate into adipocytes.

A) Western blots of Syntaxin4 (Sx4), insulin receptor beta subunit (IR), peroxisome proliferator-activated receptor-gamma (PPARγ), GLUT4 and loading control GAPDH in lysates produced from WT or Sx4 knockout (Sx4 KO) cells before (-) or after (+) the adipocyte differentiation protocol (Section 2.2.1.2). Blots are representative of n=2 independent experiments. **B)** Oil Red O lipid staining of WT (left) or Sx4 KO (right) at day 11 of differentiation. Cells are imaged at 20X magnification. Taken from Al Tobi 2018.

4.2.2 Insulin action and GLUT4 translocation in Syntaxin4 knockout cells

The insulin response in differentiated Sx4 KO adipocytes was assessed by immunoblot analysis of AKT phosphorylation, a key event in the insulin signalling pathway (reviewed in Manning and Toker 2017) and total tyrosine phosphorylation (Figure 4.2). AKT phosphorylation was unaffected in Sx4 KO cells, demonstrating that this cell line is insulin responsive. However, global tyrosine phosphorylation was down in the Sx4 KO cells (Figure 4.2, total tyrosine phosphorylation blot). Notably, the band in this panel that appears at 95kDa (marked with a red arrow) in the WT cells in response to insulin and is consistent with phosphorylation of the insulin receptor beta subunit, is much fainter in the Sx4 KO cells, although an insulin stimulated increase in the band can still be seen (Figure 4.2).

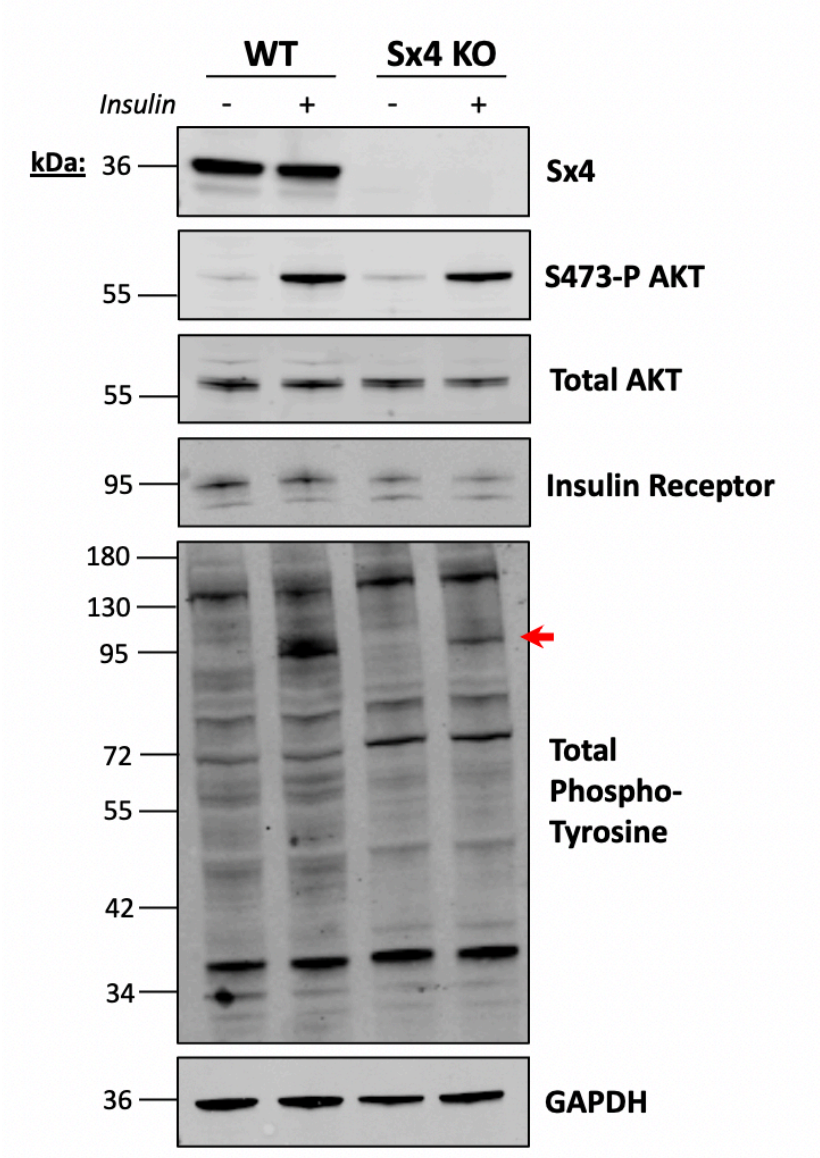

Figure 4.2 Insulin signalling in Syntaxin4 knockout 3T3-L1 adipocytes. Representative western blots of, from top to bottom, Syntaxin4 (Sx4), serine-473 phosphorylated AKT, total AKT, insulin receptor beta subunit (IR), total tyrosine phosphorylation and loading control GAPDH in WT or Sx4 knockout (Sx4 KO) 3T3-L1 adipocyte lysates, either untreated (-) or following 20 min stimulation with 100nM insulin (+). Blots are representative of n=2 independent experiments.

In Figure 4.3, a sub-cellular fractionation experiment was used to determine whether GLUT4 and IRAP, a GSV component, undergo insulin stimulated translocation in Sx4 KO 3T3-L1 adipocytes. The sub-cellular fractionation protocol (described in Section 2.2.2.3) produced the following fractions: high density microsomes (HDM), low density microsomes (LDM) and plasma membrane (PM), from Sx4 KO 3T3-L1 adipocytes that were either untreated or stimulated with 100 nM insulin for 20 minutes prior to collection. Both IRAP and GLUT4 increased in the PM fraction in response to insulin, but decreased in the LDM fraction (Figure 4.3). This showed that both GLUT4 and IRAP exhibit insulin stimulated translocation in the Sx4 KO cells.

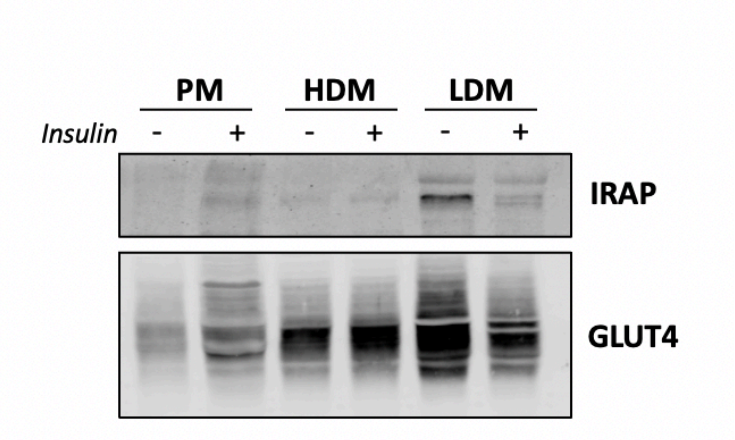

Figure 4.3 GLUT4 and IRAP translocation in Syntaxin4 knockout 3T3-L1 adipocytes.
Representative western blots of IRAP (top) and GLUT4 (bottom) in plasma membrane (PM), high density microsomes (HDM) or low density microsomes (LDM) enriched cell fractions produced from Sx4 KO 3T3-L1 adipocytes, either untreated (-) or following 20 min stimulation with 100nM insulin (+). Blots are representative of n=2 independent experiments.

4.2.3 Production of stable 3T3-L1 cell lines expressing phospho-mimetic or phospho-resistant Syntaxin4

A second goal of this chapter was to produce 3T3-L1 cell lines expressing, WT, phospho-mimetic or phospho-resistant Sx4 in a Sx4 KO background. This was done by transfecting Sx4 KO 3T3-L1 fibroblasts with pcDNA3 plasmids containing Myc-tagged WT Sx4, double phospho-mimetic Sx4 (Y115E, Y251E), shortened here to “2P”, or double phospho-resistant Sx4 (Y115F, Y251F), shortened here to “2F”, along with a Kan/G418 resistance gene. Transfected cells were then grown in G418-containing media to select for cells that had taken up the plasmid (transfection and selection protocol outlined in Section 2.2.1.3). The rationale for creating these stable cell lines is that the cells could then be differentiated into adipocytes, and the effect of phospho-mimetic or phospho-resistant Sx4 in adipocyte cell biology could be studied, particularly insulin-stimulated SNARE complex formation, GLUT4 translocation and glucose transport. Terminally differentiated 3T3-L1 adipocytes are difficult to transiently transfect compared to their fibroblast counterparts as they are not rapidly growing and dividing.

Unfortunately, despite several attempted transfections of Sx4 KO fibroblasts with the WT, 2F and 2P Sx4 plasmids following the methodology outline in Section 2.2.1.3 and using a variety of plasmid and transfection reagent concentrations, cell lines stably expressing these plasmids could not be produced. Following transfection and selection, some colonies from single

clones were produced but, repeatedly, these clones stopped growing during cell line expansion.

This work was particularly disrupted by intermittent lockdowns and loss of full-time lab access in 2020 and 2021 due to the COVID-19 pandemic, as transfection, selection, and expansion of 3T3-L1 cell lines is a lengthy process taking many weeks, and often relies on out-of-hours lab access, which was frequently unavailable during this time.

As alternative methods to produce cells expressing phospho-mimetic and phospho-resistant Sx4, both transient transfection of Sx4 KO differentiated adipocytes, and stable expression of WT, 2F and 2P Sx4 plasmids in a WT 3T3-L1 background were attempted.

Following the success of transfecting differentiated 3T3-L1 adipocytes with siRNA which will be described in Chapter 5, the same protocol and transfection agent (Section 2.2.1.4), adjusted for use with DNA plasmids, was employed to in an attempt to transiently express WT Sx4 back into Sx4 KO adipocytes. Had this procedure been a success, it could have also been used with 2P and 2F Sx4 plasmids, but unfortunately no expression of Sx4 could be induced in the Sx4 KO cells using this method, across of a range of plasmid DNA concentrations (Figure 4.4).

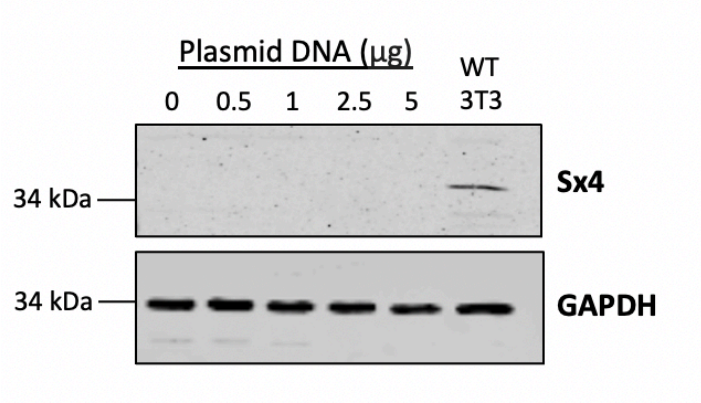

Figure 4.4 Transfection of differentiated Syntaxin4 knockout 3T3-L1 adipocytes.
Western blot of Syntaxin4 (Sx4) and loading control GAPDH in lysates produced from Sx4 KO adipocytes transfected with 0, 0.5, 1, 2.5 or 5 μg plasmid DNA containing Myc-tagged WT Sx4 at day 6 of differentiation and incubated for 3 further days prior to lysis. WT 3T3-L1 adipocyte lysate was also included as a positive control for Sx4. A single n=1 biological replicate is shown.

Finally, WT 3T3-L1 fibroblasts, rather than Sx4 KO cells, were used with the same transfection and selection protocol described above to produce cell lines stably expressing the WT, 2P and 2F Sx4 plasmids, for use in future work. This time, between 5 and 6 candidate clones for each plasmid were generated and successfully expanded. Figure 4.5 shows western blots for the Myc protein and Sx4 in lysates from each of the clones and from the parental WT 3T3-L1 fibroblasts. This confirmed that the Sx4-Myc constructs from the plasmids were expressed in all of the candidate clones, as Myc can be seen at the correct molecular weight for Sx4, 36 kDa, in all but the parental WT cells (Figure 4.5, top row). On the Sx4 blot (Figure 4.5, bottom row) a second band at a slightly higher molecular weight than endogenous Sx4 (indicated

with the red arrow) can be seen in all but the parental WT cells, providing further evidence that these cells express the Sx4-Myc constructs.

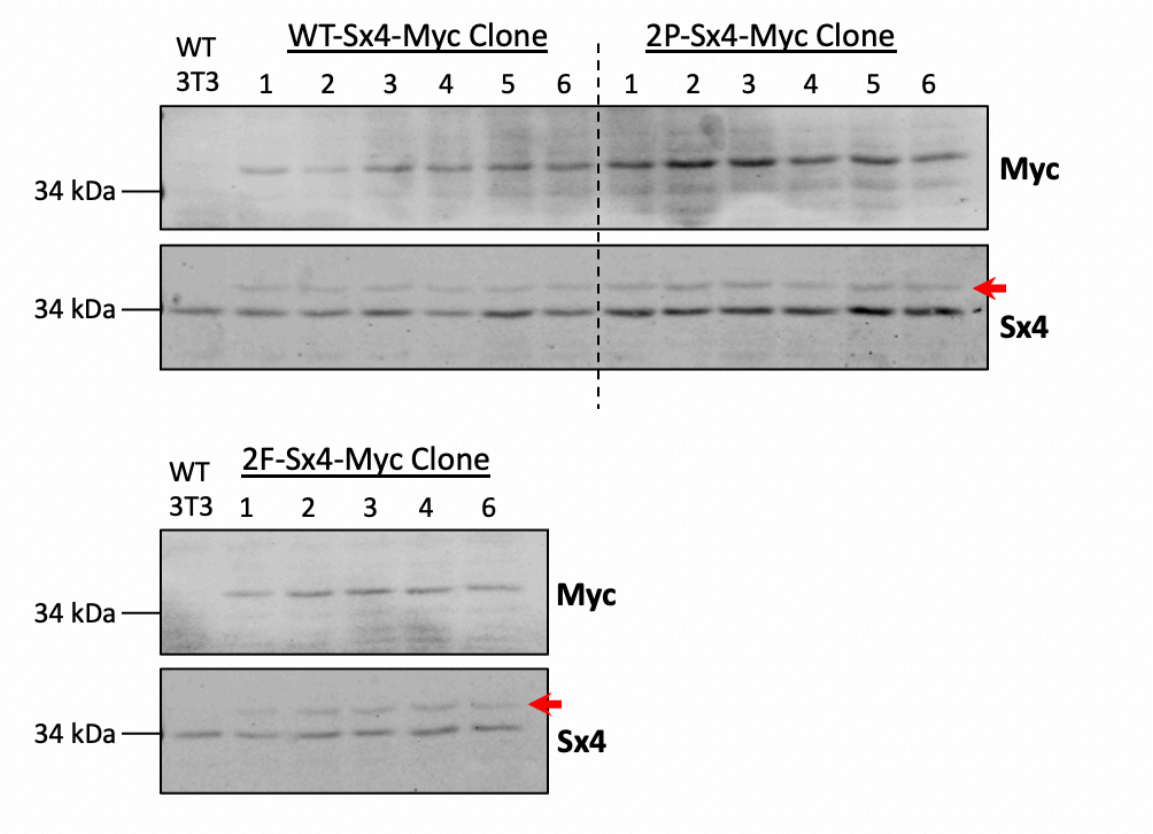

Figure 4.5 Generation of 3T3-L1 cell lines expressing Myc-tagged Sx4 constructs.
Western blot of Myc and Sx4 in lysates produced from candidate clones of WT 3T3-L1 cells stably expressing Myc-tagged WT Sx4 (WT-Sx4-Myc), double phospho-mimetic Sx4 with Y115E and Y251E (2P-Sx4-Myc), or double phospho-resistant Sx4 with Y115F and Y251F (2F-Sx4-Myc). Lysates from individual candidate colonies are numbered 1-6. 2F-Sx4-Myc clone 5 was excluded due to slow growth. Lysate from parental WT 3T3-L1 cells is also included as a control. Red arrows indicate expression of Myc-tagged Sx4.

4.3 Discussion

4.3.1 Syntaxin4 knockout cells differentiate into adipocytes

Sx4 KO 3T3-L1 cells have been shown previously by observation of morphological features and by lipid droplet detection using Oil Red O staining to be capable of differentiation into adipocytes (Black 2016, Al-Tobi 2018, Figure 4.1 panel B). Data presented in Figure 4.1 supports this, as levels of the markers of adipocyte differentiation IR, PPARγ and GLUT4 (Cristancho and Lazar 2011) increase in Sx4 KO cells that have been subjected to the differentiation protocol. These increases were not as pronounced as those seen in WT 3T3 cells following differentiation, and this is likely due to a lower proportion of Sx4 KO cells fully developing into adipocytes, which can be seen in the Oil Red O staining images in Figure 4.1 panel B. The fact that Sx4 KO 3T3-L1 cells are not as well differentiated than their WT counterparts should be considered when interpreting data from these cells. Ideally, if another Sx4 KO 3T3-L1 cell line were to be generated, a passage-matched WT control should be maintained. This could help determine whether the reduced differentiation capacity of Sx4 KO cells is due to loss of Sx4, or a simply a consequence of the cell line having been passaged a high number of times.

4.3.2 Syntaxin4 knockout cells are insulin responsive

Figures 4.2 and 4.3 demonstrated that, despite some issues with differentiation, Sx4 KO 3T3-L1 adipocytes are insulin responsive. AKT activation was unaffected by loss of Sx4, and although tyrosine phosphorylation was reduced, a clear insulin activation could still be seen (Figure 4.2). Furthermore, robust insulin stimulated translocation of GLUT4 and IRAP out of low density microsomes and into the plasma membrane was observed in the Sx4 KO adipocytes (Figure 4.3). In the 2022 Black et al study, of which this data forms a part of, maximum glucose transport in response to insulin was shown to be lower in Sx4 KO cells than in WT, however this was explained by an overall reduction in GLUT4 levels, and not by disrupted GLUT4 translocation (Black et al. 2022).

4.3.3 Syntaxin4 is not always required for insulin stimulated GLUT4 translocation

The 2022 Black et al study found a number of other effects of loss of Sx4 in 3T3-L1 adipocytes. They found that glucose transport was reduced in Sx4 KO cells, at a level consistent with the reduced levels of GLUT4 in these cells. However, ectopic expression of the HA-GLUT4-GFP construct in Sx4 KO cells showed that in these circumstances, the insulin stimulated translocation of HA-GLUT4-GFP to the plasma membrane was not affected indicating that the cells use an alternative (Sx4-independent) means to deliver GLUT4 to the cell surface or adapt to Sx4 knockout by up-regulation

of a distinct mechanism to deliver GSV to the surface. This is supported by the sub-cellular fractionation data shown here in Figure 4.3 which has revealed insulin-stimulated translocation of GLUT4 and IRAP in Sx4 knockout cells. Therefore, despite longstanding evidence that Sx4 is involved in GSV fusion with the plasma membrane (Brandie et al. 2008; Kawaguchi et al. 2010; Kioumourtzoglou, Gould, and Bryant 2014), these data show that Sx4 is not always required for insulin stimulated GLUT4 translocation to the plasma membrane.

One explanation for these findings is that there are other SNARE proteins that can take on the role of Sx4 in insulin stimulated glucose transport when Sx4 is lost. This is supported by the fact that Munc18c is able to bind Sx2 and Sx3, and by doing so increases the rate of membrane fusion events controlled by those Syntaxins (Yu et al. 2013). However, it is worth noting that expression of Sx2 and Sx3 was not altered in Sx4 KO adipocytes, so although these proteins may be able to provide redundancy for the function of Sx4, they are not upregulated in response to its loss (Black et al. 2022).

Other evidence for redundancy in the Sx4/SNAP23/VAMP2 system can be seen in the plasticity of VAMP proteins. Despite VAMP2 having been identified as the main v-SNARE involved in GSV fusion with the plasma membrane (Sadler, Bryant, and Gould 2015), an earlier study showed that VAMP3 and VAMP8 can also fulfil this role (Zhao et al. 2009). In this study,

simultaneous knockdown of VAMP2, VAMP3 and VAMP8 resulted in a total loss of insulin stimulated glucose transport, but reintroduction of any one of those proteins was sufficient to restore glucose transport.

Yet further evidence for the plasticity of SNARE proteins involved in GLUT4 translocation can be seen in a recent study which generated a Syntaxin16 (Sx16) knockout 3T3-L1 cell line. Sx16 is a Q_a-SNARE involved in glucose transport, specifically in sorting GLUT4 from endosomes into GSVs (Proctor et al. 2006). However, when Sx16 was lost from 3T3-L1 adipocytes, glucose transport was unaffected (Bremner et al. 2022). As is the case for Sx4 KO cells, loss of Sx16 can be compensated for by the cell.

Evidently, SNAREs involved in GLUT4 translocation, including components of the Sx4/SNAP23/VAMP2 SNARE complex, can be replaced if required in order to preserve the vital process of GSV fusion with the plasma membrane. This makes pulling apart the precise mechanisms of this process challenging, and future work should focus on identifying other plasma membrane associated t-SNAREs capable of facilitating insulin stimulated GSV fusion with the plasma membrane, perhaps by knockdown and reintroduction of t-SNAREs, similar to the Zhao et al VAMP-focused study. Such studies exemplify the inherent limitations of knockout experiments.

4.3.4 Stable expression of Sx4 mutants in Sx4 KO 3T3-L1 cells proved challenging

One way to circumvent these limitations is to re-express the protein of interest and compare this to specific mutations. As discussed previously, one of the initial goals of this chapter was to produce 3T3-L1 cell lines expressing WT, phospho-mimetic or phospho-resistant Sx4 in a Sx4 KO background, with the goal of studying the effect of Sx4 phosphorylation on insulin-stimulated SNARE complex formation, GLUT4 translocation and glucose transport in adipocytes. Unfortunately, this aim was not achieved, largely due to issues in expanding colonies of candidate cells following transfection and selection (see Section 4.2.3), nor was transient transfection of differentiated Sx4 KO adipocytes with the Sx4 plasmids (Figure 4.4). However, when WT 3T3-L1 cells were transfected with the same Sx4 plasmids and subjected to the same selection and expansion protocol (Section 2.2.1.3), several candidate clones expressing Myc-tagged WT, 2P or 2F Sx4 were generated (Figure 4.5).

The fact that cell lines stably expressing the Myc-tagged Sx4 constructs could be generated using WT 3T3-L1 cells, but the same protocol with the same plasmids were not effective when using Sx4 KO cells suggests that the issues arose from using the knockout cells for further transfections. 3T3-L1s are not an immortalised cell line, and so can only be passaged a limited number of times before their growth and differentiation are affected. Some

suppliers of 3T3-L1 cells do not recommend use beyond passage 13 (Zenbio 3T3-L1 Manual), and most studies on improving the differentiation of 3T3-L1s only use cells up to passage 12 (Zebisch et al. 2012; Hua et al. 2016). The parental 3T3-L1 cell line used to generate the Sx4 KO cell line would have undergone many passage steps as part of colony expansion following transfection with the CRISPR Sx4 plasmid (Black 2016, methods section). This means that the "true" passage number of the Sx4 KO cell line is unknown, and this potentially very high passage number could be the cause of the issues faced here in generating further stable cell lines from these cells. To avoid this problem in future studies, phospho-mimetic and phospho-resistant mutations to Sx4 could be introduced directly to low-passage WT 3T3-L1 cells.

4.3.5 Potential utility of the WT, 2P and 2F 3T3-L1 cell lines

The key outcome of the study presented in this chapter is that 3T3-L1 cell lines expressing Myc-tagged WT, 2P and 2F Sx4 in a WT background have been generated. Although the original aim was to express these Sx4 constructs in a Sx4 KO background, these new cell lines still provide a potentially interesting new tool for understanding the role of Sx4 in adipocyte biology.

The presence of the Myc tag on these Sx4 proteins means that they could be identified in the cell. For example, it may be of interest to use Proximity

Ligation Assay (PLA) to look at pairwise interactions between Sx4, SNAP23, VAMP2 and Munc18c in these cells under different insulin stimulation conditions (as performed in Kioumourtzoglou et al. 2014, and here in Chapter 5), to determine whether phospho-mimetic or phospho-resistant Sx4 behaves differently from WT Sx4 in insulin stimulated SNARE complex formation. Using primary antibodies against the Myc tag in these experiments could allow the altered Sx4 to be distinguished from endogenous Sx4. Although these data could be complicated by the presence of endogenous Sx4 in the cell, it is also possible that the endogenous Sx4 could act as a control in this case.

These PLA experiments using the new WT, 2P and 2F 3T3-L1 cell lines are being carried out by colleagues at the University of York at the time of writing. In the future it would be interesting to look at GLUT4 translocation using sub-cellular fractionation, and glucose uptake in all three of these cell lines, to determine where the presence of any phospho-mimetic or phospho-resistant Sx4 affects these processes.

In conclusion, although there will be limitations to the use of the new WT, 2P and 2F 3T3-L1 cell lined due to their generation in a WT background and thus in the presence of endogenous Sx4, these cell lines could still be a valuable tool for furthering our understanding of the role of Sx4 phosphorylation in SNARE complex formation and GLUT4 translocation.

Chapter 5

Investigating the Role of EHD2 in Glucose Transport

5 Investigating the Role of EHD2 in Glucose Transport

5. 1 Introduction

5.1.1 EHD2 and caveolae structure

Eps15 homology domain–containing 2 (EHD2) belongs to the EHD-containing protein family of dynamin-related ATPases involved in membrane remodelling in the endosomal system (Naslavsky and Caplan 2011). EHD2 dimers oligomerize into ring-shaped structures on highly curved membranes, leading to the activation of their intrinsic ATPase activity (Daumke et al. 2007).

EHD2 is specifically associated with caveolae and proper EHD2 assembly is dependent on cavin1 and on caveolar integrity. Unlike Caveolin and Cavin proteins, which form a caveolar coat across the whole caveolar bulb, EHD2 assembles at the caveolae neck region (Ludwig et al. 2013). EHD2 is not required for caveolae formation but contributes to their stability and turnover. In one study, an overabundance of EHD2 resulted in distortion and loss of caveolae, whereas depletion of EHD2 resulted in more short-lived caveolae (Morén et al. 2012). In another study, depletion of EHD2 increased the number of mobile caveolae vesicles emerging from the plasma membrane, showing that EHD2 was required to prevent “pinching off” of caveolae. This study also found that EHD2’s ability to confine caveolae to the plasma

membrane relied on its ability to link caveolae to actin filaments (Stoeber et al. 2012).

EHD2 undergoes a cycle of attaching to the plasma membrane and adopting an open conformation, followed by ATP binding which allows partial insertion into the membrane where oligomerization occurs. Finally, ATP hydrolysis leads to detachment of EHD2 from the membrane. It is the oligomerization of EHD2 in its membrane-bound state that is crucial for its role in restricting caveolae dynamics (Hoernke et al. 2017). One study found that EHD2 was released from the plasma membrane under mechanical stress and subsequently transported to the nucleus where it regulates the transcription of genes coding for caveolae components, demonstrating a role for EHD2 as a caveolae-based mechanotransducer (Torrino et al. 2018). These data were supported by another study that found when EHD2 was knocked out, cells were more prone to rupture when exposed to stretch forces (Yeow et al. 2017). Interestingly, this study also found that caveolae in cells lacking EHD2 lacked the characteristic clustering into higher-level structures.

To summarise, EHD2 is structural component of caveolae localised to the caveolae neck region. It is required for optimal caveolae stability and longevity and plays a role in cells' resistance to mechanical stress.

5.1.2 EHD2 in adipocyte caveolae

Caveolae are abundant in adipocytes, so it is unsurprising that EHD2 has been shown to play an important role in adipocyte function. EHD2 expression is highly upregulated during adipocyte differentiation and is localised to adipocyte caveolae (Morén et al. 2019). Knockdown of EHD2 has been shown to impair the adipocyte differentiation process, as well as affecting insulin sensitivity, lipid storage capacity, and lipolysis (Morén et al. 2019).

In a study of EHD2 KO mice (*Ehd2* -/-), several changes to adipose tissue were observed. Both fatty acid uptake and lipid droplet size increased in comparison to adipose tissue from WT mice. Increased caveolae motility was also observed in both brown and white adipose tissue of *Ehd2* -/- mice, along with elevated numbers of caveolae that had detached from the plasma membrane (Matthaeus et al. 2020). Another study using the *Ehd2* -/- mouse found an impairment in epididymal adipose tissue expansion in the knock-out mice compared to WT. Interestingly, this effect was not observed in the inguinal adipose tissue of the same mice. Furthermore, this study showed that mice lacking EHD2 had a lower proportion of small adipocytes and displayed reduced lipolysis (Fryklund et al. 2021). These data highlight the importance of EHD2 in lipid handling and metabolism in adipocytes.

A study of the lipid composition of adipocyte caveolae also highlighted a key role for EHD2. It was found that sphingomyelin stabilised caveolae to the cell

surface, whereas cholesterol and glycosphingolipids drove caveolae scission from the PM. EHD2 restricted diffusion of these lipids at the caveolae neck, which prevented caveolae scission from the plasma membrane (Hubert et al. 2020). These data provide yet more evidence that EHD2 is vital for caveolae stability in adipocytes.

A study on the effects of hypoxia on adipose tissue also implicated EHD2 in caveolae stability. The white adipose tissue of lean mice exposed to hypoxic conditions developed insulin resistance and problems with insulin signalling. Hypoxia was also shown to trigger caveolae disassembly in conjunction with downregulation of caveolar gene expression, including EHD2 (Varela-Guruceaga et al. 2020). This is of interest because hypoxia can develop in white adipose tissue in humans as a result of obesity (Trayhurn 2013). Moreover, EHD2 expression has been shown to be downregulated in the adipose tissue of two mouse models of obesity, and in obese humans (Matthaeus et al. 2020).

Given the important role of EHD2 in adipocyte function, the link between EHD2 and obesity, and the larger role caveolae play in insulin signalling, this chapter will explore the role of EHD2 in insulin signalling, GLUT4 translocation and glucose transport in adipocytes. The core aims of this study were to efficiently knockdown EHD2 expression in mature 3T3-L1 adipocytes, to investigate the effect of EHD2 knockdown on expression of

key proteins involved in insulin signalling and glucose transport, and to determine if and how EHD2 knockdown affected insulin-stimulated GLUT4 translocation and glucose transport.

5.2 Results

5.2.1 EHD2 knockdown and protein expression

In order to investigate the role of EHD2 in insulin signalling, GLUT4 translocation to the plasma membrane, and subsequent glucose transport, an siRNA knockdown of EHD2 was performed in 3T3-L1 adipocytes on day 6 of the differentiation protocol as outlined in section 2.2.1.4. These EHD2 knockdown (EHD2 KD) cells were used in all assays 4 days post-transfection. Alongside every EHD2 knockdown, cells of the same passage were transfected with scrambled RNA to produce matching control cells.

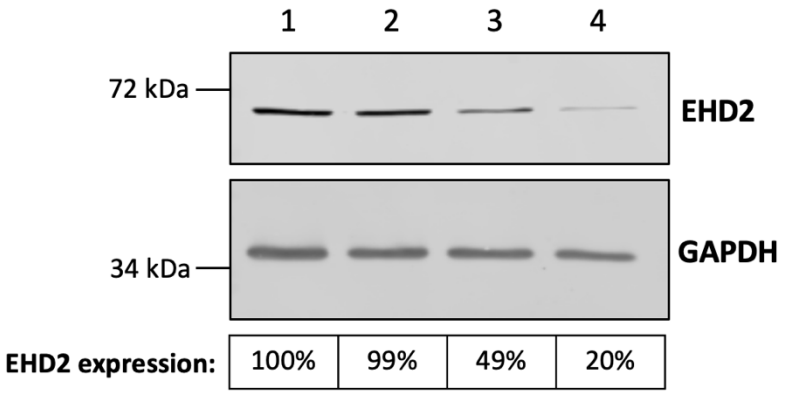

Figure 5.1 Efficient EHD2 knockdown in 3T3-L1 adipocytes.
Western blots of EHD2 and loading control GAPDH in 3T3-L1 adipocyte lysates. Lane 1 shows untreated WT adipocytes. For lanes 2-4 mature adipocytes were trypsinised and transfected with 0 nM (lane 2), 20 nM (lane 3) or 40 nM (lane 4) EHD2 siRNA, before replating. Lysates were prepared 96 hrs post transfection. EHD2 expression is shown below each lane, calculated relative to GAPDH and as a percentage of EHD2 expression in untreated WT cells. Data is representative of n=3 biological replicates.

Figure 5.1 shows the results of an initial experiment to determine which concentration of the EHD2 siRNA would yield the most efficient knockdown. 40nM siRNA (Figure 1, Lane 4) was selected on this basis and was used throughout all knockdown experiments described here. Accordingly, the control scrambled siRNA was also used at 40nM. Figure 5.1, Lane 2, also shows that the process required for this transfection, which included a trypsinisation and replating step, did not affect the expression of EHD2 when the EHD2 siRNA was excluded from the transfection mixture, as seen by comparing EHD2 levels in Lane 2 with that of Lane 3 and 4, which did contain EHD2 siRNA.

Once a suitable protocol for efficient EHD2 knockdown had been established, the effect of lowered levels of EHD2 on the expression of a range of proteins involved in glucose transport was investigated (Figure 5.2). EHD2 knockdown resulted in a reduction in Caveolin1 expression of 81.1% (±6.9%, $p=0.018$) of that of control cells, whereas Insulin Receptor (beta subunit) levels were reduced to 51.2% (±3.9%, $p<0.001$). Furthermore, EHD2 KD cells also had lowered levels of the t-SNARE SNAP23 at 63.9% (±7.3%, $p=0.002$) of control levels, and the regulatory Sec1-Munc18 protein Munc18c at 65.7% (±16.0%, $p=0.039$). No significant change was seen in levels of the t-SNARE Syntaxin4 (Sx4) or the v-SNARE VAMP2 when compared to control cells. Moreover, GLUT4 levels remained unchanged, as did the levels of Syntaxin16 (Sx16), a SNARE protein involved in intracellular sorting of

GLUT4 (Proctor et al., 2006). Insulin stimulation did not affect the levels of any of the above-mentioned proteins in either control or EHD2 KD cells (Figure 5.2, panel A).

A

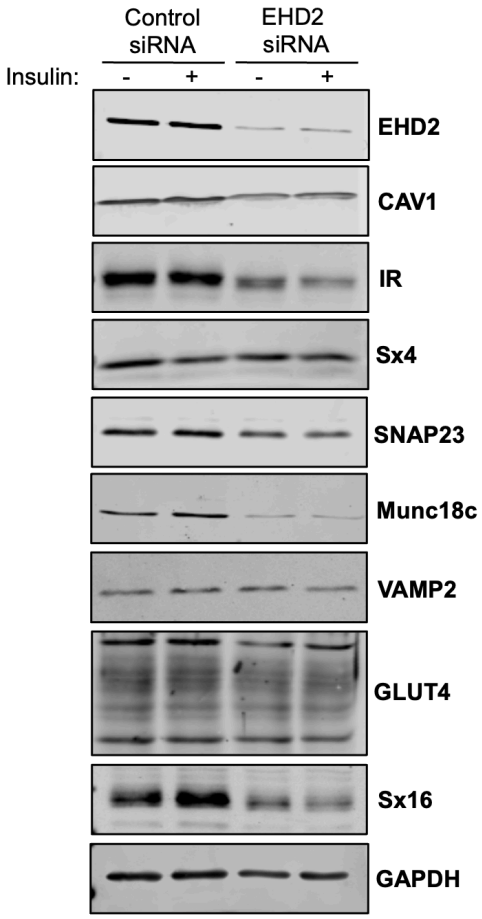
Control siRNA
EHD2 siRNA
Insulin: - + - +
EHD2
CAV1
IR
Sx4
SNAP23
Munc18c
VAMP2
GLUT4
Sx16
GAPDH

B

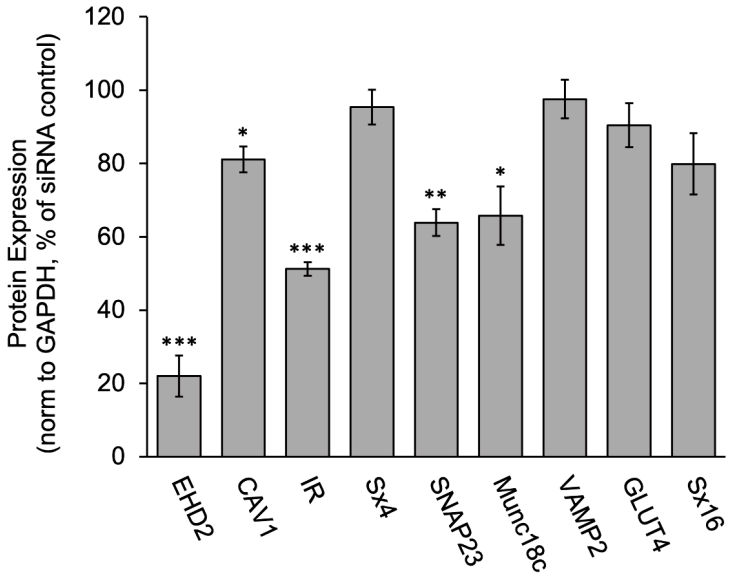
Protein Expression
(norm to GAPDH, % of siRNA control)
120
100
80
60
40
20
0
***
*
***
**
*
EHD2
CAV1
IR
Sx4
SNAP23
Munc18c
VAMP2
GLUT4
Sx16

Figure 5.2 Protein expression following EHD2 knockdown.
(A) Representative western blots of EHD2, caveolae protein Caveolin1 (CAV1), Insulin Receptor beta subunit (IR), SNARE proteins Syntaxin4 (Sx4), SNAP23, VAMP2 and Syntaxin16 (Sx16), as well as regulatory protein Munc18c and the glucose transporter GLUT4, in 3T3-L1 adipocyte lysates collected 96 h after transfection with control siRNA or EHD2 siRNA, either untreated or following 15 min stimulation with 100nM insulin. GAPDH was used as a loading control. 15 μg protein was loaded per lane.
(B) Corresponding quantification of protein expression in EHD2 siRNA knockdown adipocytes is normalised to GAPDH and expressed as a percentage of protein expression in control siRNA transfected adipocytes. Mean and SD of n = 3 independent biological replicates are shown. Statistical analysis was with unpaired t-tests, * $p < 0.05$, ** $p < 0.01$, *** $p < 0.001$.

5.2.2 Insulin action and GLUT4 translocation in EHD2 knockdown adipocytes

AKT phosphorylation, a key event in the insulin signalling pathway (reviewed in Manning and Toker 2017), was not significantly lower in EHD2 KD adipocytes than in control cells (Figure 5.3). However, immunoblotting for all phosphorylated tyrosine residues in lysates from EHD2 KD and control cells both before and after insulin stimulation revealed that global tyrosine phosphorylation was down in the EHD2 KD cells, particularly in response to insulin (Figure 5.3, bottom panel). Notably, the band in this panel that appears at 95kDa in control cell lysates in response to insulin and is consistent with phosphorylation of the insulin receptor beta subunit, is much fainter in the EHD2 KD cell lysates. This corresponds with the drop in insulin receptor beta subunit levels seen following EHD2 knockdown in Figure 5.2.

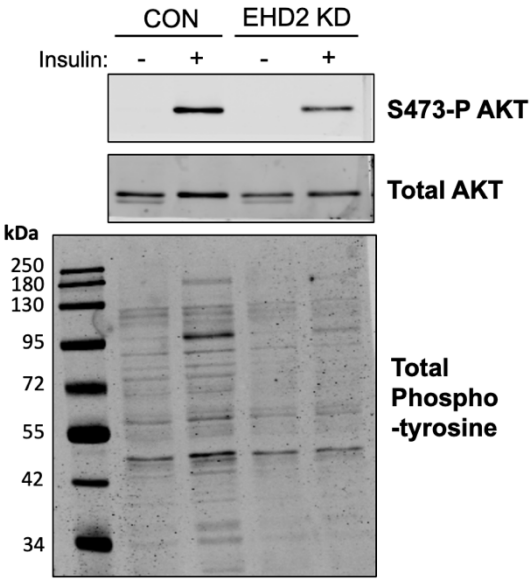

Figure 5.3 Insulin stimulated phosphorylation following EHD2 knockdown.
Western blots of serine-473 phosphorylated AKT (top panel), total AKT (middle panel) and total tyrosine phosphorylation (bottom panel) in 3T3-L1 adipocyte lysates prepared 96 h after transfection with control siRNA or EHD2 siRNA, either untreated or following 15 min stimulation with 100nM insulin. 15 μg protein was loaded per lane. Blots are representative of n=2 independent experiments.

Maximum glucose transport following 15 min 100nM insulin stimulation was lower in EHD2 KD than in control cells (Figure 5.4, panel A), at 70.7% (±19.7%, p=0.025) of the maximum transport in control cells. GLUT4 translocation in EHD2 KD and control cells was investigated using subcellular fractionation (Figure 5.4, panel B), resulting in a pellet fraction (P), which is enriched in plasma membranes, and a supernatant fraction (S) which is enriched in GLUT4 storage vesicles (GSVs) (see section 2.2.2.4). The translocation of GSV component IRAP was also investigated, along with Sx16, which has been shown to translocate with GLUT4 (Shewan et al. 2003).

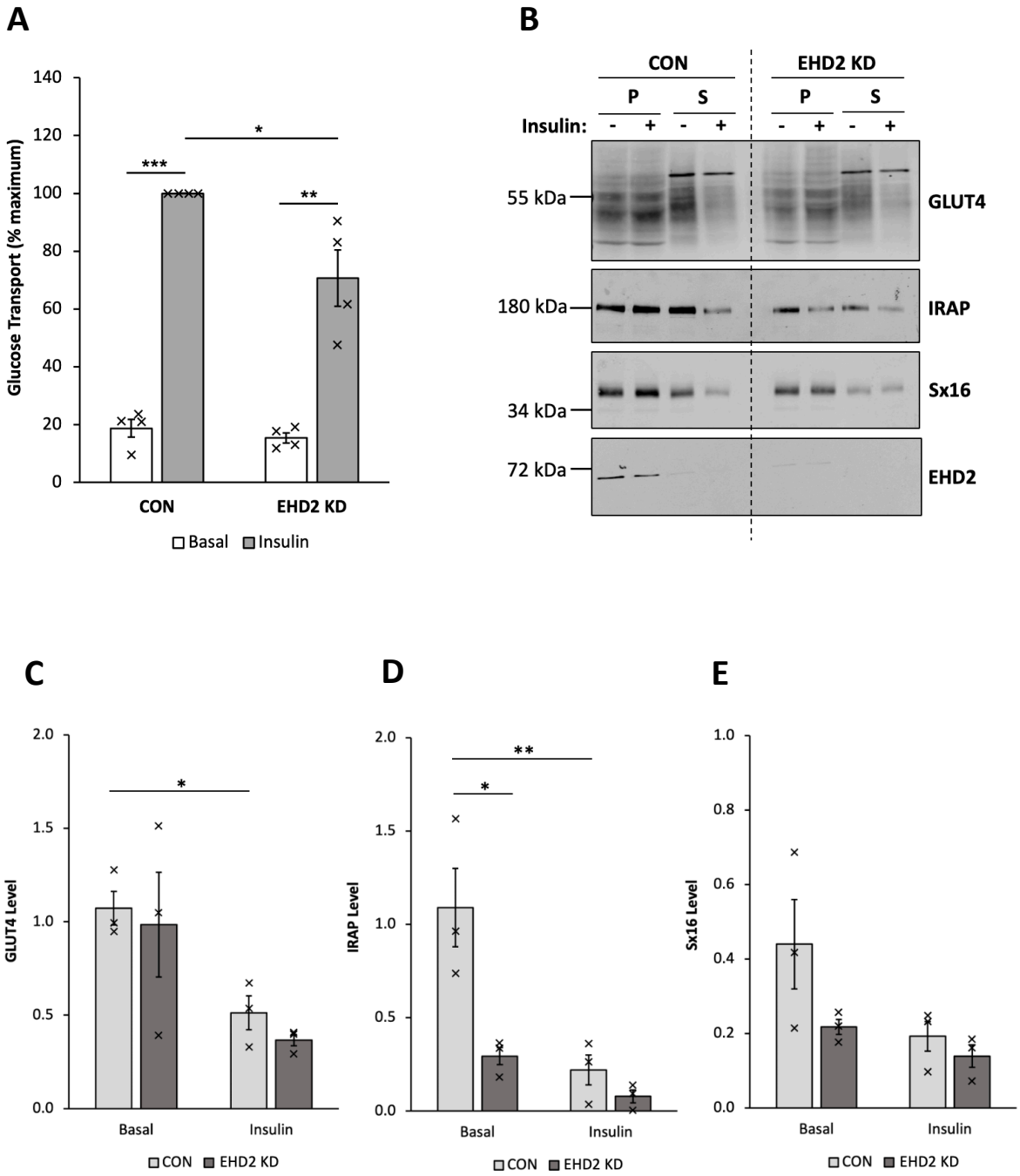

Figure 5.4 Insulin stimulated glucose transport following EHD2 knockdown.

(A) Glucose transport in control and EHD2 knockdown 3T3-L1 adipocytes. Triplicate wells of cells, 96 h after transfection with control siRNA (Control) or EHD2 siRNA (EHD2 KD), with (Insulin) or without (Basal) 15 min stimulation with 100nM insulin were used to assess uptake of 2-deoxy-D-glucose. Data

were corrected for non-specific cellular isotope uptake by performing parallel assays in the presence of 10 µM cytochalasin B. Data were then normalised to those obtained in the insulin-stimulated control adipocytes for each data set. Mean and SD of n = 4 independent experiments are shown, each 'x' on the graph is data from a sperate biological replicate and is the mean of triplicate technical replicates. Statistical analysis was with two-way ANOVA, * $p < 0.05$. **(B)** Representative western blots for GLUT4, IRAP, Syntaxin16 (Sx16) and EHD2 in fractions from a 16k subcellular fractionation. P = pellet, enriched in plasma membranes. S = supernatant, enriched in GLUT4 storage vesicles (GSV). Fractions were produced from 3T3-L1 adipocytes collected 96 h after transfection with control siRNA or EHD2 siRNA, either untreated or following 15 min stimulation with 100nM insulin. **(C)-(E)** Corresponding quantification of GLUT4 **(C)**, IRAP **(D)** and Sx16 **(E)** levels in the GSV enriched supernatant fraction from basal and insulin stimulated EHD2 KD and control cells. Mean and SD of n = 3 independent experiments are shown, each 'x' on the graph is data from a sperate biological replicate. Statistical analysis was with two-way ANOVA, no significant differences were found, except those marked * $p < 0.05$, ** $p < 0.01$, *** $p < 0.001$.

In Figure 5.4, panels C to E, protein levels in the S fraction shown in Figure 5.4 panel B, enriched in GSVs, were quantified in EHD2 KD and control cells under basal or insulin-simulated conditions. Insulin-stimulated translocation of GLUT4 out of the GSV-containing fraction was observed for both cell types, with no significant difference in the translocation of GLUT4 between control and EHD2 KD cells (Figure 5.4, panel C). Contrastingly, IRAP translocation out of GSVs in response to insulin was diminished in EHD2 KD cells, with IRAP levels in the GSV fractions following insulin stimulation dropping by 61.1% in control cells but by only 30.2% in EHD2 KD cells (Figure 5.4, panel D). However, IRAP levels in every fraction were lower in

EHD2 KD cells than in control cells (Figure 5.4, panel B), so this effect could be explained by overall lower levels of IRAP in the EHD2 KD cells.
High variability in Sx16 protein levels in each fraction meant that no significant change in Sx16 was found between EHD2 KD and control cells, or in response to insulin (Figure 5.4, panel E).

5.2.3 The effect of EHD2 knockdown on SNARE complex formation

Proximity ligation assay (PLA) is a technique that allows pairwise protein-protein interactions to be visualised in the cell (see Section 2.2.5.3). Briefly, two proteins were detected with primary antibodies in fixed and permeabilised 3T3-L1 adipocytes, in this case in either EHD2 KD or control cells. Specially designed secondary antibodies conjugated to an oligonucleotide detect those primary antibodies, and a series of reaction steps ligates and amplifies this DNA, allowing a fluorescent probe to detect and visualise the complex (see Figure 2.1). Ultimately, this means that if the proteins in question are less than 40 nm apart, and therefore closely interacting, they will be marked by a fluorescent dot (or “signal”) in the cell when imaged with a confocal microscope.

A) Caveolin1 + Insulin Receptor

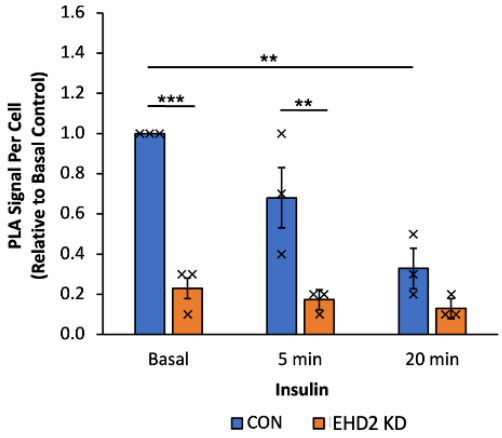

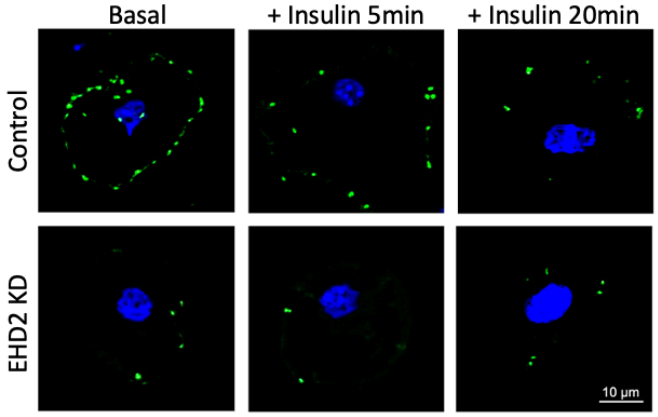

B) Syntaxin4 + Insulin Receptor

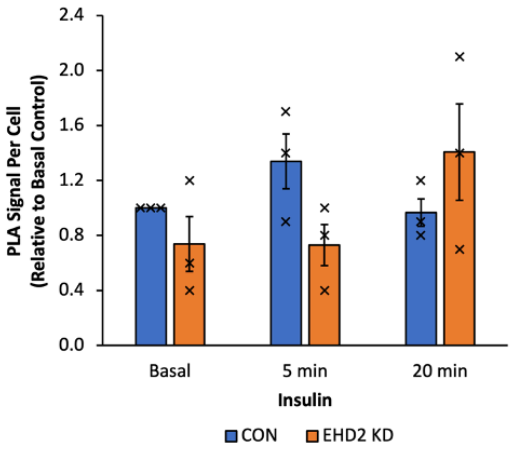

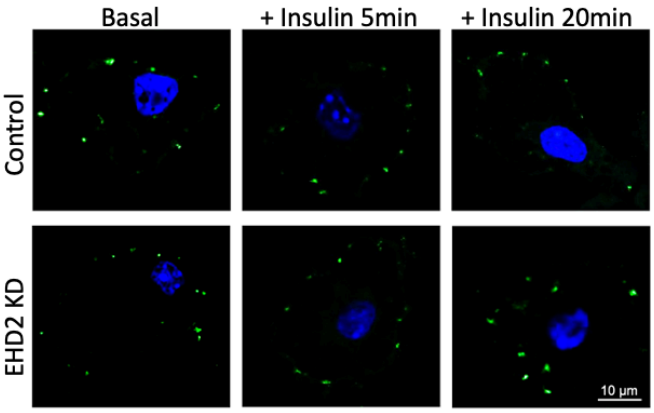

C) Syntaxin4 + VAMP2

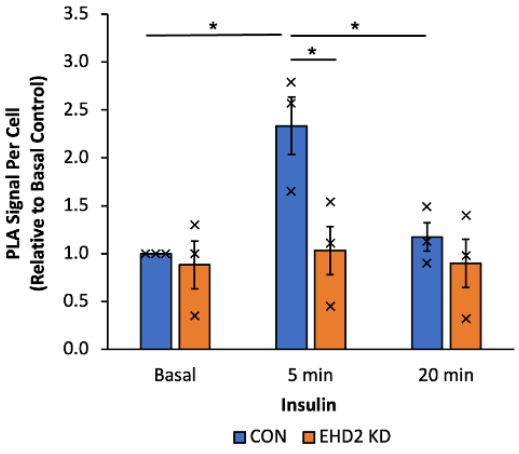

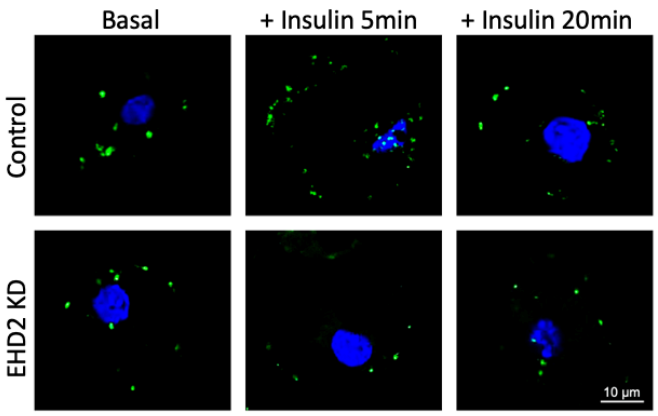

D) Syntaxin4 + SNAP23

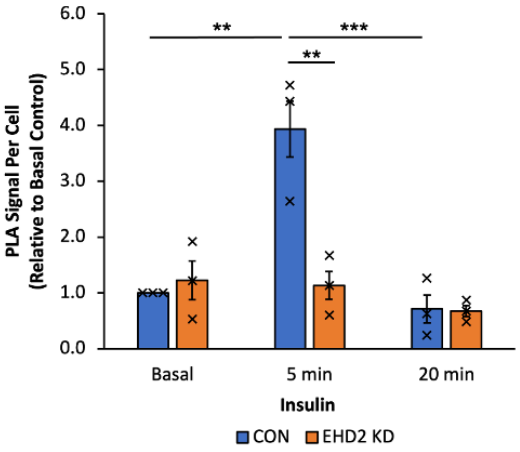

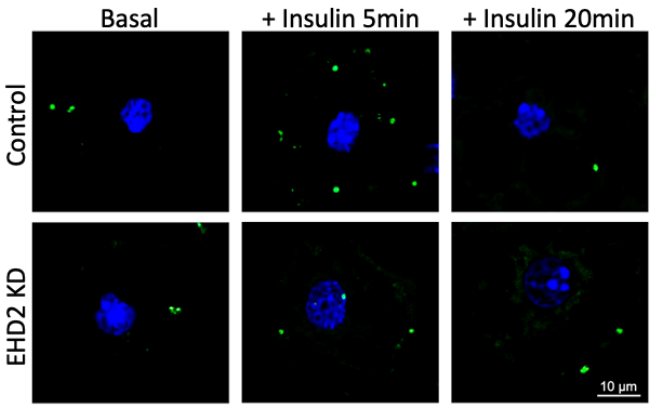

E) Syntaxin4 + Munc18c

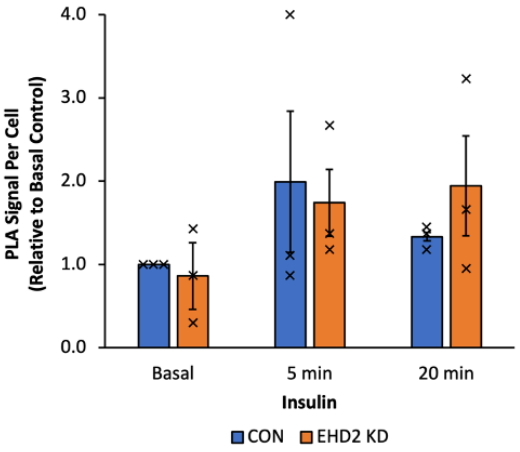

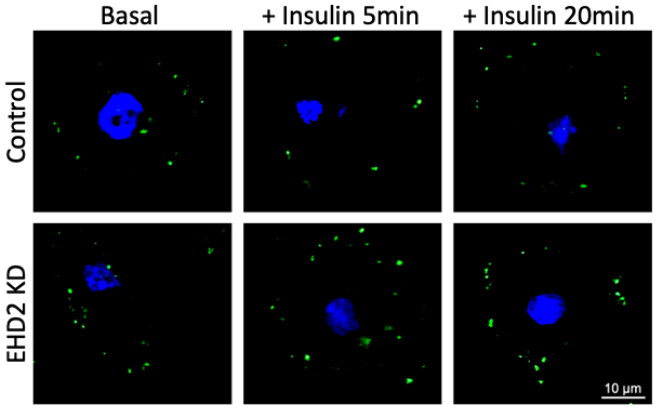

F) SNAP23 and VAMP2

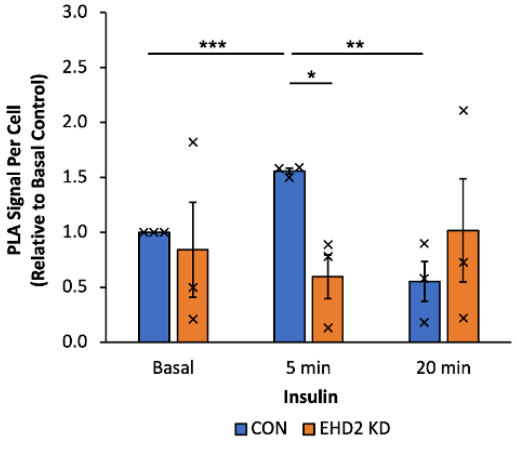

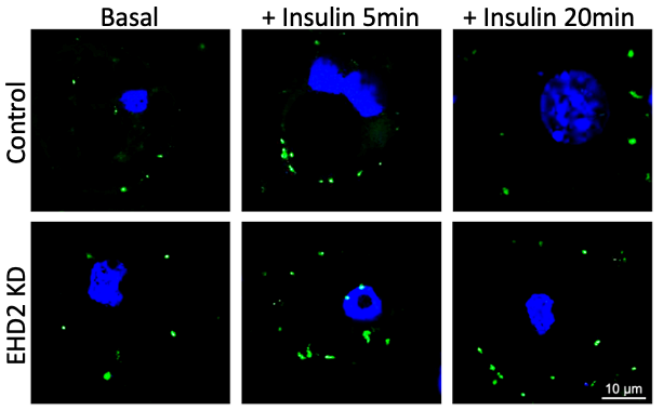

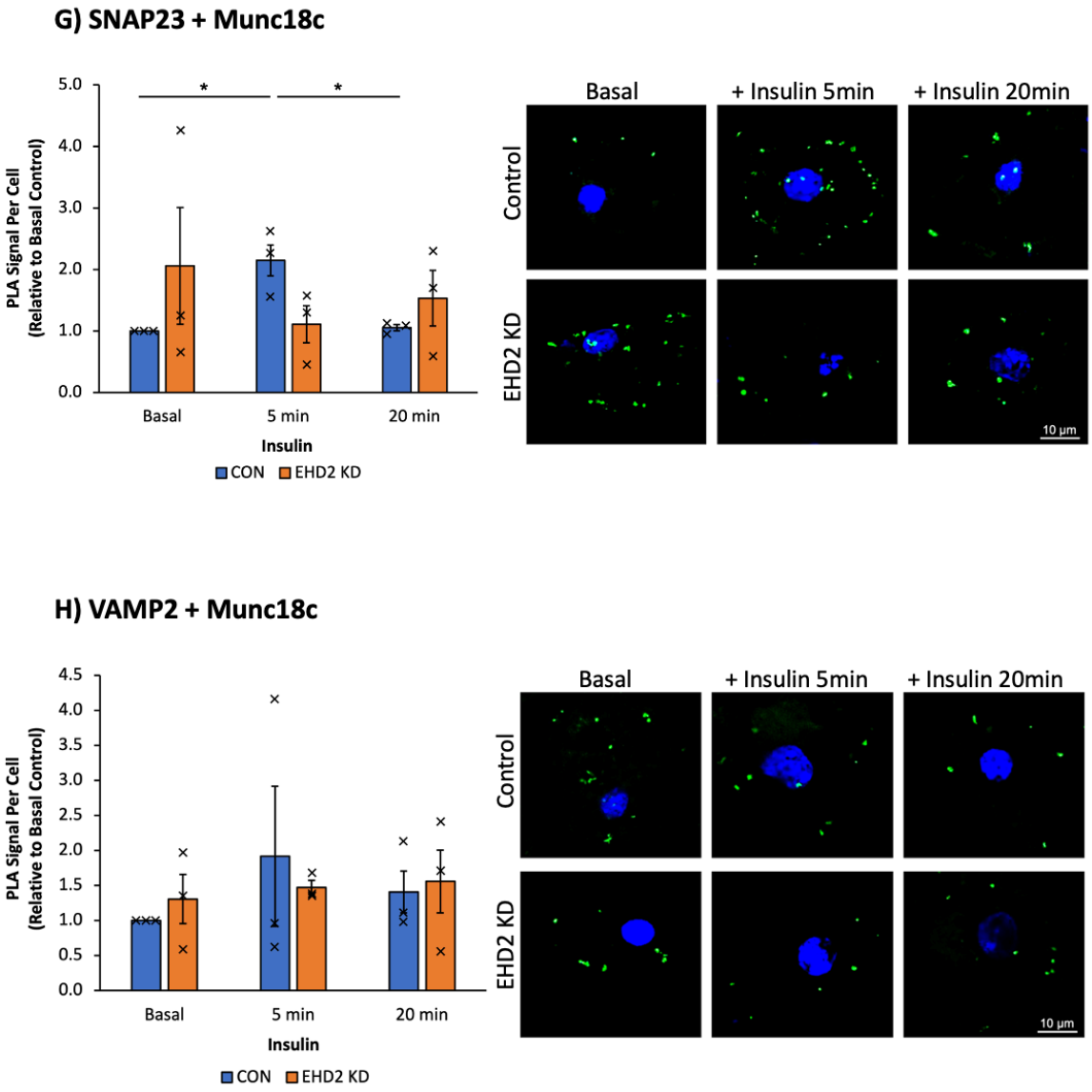

Figure 5.5 Proximity Ligation Assays with EHD2 knockdown and control 3T3-L1 adipocytes. Proximity Ligation Assay (PLA) was used to assess pairwise interactions of proteins in 3T3-L1 adipocytes, fixed 96 h after transfection with control siRNA (Control) or EHD2 siRNA (EHD2 KD), and following 0 (Basal), 5- or 20-min stimulation with 100nM insulin. Representative images, with PLA signal in green and nuclei staining with DAPI in blue, are shown alongside corresponding quantification of PLA signal per cell normalised to Basal Control for the following protein pairs: **(A)** Caveolin1 and Insulin Receptor beta subunit (IR); **(B)** Syntaxin4 (Sx4) and IR; **(C)** Sx4 and VAMP2; **(D)** Sx4 and SNAP23; **(E)** Sx4 and Munc18c; **(F)** SNAP23 and VAMP2; **(G)** SNAP23 and Munc18c; **(H)** VAMP2 and Munc18c.

Mean and SD of n = 3 independent biological replicates are shown. Typically, around 70 cells were examined in each biological replicate, and the mean values from each biological replicate are shown by the 'x' on the figures. Quantification was performed in ImageJ and statistical analysis was with two-way ANOVA, * $p < 0.05$, ** $p < 0.01$, *** $p < 0.001$. Scale bars are 10 μm.

PLA has been used here to measure the interactions of several protein pairs in both control and EHD2 KD adipocytes, under basal conditions, or following 5- or 20-minutes stimulation with 100 nm insulin.

Interactions between Caveolin1 (Cav1) and Insulin Receptor (beta subunit) (IR) were measured, initially as a proof of concept of the technique, as CAV1 and IR are known to closely interact at the plasma membrane (Lee et al. 2000), and this can be seen clearly in the Control Basal panel of Figure 5.5, panel A. Interestingly and unexpectedly, these interactions significantly decreased in number in cells after 20 min insulin stimulation. Even more striking was the dramatic loss of these signals in EHD2 KD cells across all insulin stimulation states, suggesting that loss of EHD2 disrupts interactions between CAV1 and IR.

Figure 5.5 panel B shows PLA between IR and Sx4. Interactions between these proteins did not significantly change given different insulin stimulation conditions, or between EHD2 KD and control cells. It is noteworthy that interactions between IR and Sx4 did not decrease in EHD2 KD cells, despite that fact that IR expression in these cells is around 50% lower than in control

cells (Figure 5.2). This suggests that loss of CAV1-IR interactions in EHD2 KD cells may not be wholly explained by the reduction in IR levels.

PLA was used to examine pairwise interactions between the SNARE proteins involved in GSV fusion with the plasma membrane. This technique has previously been used to demonstrate insulin-stimulated SNARE complex formation between these proteins (Kioumourtzoglou, Gould, and Bryant 2014), and so is being employed here to investigate whether loss of EHD2 affects interactions between these proteins.

For both Sx4 and VAMP2 (Figure 5.5, panel C), and Sx4 and SNAP23 (Figure 5.5, panel D) interactions between these pairs of SNARE proteins in control cells increased following 5 minutes insulin stimulation but returned to basal levels by 20 minutes of insulin stimulation. However, in the EHD2 KD cells, no insulin-stimulated rise in interactions was seen. This was also the case for interactions between SNAP23 and VAMP2 (Figure 5.5, panel F), as well as those between SNAP23 and Munc18c (Figure 5.5, panel G). This suggests that EHD2 plays a role in allowing insulin-stimulated SNARE complex formation. Neither EHD2 knockdown nor insulin stimulation significantly altered pairwise interactions between Sx4 and Munc18c (Figure 5.5, panel E), or between VAMP2 and Munc18c (Figure 5.5, panel H), in spite of Munc18c expression being downregulated in the EHD2 KD cells. These data support the hypothesis that loss of EHD2 affects insulin-

stimulated increase in SNARE complex formation only, rather than total number of interactions, as was the case for Caveolin1 and Insulin Receptor interactions.

A major difference in the findings of this study in comparison to the previous PLA study of these SNARE proteins was that here an insulin-stimulated rise in interactions between Sx4 and VAMP2, and between Sx4 and SNAP23 was observed, whereas this had not been seen previously. In that study, the cells were imaged in z-stacks, where images are taken throughout the cell, rather than in a central single plane. To determine whether these different imaging methods may have influenced the results of these experiments, z-stack and single plane images of the same cells, control 3T3-L1 adipocytes that had undergone PLA for Sx4 and VAMP2 interactions, were analysed (Figure 5.6).

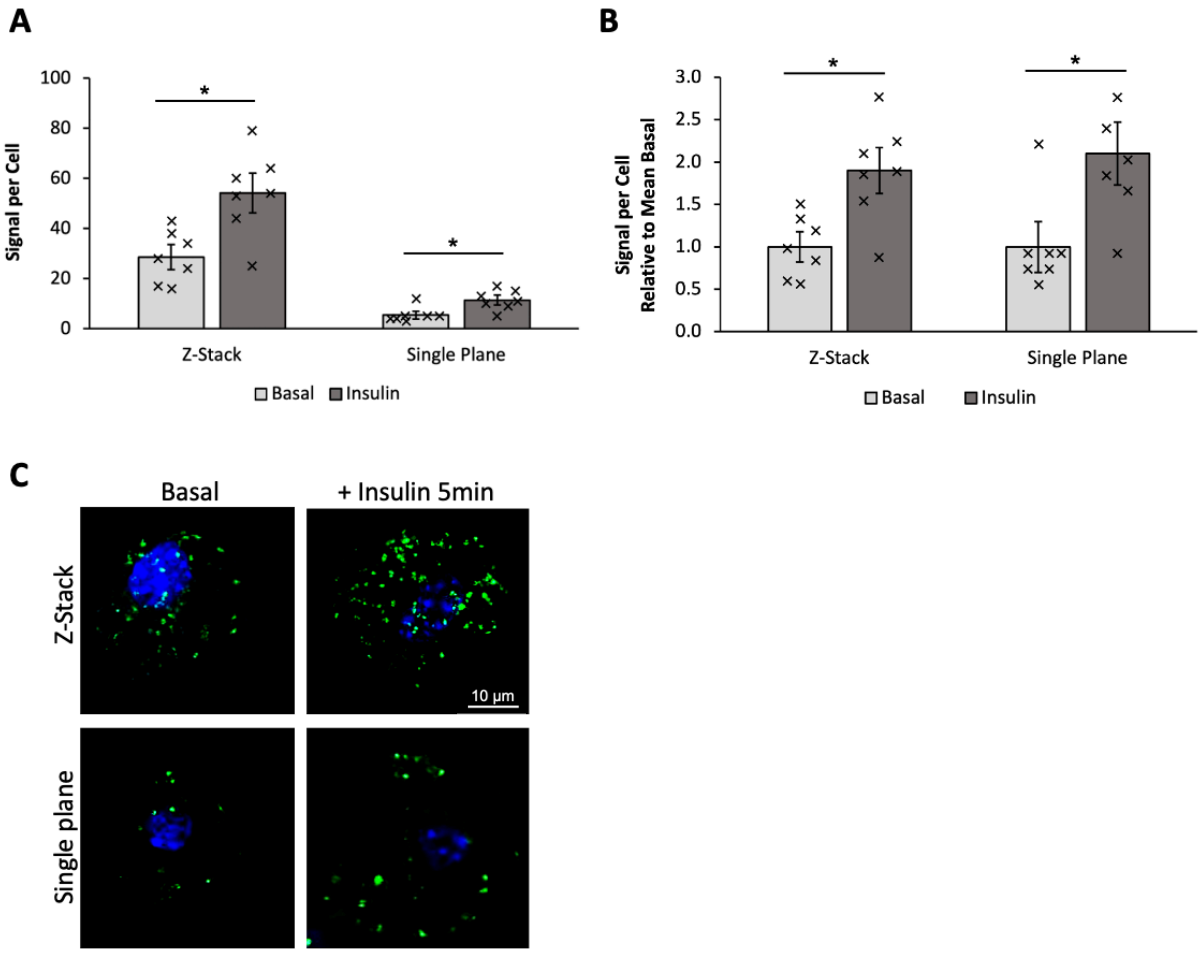

Figure 5.6 Comparison of imaging techniques for Syntaxin4-VAMP2 PLA

Z-stack and single plane imaging for proximity ligation assay of Synatxin4 and VAMP2 on 3T3-L1 adipocytes fixed 96 h after transfection with control siRNA only and following 0 (Basal) or 5 (Insulin) minutes stimulation with 100nM insulin. Mean and SD of n = 7 cells per condition are shown, with signal number for each cell shown as an 'x' on the graph. Quantification was performed in ImageJ and statistical analysis was with unpaired t-tests, * $p < 0.05$. **(A)** Raw signal per cell, **(B)** Signal per cell relative to mean signal per cell in the basal dataset. **(C)** Representative PLA images, scale bar is 10 μm.

As expected, taking Z-stacks of images captured more PLA signals than taking a single plane image (Figure 5.6, panel A). However, when the signal per cell data was adjusted relative to the mean signal per cell in the basal group, both z-stack and single plane imaging produced the same results: insulin stimulation significantly increased the number of interactions between Sx4 and VAMP2 (Figure 5.6, panel B). Therefore, the different imaging method cannot account for the difference in the PLA data presented here and that shown in the 2014 study.

5.2.4 Protein expression in caveolae of EHD2 knockdown adipocytes

As EHD2 is localised to caveolae (Morén et al. 2012), an experiment was carried out to determine whether levels of the proteins studied in the PLA experiments (CAV1, IR, and the SNARE proteins) were affected by EHD2 knockdown specifically in the caveolae by using differential centrifugation to enrich for a caveolae-fraction, as outlined in Section 2.2.2.2 (Figure 7).

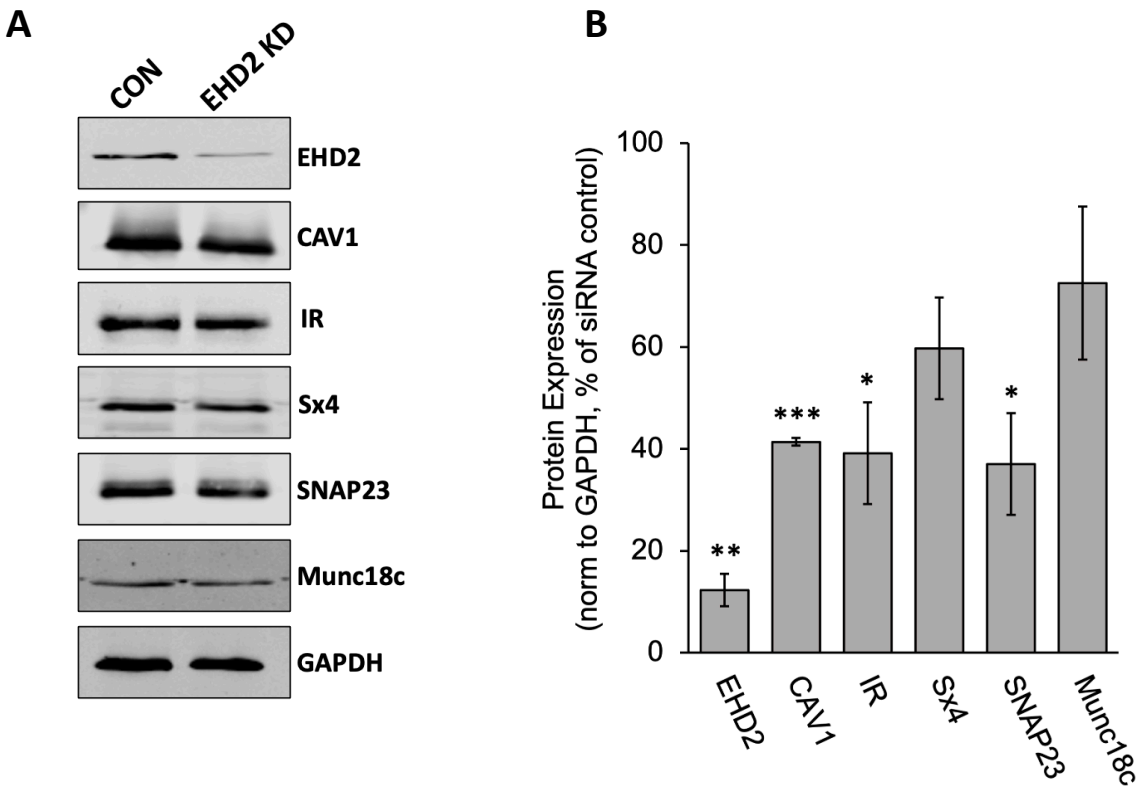

Figure 5.7 Protein expression in caveolae following EHD2 knockdown.
(A) Representative western blots of EHD2, Caveolin1 (CAV1), Insulin Receptor beta subunit (IR), Syntaxin4 (Sx4), SNAP23, and Munc18c in caveolae enriched fractions (isolated using a detergent-free method with a discontinuous sucrose gradient; fraction taken from 5-30% sucrose interface), produced from 3T3-L1 adipocytes collected 96 h after transfection with control siRNA (CON) or EHD2 siRNA (EHD2 KD). GAPDH was used as a loading control.
(B) Corresponding quantification of caveolae protein expression in EHD2 siRNA knockdown adipocytes is normalised to GAPDH and expressed as a percentage of caveolae protein expression in control siRNA transfected adipocytes. Mean and SD of n = 3 independent experiments are shown. Statistical analysis was with unpaired t-tests, * $p < 0.05$, ** $p < 0.01$, *** $p < 0.001$. Sx4 and Mucn18c levels were not significantly changed between the groups.

CAV1 levels in the caveolae-enriched fractions of EHD2 KD cells were down by 60% (SD=1.5, $p<0.001$) compared to that of control cells (Figure 5.7). Interestingly, this is a larger drop in CAV1 levels than was observed in whole cell lysates, where CAV1 was down by just 20% (Figure 5.2)- suggesting that more CAV1 is lost from caveolae than elsewhere in the cell when EHD2 levels are reduced.

IR and SNAP23 levels in the caveolae of EHD2 KD cells were also significantly lower than in control cells, although in this case the magnitude of this drop was similar to that seen in whole cell lysates. As in whole cell lysates, EHD2 KD did not affect levels of Sx4. Interestingly, Munc18c levels in caveolae enriched fractions were not significantly lower in EHD2 KD cells compared to control cells. This is in contrast to the data from whole cell lysates, where there was a drop in Munc18c expression following EHD2 knockdown.

5.2.5 Interaction between EHD2 and Syntaxin16

Syntaxin16 (Sx16) is a Q_a-SNARE involved in glucose transport alongside a number of other cellular functions in adipocytes (Bremner et al. 2022). It plays a role in sorting GLUT4 from endosomes into GSVs (Proctor et al. 2006) and following insulin stimulation, it translocates with GLUT4 to the plasma membrane (Shewan et al. 2003). Sx16 is of interest here because prior to the start of this project, a Multidimensional Protein Identification

Technology (MudPIT) analysis was performed on proteins that immunoprecipitated with Sx16 in untreated 3T3-L1 adipocytes, with the goal of discovering binding partners of Sx16 (Berends and Gould, unpublished work).

The top 7 protein matches from this analysis are shown in Figure 5.8, panel A. Of all the proteins in the Sx16 co-IP, EHD2 was identified with the highest protein score, which indicates a confident match, and the highest coverage, which indicates the proportion of a reference sequence covered by reads from the MudPIT. This strongly suggests that EHD2 can bind to Sx16 in adipocytes. The MudPIT analysis also identified Vacuolar protein sorting-associated protein 45 (Vps45), a known binding partner of Sx16 (Struthers et al. 2009), validating the approach and suggesting the results were reflecting the Sx16-interactome.

In order to further investigate this interaction, PLA was used to visualise interactions between Sx16 and EHD2 in WT 3T3-L1 adipocytes, in the basal state or following 5- or 20-minutes insulin stimulation (Figure 5.8, panels B and C). The presence of PLA signals in basal adipocytes supports the MudPIT data in the hypothesis that EHD2 binds Sx16. Strikingly, these interactions significantly decrease after 5 minutes with insulin stimulation and remain low at 20 minutes with insulin stimulation.

A

Rank by Score	Description	Score	Coverage
1	EH domain-containing protein 2	2285.04	76.98
2	Isoform 3 of Septin-9	1868.70	71.35
3	Stress-70 protein, mitochondrial	1680.34	50.81
4	Dihydrolipoyllysine-residue acetyltransferase component of pyruvate dehydrogenase complex, mitochondrial	1545.93	46.42
5	Heat shock cognate 71 kDa protein	1513.36	52.94
6	Long-chain-fatty-acid--CoA ligase 1	1509.99	48.78
7	Vacuolar protein sorting-associated protein 45	1230.21	56.32

B

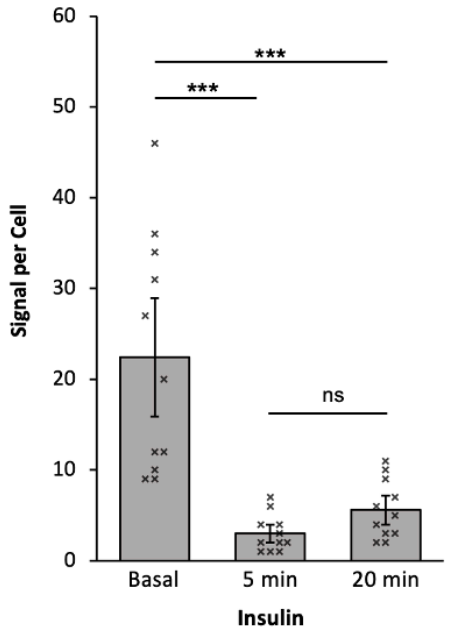

C

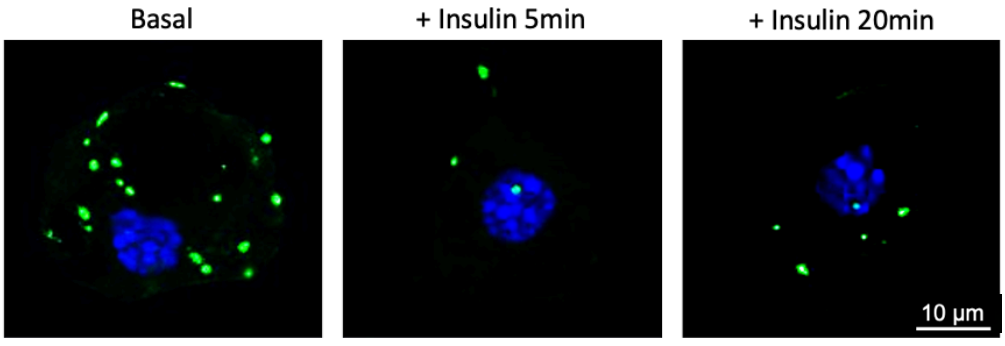

Figure 5.8 EHD2 interacts with Syntaxin16 in WT 3T3-L1 adipocytes.

(A) Top ranking results of a Multidimensional Protein Identification Technology (MudPIT) analysis performed on proteins that immunoprecipitated with Syntaxin16 (Sx16) in untreated WT 3T3-L1 adipocytes. For each protein match, Mascot software was used to calculate an overall Protein Score. This number reflects the combined scores of all observed mass spectra that can be matched to amino acid sequences within that protein. A higher score indicates a more confident match. Coverage is defined as the proportion of a reference sequence covered by reads from the MudPIT. This experiment and subsequent analysis were performed by Berend and Gould and are presently unpublished.
(B) - (C) Proximity Ligation Assay (PLA) was used to assess pairwise interactions between EHD2 and Sx16 in WT 3T3-L1 adipocytes, following 0 (Basal), 5- or 20-min stimulation with 100nM insulin. Representative images **(C)**, with PLA signal in green and nuclei staining with DAPI in blue, are shown alongside corresponding quantification of PLA signal per cell **(B)**. Data is from a single biological replicate, with mean and SD of n = 11 cells per condition. Quantification of technical repeats was performed in ImageJ and statistical analysis was with one-way ANOVA, *** $p < 0.001$. Scale bars are 10 μm. Clearly, biological replication is needed to validate these conclusions.

5.2.6 Insulin-stimulated Sx4 phosphorylation in EHD2 knock out mice

In Chapter 3, phosphorylation of Sx4 in response to insulin was investigated in 3T3-L1 adipocytes with limited success due to non-specific binding of the Sx4-Y115P and Sx4-Y251P specific antibodies in the 3T3-L1 lysates (see Section 3.2.2). The opportunity arose to investigate Sx4 phosphorylation in primary mouse adipocytes, from both WT and EHD2 knock out (ehd2 -/-) mice. Figure 5.9 shows data generated from whole cell lysates prepared from inguinal fat of individual WT and ehd2-/- mice that were fed a high-fat diet for 2 weeks. Adipocytes were either stimulated with 10nM insulin for 5 minutes or untreated (Basal) prior to lysis.

Immunoblots for total and phosho-AKT (Figure 5.9, panel B) and subsequent quantification (Figure 5.9, panel D) showed that AKT activation in response to insulin was not affected by loss of EHD2, at least after 5 minutes insulin stimulation. These data also confirm that the adipocytes were insulin responsive, similar to the results observed in EHD2 KD 3T3-L1 adipocytes in Figure 5.3.

Using immunoblot data, a representative sample of which are shown in Figure 5.9 panel A, fold change in Sx4-Y115 and Sx4-Y251 phosphorylation following insulin stimulation of adipocytes from individual mice was measured. The insulin-stimulated fold change in phosphorylation at both sites was significantly lower in the ehd2-/- mice than in WT (for Y115 $p=0.039$ for

Y251 p=0.014), with WT mice seeing a rise in Sx4 phosphorylation on average that was not seen in ehd2-/- mice (Figure 5.9, panel C). Total Sx4 levels were not altered by loss of EHD2.

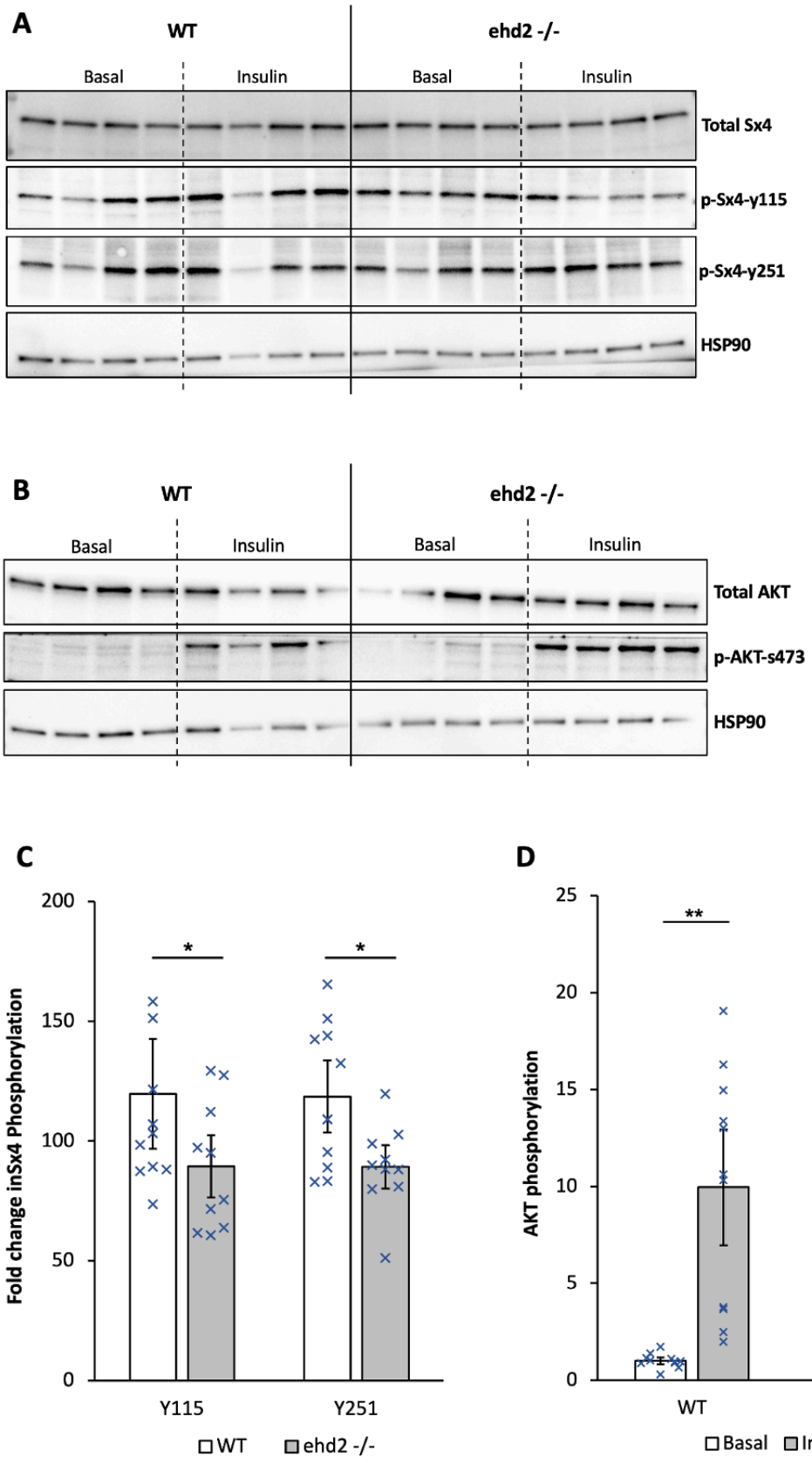
A
WT
ehd2 -/-
Basal
Insulin
Basal
Insulin
Total Sx4
p-Sx4-y115
p-Sx4-y251
HSP90
B
WT
ehd2 -/-
Basal
Insulin
Basal
Insulin
Total AKT
p-AKT-s473
HSP90
C
Fold change inSx4 Phosphorylation
200
150
100
50
0
*
*
Y115
Y251
WT
ehd2 -/-
D
AKT phosphorylation
25
20
15
10
5
0
**
**
WT
ehd2 -/-
Basal
Insulin

Figure 5.9 Insulin stimulated AKT and Syntaxin4 phosphorylation in ehd2 -/- mice.

(A) – (B) Representative western blots of **(A)** Total Syntaxin4 (Sx4), tyrosine-115 phosphorylated Sx4 and tyrosine-251 phosphorylated Sx4, and of **(B)** Total AKT, and serine-473 phosphorylated AKT in whole cell lysates prepared from inguinal fat of individual HFD WT and ehd2-/- mice. Adipocytes were stimulated with 10nM insulin for 0 (Basal) or 5 (Insulin) minutes prior to lysis. HSP90 is used as a loading control. **(C)** Quantification of fold change in Sx4 phosphorylation following 5 minutes insulin stimulation at Y115 and Y251 phosphorylation sites in WT and ehd2 -/- mice. **(D)** Quantification of s473 phosphorylated AKT in basal and insulin stimulated WT and ehd2 -/- mice adipocytes, normalised to HSP90 and total AKT levels and expressed relative to mean WT basal p-AKT-s473 levels. Mean and SD of n = 11 WT mice and n= 10 ehd2 -/- mice are shown, with data from each individual mouse shown as an 'x' on the graph. Statistical analysis was with unpaired t-tests **(C)** and two-way ANOVA **(D)**, * $p < 0.05$, ** $p < 0.01$.

5.3 Discussion

5.3.1 EHD2 knockdown causes reduction in key glucose transport protein expression

The aim of the study presented in this chapter was to determine whether EHD2 plays a role in insulin stimulated GLUT4 translocation and subsequent glucose transport in adipocytes. Once a protocol for the efficient siRNA knockdown of EHD2 in mature 3T3-L1 adipocytes was developed (Figure 5.1), expression levels of various proteins involved in GLUT4 translocation were measured in these knockdown cells and in their corresponding control cells transfected instead with scrambled siRNA (Figure 5.2). The caveolae component Cav1, and the Insulin Receptor (IR) beta subunit were down in the EHD2 KD cells. Of the proteins involved in the SNARE complex required for GLUT4 storage vesicle (GSV) fusion with the plasma membrane (Sx4, SNAP23, VAMP2 and Munc18c), SNAP23 and Munc18c levels were also reduced in the EHD2 knockdown cells.

It has been shown that EHD2 can act as a transcription factor linking caveolae dynamics to gene transcription (Torrino et al. 2018) notably affecting the transcription of Cav1 following mechanical stress. While only the transcription of caveolae components were measured in that study, the reduction in levels of other proteins in EHD2 KD cells described in Figure 5.2 could be linked to EHD2's ability to impact transcription. Loss of EHD2 has

been demonstrated to disrupt the structure and motility of caveolae (Morén et al. 2012; Matthaeus et al. 2020). Cav1, IR and SNAP23 are enriched in caveolae (Chapter 1 Figure 1), so an alternative or exacerbating cause of their reduction in EHD2 KD cells could be a loss of stability resulting from a change in caveolae structure.

5.3.2 EHD2 affects insulin response and glucose transport

Despite lower levels of IR beta subunit in EHD2 KD cells, AKT activation was not significantly affected in these cells (Figure 5.3). However, levels of total tyrosine phosphorylation in EHD2 KD cells were down compared to control cells, particularly in response to insulin (Figure 5.3, bottom panel). This is likely due to the 50% reduction in the IR beta subunit caused by EHD2 knockdown, as this subunit contains the insulin-activated tyrosine kinase component. Despite this reasonably large loss of IR activation, the fact that AKT activation remained at normal levels in EHD2 KD cells demonstrates the robustness of the insulin signalling pathway and suggests that any disruption to the insulin response in EHD2 KD cells occurs upstream of AKT activation.

Glucose transport following insulin stimulation in EHD2 KD cells was down compared to control cells, but only by 30% (Figure 5.4, panel A). This combines with the AKT and total tyrosine phosphorylation data to suggest that while EHD2 plays a role in insulin stimulated glucose transport, the process is not dependant on it. Translocation of GLUT4 out of GSVs

following insulin stimulation did not appear to be affected by loss of EHD2 (Figure 5.4, panel C). IRAP translocation was reduced in the EHD2 KD cells, but lower overall levels of IRAP in the knockdown cells make this experiment difficult to draw conclusions from (Figure 5.4, panel D). So too does Figure 5.4, panel E, in which Sx16 fails to see significant insulin stimulated translocation in either cell type, despite it being previously demonstrated that Sx16 translocates with GLUT4 (Bremner et al. 2022). It is likely that the fairly crude 16k fractionation method employed in the experiment presented in Figure 5.4 is simply not sensitive enough to pick up any changes in translocation subtle enough to only produce a 30% reduction in glucose transport.

5.3.3 EHD2 plays a role in insulin-stimulated SNARE complex formation

Proximity ligation assay (PLA) was used to assess the formation of SNARE complexes between Sx4, SNAP23 and VAMP2, as they are associated with GSV fusion with the plasma membrane. PLA allows interactions between two proteins to be measured in the cell, so all pairwise interactions between Sx4, SNAP23, VAMP2 and the regulatory protein Munc18c were studied, at three insulin stimulation states (basal, 5 minutes and 20 minutes), and in both EHD2 KD and control cells.

5.3.3.1 Insulin receptor and Caveolin1 interaction

Interactions between IR and Cav1 were also measured at these insulin stimulation states in both EHD2 KD and control cells, yielding interesting and unexpected results. In control cells, following both 5- and 20-minutes insulin stimulation, interactions between IR and Cav1 decrease significantly. In the control cell basal state panel in Figure 5A, a high number of interactions between Cav1 and IR can be seen. It is known that IR phosphorylates Cav1 in response to insulin stimulation (Kimura et al. 2002), and it is within 5 minutes of insulin stimulation that these interactions begin to decrease. This suggests that once IR has phosphorylated Cav1, these proteins move away from each other. This could be the result of IR recycling following insulin stimulation (Chen et al. 2019), another process resulting in IR moving away from caveolae following insulin stimulation, or simply a change in confirmation of Cav1 following its phosphorylation that prevents PLA detection of the interaction. In any case, this dramatic drop in IR and Cav1 interactions following insulin stimulation is not seen in EHD2 KD cells, rather, their interactions are low across all insulin stimulation times. The loss of PLA signals between control and knockdown cells here cannot be fully explained by the lower levels of IR and Cav1 in EHD2 KD cells (Figure 5.2), as interactions between Sx4 and IR (shown in Figure 5.5, panel B), were unchanged in both control and knockdown cells and were not reduced by EHD2 knockdown. As IR and Cav1 are localised to caveolae, it is likely that

the loss of their interactions caused by EHD2 KD are the result of the loss of caveolae stability associated with loss of EHD2.

5.3.3.2 SNARE protein interactions

An increase in associations between the following pairs of SNARE proteins was observed in control cells following 5 minutes insulin stimulation: Sx4 and VAMP2 (Figure 5.5, panel C); Sx4 and SNAP23 (Figure 5.5, panel D); SNAP23 and VAMP2 (Figure 5.5, panel F); SNAP23 and Munc18c (Figure 5.5, panel G). For all of these pairs, the number of associations had returned to basal levels by 20 minutes following insulin stimulation. Again, for all of these pairs, no increase in associations was seen in the EHD2 KD cells at any insulin stimulation timepoint. Pairwise associations between Sx4 and Munc18c (Figure 5.5, panel E) and between VAMP2 and Munc18c (Figure 5.5, panel H) were not affected by insulin stimulation or EHD2 knockdown.

The rationale for using PLA to study SNARE complex formation was based on a 2014 study by Kioumourtzoglou et al., in which PLA was used to measure interactions between these same pairs of SNARE proteins. These experiments were performed in WT 3T3-L1 adipocytes and had just two insulin stimulation timepoints: basal and 5 minutes (Kioumourtzoglou, Gould, and Bryant 2014). Looking in the control cells only at the basal and 5-minute insulin stimulation timepoints, for the majority of our protein pairs, the PLA experiments presented here and those in the 2014 paper yielded the same

results, with two notable exceptions. For the Sx4 and VAMP2 pair, and for the Sx4 and SNAP23 pair, the PLA experiments presented in this chapter found an increase in signals following 5 minutes insulin stimulation, whereas the previous study found no significant increase for these pairs.

As discussed in the results section of this chapter, and shown in Figure 5.6, the differing results between this and the previous SNARE PLA study could not be explained by the different imaging techniques. The previous study used z-stack images whereas here only single-plane images were taken. However, when cells with Sx4-VAMP2 PLA staining were re-imaged in z-stack formats, although the raw signal per cell numbers were greater and more closely resemble those found in the 2014 study, the proportional increase in signals in response to insulin remained the same (Figure 5.6, panels A and B). Therefore, the different imaging technique can be ruled out as an explanation of the differences between the results.

A number of methodological differences between the PLA experiments in the present study and those in the 2014 paper may have contributed to the different results for the Sx4-VAMP2 and Sx4-SNAP23 pairs. Firstly, not all antibodies used in the assay were the same between the two studies, as a number of antibodies used in the 2014 study have since been discontinued by their manufacturers. It is possible that some antibodies are better suited for use in PLA than others. For future repeats of PLA experiments to study

these SNARE proteins' interactions, a number of different antibodies for each target protein could be used. If increased PLA signal numbers following insulin stimulation were observed repeatedly, even when using different antibodies against the two target proteins, this would strengthen the evidence that interactions between those proteins do increase in response to insulin.

Secondly, different PLA kits were used for the two studies, which means the buffers, secondary antibodies and reaction enzymes were different. The 2014 study used Duolink In Situ PLA kit from Olink Bioscience, whereas the study presented here used NaveniFlex MR from Navinci. NaveniFlex MR is a newer kit that which uses improved PLA probes that have been shown to produce consistently more efficient signal generation that traditional PLA probes used in the older Duolink system (Klaesson et al. 2018). It is possible that these improved PLA probes allowed for more sensitive detection of Sx4-VAMP2 and Sx4-SNAP23 interactions, and thus the increase in these interactions following 5 minutes insulin stimulation could be observed.

Finally, another key difference between these two PLA studies is the cells themselves. The 2014 study used untreated WT 3T3-L1 adipocytes whereas the control adipocytes in this study had been trypsinised, transfected with scrambled siRNA, and re-plated before use in the assay, in order to be comparable with the EHD2 KD cells. It is possible that the transfection and replating process could have affected some cellular processes. A way to

mitigate this concern in future studies could be to include a “true WT” control of completely untreated cells alongside the scrambled RNA control and the EHD2 knockdown cells.

Regardless of the discrepancies between the results presented in this chapter and those of the previous PLA study of these SNARE proteins, a clear and consistent pattern of results emerge in Figure 5.5 which broadly agree with the previous study by Kioumourtzoglou et al. At 5 minutes post insulin stimulation, a number of pairs of the SNARE proteins required for GSV fusion with the plasma membrane (Sx4 and VAMP2; Sx4 and SNAP23; SNAP23 and VAMP2; and SNAP23 and Munc18c) exhibit increased interactions, representing insulin-stimulated SNARE complex formation. Hence our analysis using different antibodies, kits and cells largely supports the previous results and conclusions (Kioumourtzoglou, Gould, and Bryant 2014). In EHD2 KD cells, although the raw number of these interactions, measured as signals per cell, were no lower than in control cells in the basal state, the insulin-stimulated increase in these interactions at 5 minutes insulin stimulation was lost. These results are consistent with the hypothesis that knockdown of EHD2 hinders insulin-stimulated SNARE complex formation.

It is not clear whether EHD2 plays a direct role in the formation of this SNARE complex, or whether the effect of EHD2 knockdown on caveolae stability and motility is to blame for the loss of the insulin response of this

complex formation. Notably, levels of the SNARE proteins of interest in caveolae-enriched cell fractions from EHD2 KD cells (Figure 5.7) were not especially different to levels found in whole cell lysates (Figure 5.2). This demonstrates that loss of EHD2 likely does not result in greater loss of the SNARE proteins of interest from caveolae.

It may be interesting, in future work, to perform these same PLA experiments on cells that have had their caveolae disrupted, such as by cholesterol depletion (Parpal et al. 2001), or Cavin1 knockdown (Liu et al. 2008), to see if the same pattern of loss of insulin stimulated SNARE complex formation occurs. This could help ascertain whether EHD2's role in stabilising caveolae is linked to its role observed here of facilitating insulin stimulated SNARE complex formation. Additionally, PLA between EHD2 itself and the SNARE proteins in question, to find out whether those proteins directly interact, could shed light on EHD2's function.

5.3.4 EHD2 interacts with Syntaxin16

A MudPIT analysis of proteins that immunoprecipitated with Sx16 in 3T3-L1 adipocytes, performed prior to the start of this project, identified EHD2 as a binding partner of Sx16 (Figure 5.8, panel A). As part of this investigation into the role of EHD2 in glucose transport, a PLA experiment also confirmed that EHD2 and Sx16 interact in adipocytes (Figure 5.8, panels B and C).

Strikingly, these interactions significantly decreased following insulin stimulation.

Sx16 translocates to the plasma membrane with GLUT4 following insulin stimulation (Shewan et al., 2003), and it is at this point that PLA data in Figure 5.8 shows that interactions between Sx16 and EHD2 decrease. This could support the hypothesis that EHD2 plays a direct role in insulin stimulated fusion of GSVs with the plasma membrane. No firm conclusions can be drawn from this data, as only technical replicates, rather than biological replicates were carried out due to time constraints, though the initial results were striking enough to include here.

5.3.5 Insulin stimulated Syntaxin4 phosphorylation is affected in ehd2 -/- mice

AKT and Syntaxin4 (Sx4) phosphorylation were studied in primary adipocytes from inguinal fat of WT and ehd2-/- mice. AKT activation following 5 minutes insulin stimulation was not affected by loss of EHD2 in the mouse adipocytes. However, fold change in Sx4 phosphorylation following insulin stimulation, at both the Y115 and Y251 phosphorylation sites was lower in ehd2 -/- mice than in WT (Figure 5.9).

As discussed in chapter 3, Sx4 is known to be phosphorylated on Y115 and Y251 in response to insulin, and phosphorylation at these residues increases

its rate of SNARE complex formation with SNAP23 and VAMP2. Again, as discussed in chapter 3, it is likely that the insulin receptor itself phosphorylates Sx4 at Y115 and Y251 in response to activation by insulin (Schmelzle et al. 2006, Black 2016, Al Tobi 2018).

Loss of EHD2, at least in mice adipocytes, appears to reduce insulin stimulated Sx4 phosphorylation. This, when combined with the PLA data from 3T3-L1 adipocytes, may explain the loss of insulin stimulated interactions between Sx4 and its binding partners. Unfortunately, it was not possible to confirm the effect of EHD2 knockdown on Sx4 phosphorylation in 3T3-L1 adipocytes, as the phospho-specific antibodies against Sx4-Y115-P and Sx4-Y251-P did not work as reliably in 3T3-L1 lysates as they did in primary adipocyte lysates. However, future work on this project should see PLA with the SNARE proteins performed in primary adipocytes from both WT and ehd2 -/- mice, to find out whether the results from 3T3-L1 adipocytes can be replicated in primary cells, further solidifying the link between EHD2, Sx4 phosphorylation and GSV SNARE complex formation.

5.3.6 Conclusions

Taken together, the data presented here suggest a role for EHD2 in insulin stimulated glucose transport in adipocytes. EHD2 is required to maintain normal levels of the Insulin Receptor beta subunit, as well as SNAP23 and Munc18c, a SNARE and SNARE-associated protein respectively, which are

involved in the fusion of GSVs with the plasma membrane in response to insulin (Figure 5.2). While AKT phosphorylation was unaffected by EHD2 knockdown, total tyrosine phosphorylation levels were affected (Figure 5.3) and this is likely linked to the lower levels of IR beta, the key insulin responsive tyrosine kinase. Moreover, at least in primary mouse adipocytes, loss of EHD2 reduced insulin stimulated phosphorylation of the SNARE protein Sx4, a process linked to its ability to form SNARE complexes with SNAP23 and VAMP2, ultimately leading to fusion of GSVs with the plasma membrane (Figure 5.9).

One of the key findings of this study was that when EHD2 levels are reduced, interactions between multiple pairs of the SNARE proteins involved in GSV fusion with the plasma membrane no longer increase following 5 minutes insulin stimulation (Figure 5.5). This suggests that EHD2 is involved in the insulin stimulated SNARE complex formation, occurring within 5 minutes of insulin exposure, that leads to GSV fusion with the plasma membrane and subsequent GLUT4 translocation. This is backed up by the glucose transport data shown in Figure 5.4, panel A, which demonstrates that glucose uptake in response to insulin is reduced in EHD2 knockdown cells. The interaction between EHD2 and Sx16 that was reduced upon insulin stimulation (Figure 5.8) also hints at a role for EHD2 in glucose transport.

GLUT4 translocation did not appear to be affected by EHD2 knockdown (Figure 5.4, panel C), which would appear to contradict the PLA and glucose uptake data. However, the translocation assay used here is not sensitive to small changes and was performed following 20 minutes insulin stimulation rather than at 5 minutes where the effect in the PLA experiments was seen. This adds weight to the argument that EHD2 is involved in the initial SNARE complex formation and GSV fusion with the plasma membrane within 5 minutes of insulin stimulation. This hypothesis is also supported by a study that used TIRF microscopy to study GLUT4 distribution, which found that around 50% of GLUT4-containing structures they identified were localised with 100 nm of the plasma membrane (Stenkula et al. 2010). This pool of GSVs held close to the plasma membrane may be responsible for the initial spike in SNARE protein interactions observed in Figure 5.5 that was abrogated by EHD2 knockdown.

The mechanism, or mechanisms, of how precisely EHD2 affects the processes of GSV fusion, GLUT4 translocation and glucose transport in adipocytes are not yet clear. However, EHD2's key role in stabilising caveolae, where IR and Sx4 are localised, suggests that these membrane structures may hold the answers. This work illustrates the need for more research into EHD2 and caveolae, as it has the potential to unlock a better understanding of glucose transport and insulin resistance in adipocytes.

Chapter 6

Discussion and Conclusions

6 Discussion and Conclusions

6.1 Key findings

In Chapter 3, the Insulin Receptor (IR) and Syntaxin4 (Sx4) were found to co-localise at the adipocyte plasma membrane, with PLA data showing that these proteins are within 400 nM of one another, supporting the hypothesis that IR directly phosphorylates Sx4 in adipocytes. Both IR and Sx4 were also found to co-localise with caveolae component Caveolin1 (Cav1) at the plasma membrane, suggesting that their interaction takes place in caveolae, and thus emphasising the importance of adipocyte caveolae in insulin action.

In Chapter 4, 3T3-L1 cells lacking Sx4 were confirmed to be able to differentiate into adipocytes, and AKT activation and GLUT4 translocation in these cells were found to be unaffected by the loss of Syntaxin4, suggesting that there is redundancy built into the SNARE machinery required for GLUT4 translocation, and highlighting the complexity of this system. Furthermore, cells stably expressing WT, phosphomimetic and phosphoresistant Sx4 in a WT 3T3-L1 background were generated. The potential future use of these new cell lines for probing the effects and importance of Sx4 phosphorylation was discussed in Section 4.3.5.

In Chapter 5, it was found that reduction of the caveolae component EHD2 by siRNA knockdown in 3T3-L1 adipocytes resulted in reduced expression of

Cav1, IR and membrane trafficking proteins SNAP23 and Munc18c. EHD2 knockdown was also found to reduce the maximum rate of insulin stimulated glucose uptake in these cells. Furthermore, PLA experiments revealed that knockdown of EHD2 disrupted insulin stimulated pairwise interactions between a number of SNARE proteins involved in GSV fusion with the plasma membrane (Sx4 and VAMP2; Sx4 and SNAP23; SNAP23 and VAMP2; and SNAP23 and Munc18c), suggesting that EHD2 is involved in the insulin stimulated formation of the Sx4/SNAP23/VAMP2 SNARE complex that drives GLUT4 translocation to the plasma membrane in response to insulin.

It was also found that in primary mouse adipocytes, loss of EHD2 led to a reduced insulin-stimulated fold change in Sx4 phosphorylation. Given that loss of EHD2 is known to disrupt adipocyte caveolae (Matthaeus et al. 2020; Hubert et al. 2020), these data further support the hypothesis explored in Chapter 3 that IR directly phosphorylates Sx4 in caveolae. These data also highlight the importance of caveolae as a signalling platform linking signals from IR to the membrane trafficking machinery required to drive GLUT4 translocation and glucose transport.

6.2 Future work

6.2.1 Interaction between EHD2 and SNARE proteins

In Chapter 5, Section 5.2.5, the interaction between Syntaxin16 (Sx16) (which plays a role in sorting GLUT4 from endosomes into GSVs (Proctor et al. 2006)) and EHD2 was investigated because of a Multidimensional Protein Identification Technology (MudPIT) analysis that revealed EHD2 as a likely binding partner of Sx16 in adipocytes (Berends and Gould, unpublished work). A PLA experiment with a single biological replicate suggested that EHD2 and Sx16 are in close proximity in the cell, but that this interaction decreases with insulin stimulation. In future work, this interaction should be probed with further IF and PLA co-localisation experiments. Additionally, PLA could be used to examine interactions between EHD2 and number of SNARE proteins in WT adipocytes, particularly Sx4, SNAP23 and VAMP2. Interrogating whether EHD2 directly interacts with these SNARE proteins, and how these interactions change following insulin stimulation, could help elucidate whether EHD2's role in insulin stimulated formation of the Sx4/SNAP23/VAMP2 SNARE complex involves direct interaction of EHD2 with these proteins, or is a secondary effect of caveolae disruption caused by the loss of EHD2.

6.2.2 Insulin stimulated EHD2 phosphorylation

Another way in which the present study could be expanded upon is in the role of tyrosine phosphorylation in the GLUT4 trafficking machinery.

The Schmelzle et al 2006 study that explored insulin stimulated tyrosine phosphorylation in 3T3-L1 adipocytes revealed that Sx4 and Munc18c become tyrosine phosphorylated in response to insulin. A wealth of subsequent evidence has shown that this phosphorylation is vital for these proteins' ability to regulate the SNARE complex formation that drives GLUT4 translocation (Kioumourtzoglou, Gould, and Bryant 2014; Black 2016; Al Tobi 2018). The same 2006 study found that EHD2 phosphorylation on Y453 increases by ≥3 times in response to insulin stimulation in 3T3-L1 adipocytes (Schmelzle et al. 2006). At the time of writing, no further studies on the insulin stimulated phosphorylation of EHD2 and its potential effects have been published. Given EHD2's location in the caveolae neck region, where IR is also found (Foti et al. 2007), it is a reasonable hypothesis that IR could directly phosphorylate EHD2. The feasibility of this could be tested using *in vitro* CIRK phosphorylation, as has been done for the phosphorylation of Munc18c (Aran, Bryant, and Gould 2011). Furthermore, co-localisation between EHD2 and IR could be examined using IF and PLA techniques in a similar manner to the IR and Sx4 co-localisation experiments in Section 3.2.3. *f*

A further question that arises from these data is whether the insulin stimulated phosphorylation of EHD2 is linked to its role in insulin stimulated SNARE complex formation explored in Chapter 5. In vitro studies could be useful in probing this question. The accelerating effect of Munc18c

phosphorylation on Sx4/SNAP23/VAMP2 SNARE complex formation was uncovered by incubating the SNARE proteins with WT or phosphomimetic Munc18c and measuring SNARE complex formation over time (Kioumourtzoglou, Gould, and Bryant 2014). A similar experiment could be done, instead incubating Sx4, SNAP23 and VAMP2 either alone, with WT EHD2, or with phosphomimetic EHD2 (EHD2 Y453E), and measuring the effect of the incubations on the rate of SNARE complex formation. This would not only indicate whether EHD2 itself can directly influence SNARE complex formation, but whether the insulin stimulated phosphorylation of EHD2 on Y453 enhances SNARE complex formation. Following this, CRISPR-Cas9 technology could be employed to generate 3T3-L1 cell lines either lacking EHD2 altogether, or expressing a phosphomimetic or phosphoresistant form of EHD2. This would allow a range of experiments probing the effect of EHD2 phosphorylation on Sx4/SNAP23/VAMP2 SNARE complex formation using PLA on these cell liens, on GLUT4 translocation using immunofluorescence and sub cellular fractionation approaches, and on glucose transport using the glucose uptake assay described here.

6.2.3 GLUT4 translocation to caveolae

As discussed at length in Section 1.5.2, there has been much debate over whether GLUT4 translocates directly to caveolae in adipocytes, with the question left largely unanswered. The data presented in Section 5.2.3 demonstrated that EHD2 plays a role in insulin stimulated formation of the

Sx4/SNAP23/VAMP2 SNARE complex, which functionally links caveolae to the SNARE complex which allows GSV fusion with the plasma membrane. This could suggest that GSV fusion with the plasma membrane occurs at the caveolae, which would mean that GLUT4 does translocate to caveolae. Some of the difficulty in observing GLUT4 in caveolae could be due to the fact that insulin has been shown to promote GLUT4 dispersal throughout the plasma membrane (Stenkula et al. 2010), meaning GLUT4 may rapidly move away from caveolae.

PLA could be used to further probe the question of whether GLUT4 translocates to the caveolae, by examining pairwise interactions between GLUT4 and caveolae components such as Cav1 and EHD2, both under basal conditions and under a range of insulin stimulation timepoints. Alternatively, more modern microscopy techniques could be employed to better understand how GLUT4 translocates to the plasma membrane, such as single molecule localization microscopy (SMLM). One type of SMLM, direct stochastic optical reconstruction microscopy (dSTORM) has been used to quantitatively image GLUT4 in the plasma membrane of 3T3-L1adipocytes (Herdly et al. 2023). Dual-colour dSTORM, which would be required to use the technique to measure co-localisation between GLUT4 and Cav1, has been done in a number of studies (Maß, Holtmannspötter, and Zachgo 2020; Puthukodan et al. 2023), and so it may be possible to determine whether GLUT4 initially translocates to caveolae by using SMLM techniques to

measure co-localisation in extremely high resolution between GLUT4 and Cav1 at the adipocyte plasma membrane under a range of insulin stimulation timepoints.

6.3 Conclusions

The data presented in this thesis provide new insights into the mechanisms linking signals from the insulin receptor to the SNARE membrane fusion machinery required for insulin stimulated GLUT4 translocation to the plasma membrane. Sx4, a key SNARE protein in GSV fusion with the plasma membrane, has been found to be in close proximity to both IR and caveolae component Cav1, revealing caveolae as a potential site of IR phosphorylation of Sx4. Furthermore, the caveolae component EHD2 has been shown to play a key role in insulin stimulated SNARE complex formation and subsequent glucose transport, highlighting the importance of caveolae in insulin action and glucose transport in adipocytes. Insulin stimulated GLUT4 translocation to the plasma membrane, which is controlled by the SNARE proteins examined here, is disrupted in people with type 2 diabetes and insulin resistance (Zierath et al. 1996; Gonzalez et al. 2011; Tan et al. 2015), and so achieving greater clarity on this process could prove vital for our understanding of these complex conditions.

Appendices

Appendix I. Plasmid map

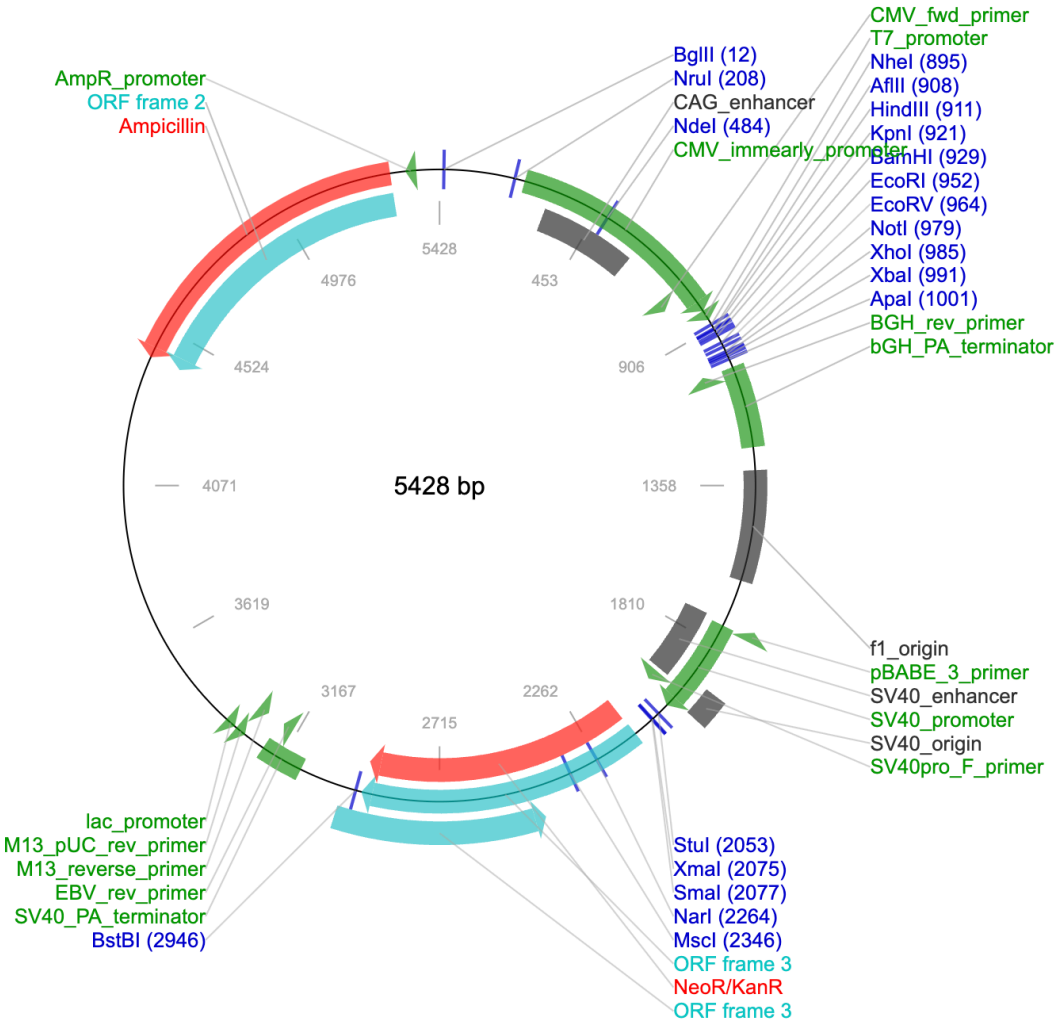

Appendix I. Map of original empty pcDNA3.1 plasmid used to generate Myc-tagged WT Syntaxin4 (Sx4), double phospho-mimetic Sx4 (Y115E, Y251E), or double phospho-resistant Sx4 (Y115F, Y251F) expression plasmids. Map suppled from Addgene Vector Database.

References

Araki, E., C. R. Kahn, and M. Shichiri. 1994. “Characterization of the IRS-1 (Insulin Receptor Substrate-1) Gene and Its Promoter.” *Nihon Rinsho, Japanese Journal of Clinical Medicine* 52 (10): 2659–64. https://pubmed.ncbi.nlm.nih.gov/7983795/.

Aran, Veronica, Nia J Bryant, and Gwyn W Gould. 2011. “Tyrosine Phosphorylation of Munc18c on Residue 521 Abrogates Binding to Syntaxin 4.” *BMC Biochemistry* 12 (1): 19. https://doi.org/10.1186/1471-2091-12-19.

Baker, Richard W., and Frederick M. Hughson. 2016. “Chaperoning SNARE Assembly and Disassembly.” *Nature Reviews Molecular Cell Biology*. Nature Publishing Group. https://doi.org/10.1038/nrm.2016.65.

Bakke, Jesse, Ahmed Bettaieb, Naoto Nagata, Kosuke Matsuo, and Fawaz G. Haj. 2013. “Regulation of the SNARE-Interacting Protein Munc18c Tyrosine Phosphorylation in Adipocytes by Protein-Tyrosine Phosphatase 1B.” *Cell Communication and Signaling* 11 (1): 1–12. https://doi.org/10.1186/1478-811X-11-57/FIGURES/6.

Bennett, Mark K., JoséE E. Garcia-Arrarás, Lisa A. Elferink, Karen Peterson, Anne M. Fleming, Christopher D. Hazuka, and Richard H. Scheller. 1993. “The Syntaxin Family of Vesicular Transport Receptors.” *Cell* 74 (5): 863–73. https://doi.org/10.1016/0092-8674(93)90466-4.

Black, Hannah L., Rachel Livingstone, Cynthia C. Mastick, Mohammed Al Tobi, Holly Taylor, Angéline Geiser, Laura Stirrat, et al. 2022. “Knockout of Syntaxin-4 in 3T3-L1 Adipocytes Reveals New Insight into GLUT4 Trafficking and Adiponectin Secretion.” *Journal of Cell Science* 135 (1). https://doi.org/10.1242/JCS.258375.

Black, Hannah Lucy. 2016. “Impact of Tyrosine Phosphorylation of Syntaxin 4 and Munc18c on GLUT4 Translocation.” http://theses.gla.ac.uk/8181/1/2016BlackPhD.pdf.

Bloch, Robert. 1973. “Inhibition of Glucose Transport in the Human Erythrocyte by Cytochalasin B.” *Biochemistry* 12 (23): 4799–4801. https://doi.org/10.1021/BI00747A036.

Blot, Vincent, and Timothy E. McGraw. 2006. “GLUT4 Is Internalized by a Cholesterol-Dependent Nystatin-Sensitive Mechanism Inhibited by Insulin.” *The EMBO Journal* 25 (24): 5648–58. https://doi.org/10.1038/SJ.EMBOJ.7601462.

Blouin, Cédric M., Cécilia Prado, Karen K. Takane, Françoise Lasnier, Adolfo Garcia-Ocana, Pascal Ferré, Isabelle Dugail, and Eric Hajduch. 2010. “Plasma Membrane Subdomain Compartmentalization Contributes to Distinct Mechanisms of Ceramide Action on Insulin Signaling.” *Diabetes* 59 (3): 600–610. https://doi.org/10.2337/DB09-0897.

Bolte, S., and F. P. Cordelières. 2006. “A Guided Tour into Subcellular Colocalization Analysis in Light Microscopy.” *Journal of Microscopy* 224 (Pt 3): 213–32. https://doi.org/10.1111/J.1365-2818.2006.01706.X.

Brandie, Fiona M., Veronica Aran, Avani Verma, James A. McNew, Nia J. Bryant, and Gwyn W. Gould. 2008. “Negative Regulation of Syntaxin4/SNAP-23/VAMP2-Mediated Membrane Fusion by Munc18c In Vitro.” *PLoS ONE* 3 (12). https://doi.org/10.1371/journal.pone.0004074.

Brännmark, Cecilia, Emma I. Kay, Unn Örtegren Kugelberg, Belén Chanclón, Man Mohan Shrestha, Ingrid Wernstedt Asterholm, Peter Strålfors, and Charlotta S. Olofsson. 2020. “Adiponectin Is Secreted via Caveolin 1-Dependent Mechanisms in White Adipocytes.” *The Journal of Endocrinology* 247 (1): 25–38. https://doi.org/10.1530/JOE-20-0078.

Bremner, Shaun K., Woroud S. Al Shammari, Roderick S. Milligan, Brian D. Hudson, Calum Sutherland, Nia J. Bryant, and Gwyn W. Gould. 2022. “Pleiotropic Effects of Syntaxin16 Identified by Gene Editing in Cultured Adipocytes.” *Frontiers in Cell and Developmental Biology* 10 (November). https://doi.org/10.3389/FCELL.2022.1033501.

Bruno, Joanne, Alexandria Brumfield, Natasha Chaudhary, David Iaea, and Timothy E. McGraw. 2016. “SEC16A Is a RAB10 Effector Required for Insulinstimulated GLUT4 Trafficking in Adipocytes.” *Journal of Cell Biology* 214 (1): 61–76. https://doi.org/10.1083/jcb.201509052.

Bryant, Nia J., and Gwyn W. Gould. 2011. “SNARE Proteins Underpin Insulin-Regulated GLUT4 Traffic.” *Traffic* 12 (6): 657–64. https://doi.org/10.1111/j.1600-0854.2011.01163.x.

Callera, G.E., Thiago Bruder-Nascimento, and R.M. Touyz. 2017. “Assessment of Caveolae/Lipid Rafts in Isolated Cells,” no. January 2017: 251–68. https://doi.org/10.1007/978-1-4939-6625-7.

Camus, Stéphane, Marine Camus, Carmen Figueras-Novoa, Gaelle Boncompain, L. Sadacca, Christopher Esk, Anne Bigot, et al. 2019. “CHC22 Clathrin Mediates Traffic from Early Secretory Compartments for Human GLUT4 Pathway Biogenesis.” *Journal of Cell Biology*. https://doi.org/10.1083/jcb.201812135.

Chen, Yang, Lili Huang, Xinzhou Qi, and Chen Chen. 2019. “Insulin Receptor

Trafficking: Consequences for Insulin Sensitivity and Diabetes." *International Journal of Molecular Sciences* 20 (20). https://doi.org/10.3390/IJMS20205007.

Chen, Yu, Yan Wang, Jinzhong Zhang, Yongqiang Deng, Li Jiang, Eli Song, Xufeng S. Wu, John A. Hammer, Tao Xu, and Jennifer Lippincott-Schwartz. 2012. "Rab10 and Myosin-va Mediate Insulin-Stimulated GLUT4 Storage Vesicle Translocation in Adipocytes." *Journal of Cell Biology* 198 (4): 545–60. https://doi.org/10.1083/jcb.201111091.

Cristancho, Ana G., and Mitchell A. Lazar. 2011. "Forming Functional Fat: A Growing Understanding of Adipocyte Differentiation." *Nature Reviews. Molecular Cell Biology* 12 (11): 722. https://doi.org/10.1038/NRM3198.

Cushman, S. W., and L. J. Wardzala. 1980. "Potential Mechanism of Insulin Action on Glucose Transport in the Isolated Rat Adipose Cell. Apparent Translocation of Intracellular Transport Systems to the Plasma Membrane." *Journal of Biological Chemistry* 255 (10): 4758–62.

D'Andrea-Merrins, Matthew, Louise Chang, Alice D. Lam, Stephen A. Ernst, and Edward L. Stuenkel. 2007. "Munc18c Interaction with Syntaxin 4 Monomers and SNARE Complex Intermediates in GLUT4 Vesicle Trafficking." *The Journal of Biological Chemistry* 282 (22): 16553–66. https://doi.org/10.1074/JBC.M610818200.

Daumke, Oliver, Richard Lundmark, Yvonne Vallis, Sascha Martens, P. Jonathan G. Butler, and Harvey T. McMahon. 2007. "Architectural and Mechanistic Insights into an EHD ATPase Involved in Membrane Remodelling." *Nature* 449 (7164): 923–27. https://doi.org/10.1038/NATURE06173.

Diabetes UK. 2019. "Us, Diabetes and a Lot of Facts and Stats," 1–48. https://www.diabetes.org.uk/resources-s3/2019-11/facts-stats-update-oct-2019.pdf.

Duan, Xiaowen, Dougall M. Norris, Sean J. Humphrey, Pengyi Yang, Kristen C. Cooke, Will P. Bultitude, Benjamin L. Parker, et al. 2022. "Trafficking Regulator of GLUT4-1 (TRARG1) Is a GSK3 Substrate." *Biochemical Journal* 479 (11): 1237–56. https://doi.org/10.1042/BCJ20220153.

Dulubova, Irina, Shuzo Sugita, Sandra Hill, Masahiro Hosaka, Imma Fernandez, Thomas C. Südhof, and Josep Rizo. 1999. "A Conformational Switch in Syntaxin during Exocytosis: Role of Munc18." *The EMBO Journal* 18 (16): 4372–82. https://doi.org/10.1093/EMBOJ/18.16.4372.

Ebina, Yousuke, Leland Ellis, Kurt Jarnagin, Marc Edery, Laszlo Graf, Eric Clauser, Jing hsiung Ou, et al. 1985. “The Human Insulin Receptor CDNA: The Structural Basis for Hormone-Activated Transmembrane Signalling.” *Cell*. https://doi.org/10.1016/0092-8674(85)90334-4.

Eguez, Lorena, Adrian Lee, Jose A. Chavez, Cristinel P. Miinea, Susan Kane, Gustav E. Lienhard, and Timothy E. McGraw. 2005. “Full Intracellular Retention of GLUT4 Requires AS160 Rab GTPase Activating Protein.” *Cell Metabolism* 2 (4): 263–72. https://doi.org/10.1016/j.cmet.2005.09.005.

Fagerholm, Siri, Unn Örtegren, Margareta Karlsson, Iida Ruishalme, and Peter Strålfors. 2009. “Rapid Insulin-Dependent Endocytosis of the Insulin Receptor by Caveolae in Primary Adipocytes.” *PloS One* 4 (6). https://doi.org/10.1371/JOURNAL.PONE.0005985.

Fasshauer, Dirk, R. Bryan Sutton, Axel T. Brunger, and Reinhard Jahn. 1998. “Conserved Structural Features of the Synaptic Fusion Complex: SNARE Proteins Reclassified as Q- and R-SNAREs.” *Proceedings of the National Academy of Sciences of the United States of America* 95 (26): 15781–86. https://doi.org/10.1073/pnas.95.26.15781.

Fernandez, Imma, Josep Ubach, Irina Dulubova, Xiangyang Zhang, Thomas C. Südhof, and Josep Rizo. 1998. “Three-Dimensional Structure of an Evolutionarily Conserved N-Terminal Domain of Syntaxin 1A.” *Cell* 94 (6): 841–49. https://doi.org/10.1016/S0092-8674(00)81742-0.

Foti, Michelangelo, Geneviève Porcheron, Margot Fournier, Christine Maeder, and Jean Louis Carpentier. 2007. “The Neck of Caveolae Is a Distinct Plasma Membrane Subdomain That Concentrates Insulin Receptors in 3T3-L1 Adipocytes.” *Proceedings of the National Academy of Sciences of the United States of America* 104 (4): 1242–47. https://doi.org/10.1073/pnas.0610523104.

Fryklund, Claes, Björn Morén, Shrenika Shah, Mario Grossi, Eva Degerman, Claudia Matthaeus, and Karin G. Stenkula. 2021. “EH Domain-Containing 2 Deficiency Restricts Adipose Tissue Expansion and Impairs Lipolysis in Primary Inguinal Adipocytes.” *Frontiers in Physiology* 12 (September). https://doi.org/10.3389/FPHYS.2021.740666.

Garrido-Sanchez, Lourdes, Xavier Escote, Leticia Coin-Aragüez, Jose Carlos Fernandez-Garcia, Rajaa El Bekay, Joan Vendrell, Eduardo Garcia-Fuentes, and Francisco J. Tinahones. 2013. “Munc18c in Adipose Tissue Is Downregulated in Obesity and Is Associated with Insulin.” *PLOS ONE* 8 (5): e63937. https://doi.org/10.1371/JOURNAL.PONE.0063937.

González-Muñoz, Elena, Carmen López-Iglesias, Maria Calvo, Manuel Palacín, Antonio Zorzano, and Marta Camps. 2009. “Caveolin-1 Loss of Function Accelerates Glucose Transporter 4 and Insulin Receptor Degradation in 3T3-L1 Adipocytes.” *Endocrinology* 150 (8): 3493–3502. https://doi.org/10.1210/en.2008-1520.

Gonzalez, Eva, Emily Flier, Dorothee Molle, Domenico Accili, and Timothy E. McGraw. 2011. “Hyperinsulinemia Leads to Uncoupled Insulin Regulation of the GLUT4 Glucose Transporter and the FoxO1 Transcription Factor.” *Proceedings of the National Academy of Sciences of the United States of America* 108 (25): 10162–67. https://doi.org/10.1073/pnas.1019268108.

Gonzalez, Eva, and Timothy E. McGraw. 2009. “Insulin-Modulated Akt Subcellular Localization Determines Akt Isoform-Specific Signaling.” *Proceedings of the National Academy of Sciences of the United States of America* 106 (17): 7004–9. https://doi.org/10.1073/pnas.0901933106.

Goodyear, Laurie J., Michael F. Hirshman, Raffaele Napoli, Jorge Calles, Jeffrey F. Markuns, Olle Ljungqvist, and Edward S. Horton. 1996. “Glucose Ingestion Causes GLUT4 Translocation in Human Skeletal Muscle.” *Diabetes* 45 (8): 1051–56. https://doi.org/10.2337/diab.45.8.1051.

Gustavsson, Johanna, Santiago Parpal, Margareta Karlsson, Cecilia Ramsing, Hans Thorn, Marie Borg, Margaretha Lindroth, Kajsa Holmgren Peterson, Karl-Eric Magnusson, and Peter Strålfors. 1999. “Localization of the Insulin Receptor in Caveolae of Adipocyte Plasma Membrane.” *The FASEB Journal* 13 (14): 1961–71. https://doi.org/10.1096/fasebj.13.14.1961.

Gustavsson, Johanna, Santiago Parpal, and Peter Strålfors. 1996. “Insulin-Stimulated Glucose Uptake Involves the Transition of Glucose Transporters to a Caveolae-Rich Fraction within the Plasma Membrane: Implications for Type II Diabetes.” *Molecular Medicine* 2 (3): 367. https://doi.org/10.1007/bf03401634.

Haeusler, Rebecca A., Timothy E. McGraw, and Domenico Accili. 2018. “Metabolic Signalling: Biochemical and Cellular Properties of Insulin Receptor Signalling.” *Nature Reviews Molecular Cell Biology* 19 (1): 31–44. https://doi.org/10.1038/nrm.2017.89.

Hancock, Melissa L., Rebecca C. Meyer, Meeta Mistry, Radhika S. Khetani, Alexandre Wagschal, Taehwan Shin, Shannan J. Ho Sui, Anders M. Näär, and John G. Flanagan. 2019. “Insulin Receptor Associates with

Promoters Genome-Wide and Regulates Gene Expression." *Cell* 177 (3): 722-736.e22. https://doi.org/10.1016/j.cell.2019.02.030.

Herdly, Lucas, Peter W. Tinning, Angéline Geiser, Holly Taylor, Gwyn W. Gould, and Sebastian van de Linde. 2023. "Benchmarking Thiolate-Driven Photoswitching of Cyanine Dyes." *The Journal of Physical Chemistry. B* 127 (3): 732–41. https://doi.org/10.1021/ACS.JPCB.2C06872.

Higuchi, Yusuke, Takehiro Ogata, Naohiko Nakanishi, Masahiro Nishi, Akira Sakamoto, Yumika Tsuji, Shinya Tomita, and Satoaki Matoba. 2022. "Requirement of Cavin-2 for the Expression and Stability of IRβ in Adequate Adipocyte Differentiation." *Molecular Metabolism* 55 (January). https://doi.org/10.1016/J.MOLMET.2021.101416.

Hoernke, Maria, Jagan Mohan, Elin Larsson, Jeanette Blomberg, Dana Kahra, Sebastian Westenhoff, Christian Schwieger, and Richard Lundmark. 2017. "EHD2 Restrains Dynamics of Caveolae by an ATP-Dependent, Membrane-Bound, Open Conformation." *Proceedings of the National Academy of Sciences of the United States of America* 114 (22): E4360–69. https://doi.org/10.1073/PNAS.1614066114.

Hua, Yongjie, Shanshan Ke, Yao Wang, David M. Irwin, Shuyi Zhang, and Zhe Wang. 2016. "Prolonged Treatment with 3-Isobutyl-1-Methylxanthine Improves the Efficiency of Differentiating 3T3-L1 Cells into Adipocytes." *Analytical Biochemistry* 507 (August): 18–20. https://doi.org/10.1016/J.AB.2016.05.007.

Hubert, Madlen, Elin Larsson, Naga Venkata Gayathri Vegesna, Maria Ahnlund, Annika I. Johansson, Lindon W.K. Moodie, and Richard Lundmark. 2020. "Lipid Accumulation Controls the Balance between Surface Connection and Scission of Caveolae." *ELife* 9 (May): 1–31. https://doi.org/10.7554/ELIFE.55038.

Ishikura, Shuhei, Philip J. Bilan, and Amira Klip. 2007. "Rabs 8A and 14 Are Targets of the Insulin-Regulated Rab-GAP AS160 Regulating GLUT4 Traffic in Muscle Cells." *Biochemical and Biophysical Research Communications* 353 (4): 1074–79. https://doi.org/10.1016/j.bbrc.2006.12.140.

Jahn, Reinhard. 2000. "Sec1/Munc18 Proteins: Mediators of Membrane Fusion Moving to Center Stage." *Neuron*. Cell Press. https://doi.org/10.1016/S0896-6273(00)00029-5.

Jaldin-Fincati, Javier R., Martin Pavarotti, Scott Frendo-Cumbo, Philip J. Bilan, and Amira Klip. 2017. "Update on GLUT4 Vesicle Traffic: A Cornerstone of Insulin Action." *Trends in Endocrinology and Metabolism*.

https://doi.org/10.1016/j.tem.2017.05.002.

Jedrychowski, Mark P., Carlos A. Gartner, Steven P. Gygi, Li Zhou, Joachim Herz, Konstantin V. Kandror, and Paul F. Pilch. 2010. “Proteomic Analysis of GLUT4 Storage Vesicles Reveals LRP1 to Be an Important Vesicle Component and Target of Insulin Signaling.” *Journal of Biological Chemistry* 285 (1): 104–14. https://doi.org/10.1074/jbc.M109.040428.

Jewell, Jenna L, Eunjin Oh, Latha Ramalingam, Michael A Kalwat, Vincent S Tagliabracci, Lixuan Tackett, Jeffrey S Elmendorf, and Debbie C Thurmond. 2011. “Munc18c Phosphorylation by the Insulin Receptor Links Cell Signaling Directly to SNARE Exocytosis.” *The Journal of Cell Biology* 193 (1): 185–99. https://doi.org/10.1083/jcb.201007176.

Kahn, B B. 1994. “Dietary Regulation of Glucose Transporter Gene Expression: Tissue Specific Effects in Adipose Cells and Muscle.” *The Journal of Nutrition* 124 (8 Suppl): 1289S-1295S. https://doi.org/10.1093/jn/124.suppl_8.1289S.

Kajno, Esi, Timothy E. McGraw, and Eva Gonzalez. 2015. “Development of a New Model System to Dissect Isoform Specific Akt Signalling in Adipocytes.” *Biochemical Journal* 468 (3): 425–34. https://doi.org/10.1042/BJ20150191.

Karhan, Asuman Nur, Jamila Zammouri, Martine Auclair, Emilie Capel, Feramuz Demir Apaydin, Fehmi Ates, Marie Christine Verpont, et al. 2021. “Biallelic CAV1 Null Variants Induce Congenital Generalized Lipodystrophy with Achalasia.” *European Journal of Endocrinology* 185 (6): 841–54. https://doi.org/10.1530/EJE-21-0915.

Karlsson, Margareta, Hans Thorn, Anna Danielsson, Karin G. Stenkula, Anita Öst, Johanna Gustavsson, Fredrik H. Nystrom, and Peter Strålfors. 2004. “Colocalization of Insulin Receptor and Insulin Receptor Substrate-1 to Caveolae in Primary Human Adipocytes: Cholesterol Depletion Blocks Insulin Signalling for Metabolic and Mitogenic Control.” *European Journal of Biochemistry* 271 (12): 2471–79. https://doi.org/10.1111/j.1432-1033.2004.04177.x.

Karlsson, Margareta, Hans Thorn, Santiago Parpal, Peter Strålfors, and Johanna Gustavsson. 2002. “Insulin Induces Translocation of Glucose Transporter GLUT4 to Plasma Membrane Caveolae in Adipocytes.” *The FASEB Journal : Official Publication of the Federation of American Societies for Experimental Biology* 16 (2): 249–51. https://doi.org/10.1096/fj.01-0646fje.

Kasuga, Masato, Yehiel Zick, Diana L. Blithe, Marco Crettaz, and C. Ronald Kahn. 1982. “Insulin Stimulates Tyrosine Phosphorylation of the Insulin Receptor in a Cell-Free System.” *Nature* 298 (5875): 667–69. https://doi.org/10.1038/298667a0.

Kawaguchi, Takayuki, Yoshikazu Tamori, Hajime Kanda, Mari Yoshikawa, Sanshiro Tateya, Naonobu Nishino, and Masato Kasuga. 2010. “The T-SNAREs Syntaxin4 and SNAP23 but Not v-SNARE VAMP2 Are Indispensable to Tether GLUT4 Vesicles at the Plasma Membrane in Adipocyte.” *Biochemical and Biophysical Research Communications* 391 (3): 1336–41. https://doi.org/10.1016/J.BBRC.2009.12.045.

Keller, Susanna R., Ann C. Davis, and Kevin B. Clairmont. 2002. “Mice Deficient in the Insulin-Regulated Membrane Aminopeptidase Show Substantial Decreases in Glucose Transporter GLUT4 Levels but Maintain Normal Glucose Homeostasis.” *Journal of Biological Chemistry* 277 (20): 17677–86. https://doi.org/10.1074/jbc.M202037200.

Kim, C. A., Marc Delépine, Emilie Boutet, Haquima El Mourabit, Soazig Le Lay, Muriel Meier, Mona Nemani, et al. 2008. “Association of a Homozygous Nonsense Caveolin-1 Mutation with Berardinelli-Seip Congenital Lipodystrophy.” *The Journal of Clinical Endocrinology and Metabolism* 93 (4): 1129–34. https://doi.org/10.1210/JC.2007-1328.

Kimura, Akiko, Silvia Mora, Satoshi Shigematsu, Jeffrey E. Pessin, and Alan R. Saltiel. 2002. “The Insulin Receptor Catalyzes the Tyrosine Phosphorylation of Caveolin-1.” *The Journal of Biological Chemistry* 277 (33): 30153–58. https://doi.org/10.1074/JBC.M203375200.

Kioumourtzoglou, D., G. W. Gould, and N. J. Bryant. 2014. “Insulin Stimulates Syntaxin4 SNARE Complex Assembly via a Novel Regulatory Mechanism.” *Molecular and Cellular Biology* 34 (7): 1271–79. https://doi.org/10.1128/mcb.01203-13.

Kitamura, Tadahiro, C. Ronald Kahn, and Domenico Accili. 2003. “Insulin Receptor Knockout Mice.” *Annual Review of Physiology* 65: 313–32. https://doi.org/10.1146/ANNUREV.PHYSIOL.65.092101.142540.

Klaesson, Axel, Karin Grannas, Tonge Ebai, Johan Heldin, Björn Koos, Mattias Leino, Doroteya Raykova, et al. 2018. “Improved Efficiency of in Situ Protein Analysis by Proximity Ligation Using UnFold Probes.” *Scientific Reports* 8 (1). https://doi.org/10.1038/S41598-018-23582-1.

Klip, Amira, Timothy E. McGraw, and David E. James. 2019. “Thirty Sweet Years of GLUT4.” *Journal of Biological Chemistry* 294 (30): 11369–81. https://doi.org/10.1074/jbc.rev119.008351.

Kohn, A D, K S Kovacina, and R A Roth. 1995. “Insulin Stimulates the Kinase Activity of RAC-PK, a Pleckstrin Homology Domain Containing Ser/Thr Kinase.” *The EMBO Journal* 14 (17): 4288–95. http://www.ncbi.nlm.nih.gov/pubmed/7556070.

Kuhné, Michelle R., Zhizhuang Zhao, Joie Rowles, Brian E. Lavan, Shi Hsiang Shen, Edmond H. Fischer, and Gustav E. Lienhard. 1994. “Dephosphorylation of Insulin Receptor Substrate 1 by the Tyrosine Phosphatase PTP2C.” *Journal of Biological Chemistry* 269 (22): 15833–37.

Kweon, Dae Hyuk, Byoungjae Kong, and Yeon Kyun Shin. 2017. “Hemifusion in Synaptic Vesicle Cycle.” *Frontiers in Molecular Neuroscience* 10 (March). https://doi.org/10.3389/FNMOL.2017.00065.

Lamaze, Christophe, Nicolas Tardif, Melissa Dewulf, Stéphane Vassilopoulos, and Cédric M. Blouin. 2017. “The Caveolae Dress Code: Structure and Signaling.” *Current Opinion in Cell Biology*. Elsevier Ltd. https://doi.org/10.1016/j.ceb.2017.02.014.

Lavan, Brian E., William S. Lane, and Gustav E. Lienhard. 1997. “The 60-KDa Phosphotyrosine Protein in Insulin-Treated Adipocytes Is a New Member of the Insulin Receptor Substrate Family.” *The Journal of Biological Chemistry* 272 (17): 11439–43. https://doi.org/10.1074/JBC.272.17.11439.

Lawrence, Michael C. 2021. “Understanding Insulin and Its Receptor from Their Three-Dimensional Structures.” *Molecular Metabolism* 52 (October). https://doi.org/10.1016/J.MOLMET.2021.101255.

Lee, H., D. Volonte, F. Galbiati, P. Iyengar, D. M. Lublin, D. B. Bregman, M. T. Wilson, et al. 2000. “Constitutive and Growth Factor-Regulated Phosphorylation of Caveolin-1 Occurs at the Same Site (Tyr-14) in Vivo: Identification of a c-Src/Cav-1/Grb7 Signaling Cassette.” *Molecular Endocrinology (Baltimore, Md.)* 14 (11): 1750–75. https://doi.org/10.1210/MEND.14.11.0553.

Liu, Libin, Dennis Brown, Mary McKee, Nathan K. LeBrasseur, Dan Yang, Kenneth H. Albrecht, Katya Ravid, and Paul F. Pilch. 2008. “Deletion of Cavin/PTRF Causes Global Loss of Caveolae, Dyslipidemia, and Glucose Intolerance.” *Cell Metabolism* 8 (4): 310–17. https://doi.org/10.1016/J.CMET.2008.07.008.

Livingstone, Rachel. 2021. “The Role of Syntaxin 4 in the Regulation of Glucose Transport in Fat and Muscle.”

López-Cano, Marc, Víctor Fernández-Dueñas, and Francisco Ciruela. 2019. "Proximity Ligation Assay Image Analysis Protocol: Addressing Receptor-Receptor Interactions." *Methods in Molecular Biology (Clifton, N.J.)* 2040: 41–50. https://doi.org/10.1007/978-1-4939-9686-5_3.

Ludwig, Alexander, Gillian Howard, Carolina Mendoza-Topaz, Thomas Deerinck, Mason Mackey, Sara Sandin, Mark H. Ellisman, and Benjamin J. Nichols. 2013. "Molecular Composition and Ultrastructure of the Caveolar Coat Complex." *PLoS Biology* 11 (8). https://doi.org/10.1371/JOURNAL.PBIO.1001640.

Manning, Brendan D., and Alex Toker. 2017. "AKT/PKB Signaling: Navigating the Network." *Cell*. Cell Press. https://doi.org/10.1016/j.cell.2017.04.001.

Maß, Lucia, Michael Holtmannspötter, and Sabine Zachgo. 2020. "Dual-Color 3D-DSTORM Colocalization and Quantification of ROXY1 and RNAPII Variants throughout the Transcription Cycle in Root Meristem Nuclei." *The Plant Journal : For Cell and Molecular Biology* 104 (5): 1423–36. https://doi.org/10.1111/TPJ.14986.

Matthaeus, Claudia, Ines Lahmann, Séverine Kunz, Wenke Jonas, Arthur Alves Melo, Martin Lehmann, Elin Larsson, et al. 2020. "EHD2-Mediated Restriction of Caveolar Dynamics Regulates Cellular Fatty Acid Uptake." *Proceedings of the National Academy of Sciences of the United States of America* 117 (13): 7471–81. https://doi.org/10.1073/PNAS.1918415117/-/DCSUPPLEMENTAL.

Matthaeus, Claudia, and Justin W. Taraska. 2021. "Energy and Dynamics of Caveolae Trafficking." *Frontiers in Cell and Developmental Biology* 8 (January). https://doi.org/10.3389/FCELL.2020.614472.

McNew, J A, F Parlati, R Fukuda, R J Johnston, K Paz, F Paumet, T H Söllner, and J E Rothman. 2000. "Compartmental Specificity of Cellular Membrane Fusion Encoded in SNARE Proteins." *Nature* 407 (6801): 153–59. https://doi.org/10.1038/35025000.

Min, Jing, Shuichi Okada, Makoto Kanzaki, Jeffrey S. Elmendorf, Kenneth J. Coker, Brian P. Ceresa, Li Jyun Syu, Yoichi Noda, Alan R. Saltiel, and Jeffrey E. Pessin. 1999. "Synip: A Novel Insulin-Regulated Syntaxin 4–Binding Protein Mediating GLUT4 Translocation in Adipocytes." *Molecular Cell* 3 (6): 751–60. https://doi.org/10.1016/S1097-2765(01)80007-1.

Morén, Björn, Björn Hansson, Florentina Negoita, Claes Fryklund, Richard Lundmark, Olga Göransson, and Karin G. Stenkula. 2019. "EHD2

Regulates Adipocyte Function and Is Enriched at Cell Surface-Associated Lipid Droplets in Primary Human Adipocytes." *Molecular Biology of the Cell* 30 (10): 1147–59. https://doi.org/10.1091/MBC.E18-10-0680.

Morén, Björn, Claudio Shah, Mark T. Howes, Nicole L. Schieber, Harvey T. McMahon, Robert G. Parton, Oliver Daumke, and Richard Lundmark. 2012. "EHD2 Regulates Caveolar Dynamics via ATP-Driven Targeting and Oligomerization." *Molecular Biology of the Cell* 23 (7): 1316–29. https://doi.org/10.1091/MBC.E11-09-0787.

Moreno-Castellanos, Natalia, Amaia Rodríguez, Yoana Rabanal-Ruiz, Alejandro Fernández-Vega, José López-Miranda, Rafael Vázquez-Martínez, Gema Frühbeck, and María M. Malagón. 2017. "The Cytoskeletal Protein Septin 11 Is Associated with Human Obesity and Is Involved in Adipocyte Lipid Storage and Metabolism." *Diabetologia* 60 (2): 324–35. https://doi.org/10.1007/S00125-016-4155-5.

Müller, Günter, Christian Jung, Susanne Wied, Stefan Welte, Holger Jordan, and Wendelin Frick. 2001. "Redistribution of Glycolipid Raft Domain Components Induces Insulin-Mimetic Signaling in Rat Adipocytes." *Molecular and Cellular Biology* 21 (14): 4553–67. https://doi.org/10.1128/MCB.21.14.4553-4567.2001.

Naslavsky, Naava, and Steve Caplan. 2011. "EHD Proteins: Key Conductors of Endocytic Transport." *Trends in Cell Biology* 21 (2): 122–31. https://doi.org/10.1016/J.TCB.2010.10.003.

Ng, Yvonne, Georg Ramm, James G. Burchfield, Adelle C.F. Coster, Jacqueline Stöckli, and David E. James. 2010. "Cluster Analysis of Insulin Action in Adipocytes Reveals a Key Role for Akt at the Plasma Membrane." *Journal of Biological Chemistry* 285 (4): 2245–57. https://doi.org/10.1074/jbc.M109.060236.

Nilsson, Rebecka, Faiyaz Ahmad, Karl Swärd, Ulrika Andersson, Marie Weston, Vincent Manganiello, and Eva Degerman. 2006. "Plasma Membrane Cyclic Nucleotide Phosphodiesterase 3B (PDE3B) Is Associated with Caveolae in Primary Adipocytes." *Cellular Signalling* 18 (10): 1713–21. https://doi.org/10.1016/J.CELLSIG.2006.01.010.

Okada, Shuichi, Kihachi Ohshima, Yutaka Uehara, Hiroyuki Shimizu, Koshi Hashimoto, Masanobu Yamada, and Masatomo Mori. 2007. "Synip Phosphorylation Is Required for Insulin-Stimulated Glut4 Translocation." *Biochemical and Biophysical Research Communications* 356 (1): 102–6. https://doi.org/10.1016/J.BBRC.2007.02.095.

Örtegren, Unn, Lan Yin, Anita Öst, Helen Karlsson, Fredrik H. Nystrom, and Peter Strålfors. 2006. “Separation and Characterization of Caveolae Subclasses in the Plasma Membrane of Primary Adipocytes; Segregation of Specific Proteins and Functions.” *The FEBS Journal* 273 (14): 3381–92. https://doi.org/10.1111/J.1742-4658.2006.05345.X.

Palacios-Ortega, Sara, Maider Varela-Guruceaga, Miriam Algarabel, Fermín Ignacio Milagro, J. Alfredo Martínez, and Carlos De Miguel. 2015. “Effect of TNF-Alpha on Caveolin-1 Expression and Insulin Signaling during Adipocyte Differentiation and in Mature Adipocytes.” *Cellular Physiology and Biochemistry* 36 (4): 1499–1516. https://doi.org/10.1159/000430314.

Palacios-Ortega, Sara, Maider Varela-Guruceaga, Fermín Ignacio Milagro, José Alfredo Martínez, and Carlos De Miguel. 2014. “Expression of Caveolin 1 Is Enhanced by DNA Demethylation during Adipocyte Differentiation. Status of Insulin Signaling.” *PLoS ONE* 9 (4). https://doi.org/10.1371/journal.pone.0095100.

Pan, Xiang, Nava Zaarur, Maneet Singh, Peter Morin, and Konstantin V. Kandror. 2017. “Sortilin and Retromer Mediate Retrograde Transport of Glut4 in 3T3-L1 Adipocytes.” *Molecular Biology of the Cell* 28 (12): 1667–75. https://doi.org/10.1091/mbc.E16-11-0777.

Parpal, Santiago, Margareta Karlsson, Hans Thorn, and Peter Strålfors. 2001. “Cholesterol Depletion Disrupts Caveolae and Insulin Receptor Signaling for Metabolic Control via Insulin Receptor Substrate-1, but Not for Mitogen-Activated Protein Kinase Control.” *Journal of Biological Chemistry* 276 (13): 9670–78. https://doi.org/10.1074/jbc.M007454200.

Pilch, Paul F., Ricardo P. Souto, Libin Liu, Mark P. Jedrychowski, Eric A. Berg, Catherine E. Costello, and Steven P. Gygi. 2007. “Cellular Spelunking: Exploring Adipocyte Caveolae.” *Journal of Lipid Research* 48 (10): 2103–11. https://doi.org/10.1194/jlr.R700009-JLR200.

Proctor, Kirsty M., Steven C.M. Miller, Nia J. Bryant, and Gwyn W. Gould. 2006. “Syntaxin 16 Controls the Intracellular Sequestration of GLUT4 in 3T3-L1 Adipocytes.” *Biochemical and Biophysical Research Communications*. https://doi.org/10.1016/j.bbrc.2006.06.135.

Puthukodan, Sujitha, Martina Hofmann, Mario Mairhofer, Hannah Janout, Jonas Schurr, Fabian Hauser, Christoph Naderer, et al. 2023. “Purification Analysis, Intracellular Tracking, and Colocalization of Extracellular Vesicles Using Atomic Force and 3D Single-Molecule Localization Microscopy.” *Analytical Chemistry* 95 (14). https://doi.org/10.1021/ACS.ANALCHEM.3C00144.

Ramm, Georg, Mark Larance, Michael Guilhaus, and David E. James. 2006. "A Role for 14-3-3 in Insulin-Stimulated GLUT4 Translocation through Its Interaction with the RabGAP AS160." *Journal of Biological Chemistry* 281 (39): 29174–80. https://doi.org/10.1074/jbc.M603274200.

Razani, Babak, Terry P. Combs, Xiao Bo Wang, Philippe G. Frank, David S. Park, Robert G. Russell, Maomi Li, et al. 2002. "Caveolin-1-Deficient Mice Are Lean, Resistant to Diet-Induced Obesity, and Show Hypertriglyceridemia with Adipocyte Abnormalities." *Journal of Biological Chemistry* 277 (10): 8635–47. https://doi.org/10.1074/jbc.M110970200.

Regazzetti, Claire, Karine Dumas, Sandra Lacas-Gervais, Faustine Pastor, Pascal Peraldi, Stéphanie Bonnafous, Isabelle Dugail, et al. 2015. "Hypoxia Inhibits Cavin-1 and Cavin-2 Expression and down-Regulates Caveolae in Adipocytes." *Endocrinology* 156 (3): 789–801. https://doi.org/10.1210/EN.2014-1656.

Robinson, Linda J., Suhong Pang, Diana S. Harris, John Heuser, and David E. James. 1992. "Translocation of the Glucose Transporter (GLUT4) to the Cell Surface in Permeabilized 3T3-L1 Adipocytes: Effects of ATP Insulin, and GTP Gamma S and Localization of GLUT4 to Clathrin Lattices." *The Journal of Cell Biology* 117 (6): 1181–96. https://doi.org/10.1083/JCB.117.6.1181.

Rodbell, M. 1964. "Metabolism of Isolated Fat Cells." *The Journal of Biological Chemistry* 239: 375–80. https://pubmed.ncbi.nlm.nih.gov/14169133/.

Ros-Baró, Anna, Carmen López-Iglesias, Sandra Peiró, David Bellido, Manuel Palacín, Antonio Zorzano, and Marta Camps. 2001. "Lipid Rafts Are Required for GLUT4 Internalization in Adipose Cells." *Proceedings of the National Academy of Sciences of the United States of America* 98 (21): 12050–55. https://doi.org/10.1073/pnas.211341698.

Sadler, Jessica B. A., Nia J. Bryant, and Gwyn W. Gould. 2015. "Characterization of VAMP Isoforms in 3T3-L1 Adipocytes: Implications for GLUT4 Trafficking." Edited by Patrick J. Brennwald. *Molecular Biology of the Cell* 26 (3): 530–36. https://doi.org/10.1091/mbc.E14-09-1368.

Sadler, Jessica B.A., Christopher A. Lamb, Gwyn W. Gould, and Nia J. Bryant. 2016. "Complete Membrane Fractionation of 3T3-L1 Adipocytes." *Cold Spring Harbor Protocols* 2016 (2): 193–98. https://doi.org/10.1101/PDB.PROT083691.

Sano, Hiroyuki, Lorena Eguez, Mary N. Teruel, Mitsunori Fukuda, Tuan D.

Chuang, Jose A. Chavez, Gustav E. Lienhard, and Timothy E. McGraw. 2007. “Rab10, a Target of the AS160 Rab GAP, Is Required for Insulin-Stimulated Translocation of GLUT4 to the Adipocyte Plasma Membrane.” *Cell Metabolism* 5 (4): 293–303. https://doi.org/10.1016/j.cmet.2007.03.001.

Sano, Hiroyuki, Susan Kane, Eiko Sano, Cristinel P. Mîinea, John M. Asara, William S. Lane, Charles W. Garner, and Gustav E. Lienhard. 2003. “Insulin-Stimulated Phosphorylation of a Rab GTPase-Activating Protein Regulates GLUT4 Translocation.” *Journal of Biological Chemistry* 278 (17): 14599–602. https://doi.org/10.1074/jbc.C300063200.

Scherer, Philipp E., Michael P. Lisanti, Giulia Baldini, Massimo Sargiacomo, Cynthia Corley Mastick, and Harvey F. Lodish. 1994. “Induction of Caveolin during Adipogenesis and Association of GLUT4 with Caveolin-Rich Vesicles.” *Journal of Cell Biology* 127 (5): 1233–43. https://doi.org/10.1083/jcb.127.5.1233.

Schmelzle, Katrin, Susan Kane, Scott Gridley, Gustav E. Lienhard, and Forest M. White. 2006. “Temporal Dynamics of Tyrosine Phosphorylation in Insulin Signaling.” *Diabetes* 55 (8): 2171–79. https://doi.org/10.2337/db06-0148.

Sekimoto, Junji, Kazuya Kabayama, Kazutoshi Gohara, and Jin Ichi Inokuchi. 2012. “Dissociation of the Insulin Receptor from Caveolae during TNFα-Induced Insulin Resistance and Its Recovery by D-PDMP.” *FEBS Letters* 586 (2): 191–95. https://doi.org/10.1016/J.FEBSLET.2011.12.019.

Shewan, Annette M., Ellen M. Van Dam, Sally Martin, Tang Bor Luen, Wanjin Hong, Nia J. Bryant, and David E. James. 2003. “GLUT4 Recycles via a Trans-Golgi Network (TGN) Subdomain Enriched in Syntaxins 6 and 16 but Not TGN38: Involvement of an Acidic Targeting Motif.” *Molecular Biology of the Cell* 14 (3): 973–86. https://doi.org/10.1091/mbc.E02-06-0315.

Shigematsu, Satoshi, Robert T. Watson, Ahmir H. Khan, and Jeffrey E. Pessin. 2003. “The Adipocyte Plasma Membrane Caveolin Functional/Structural Organization Is Necessary for the Efficient Endocytosis of GLUT4.” *The Journal of Biological Chemistry* 278 (12): 10683–90. https://doi.org/10.1074/JBC.M208563200.

Slot, Jan W., Hans J. Geuze, Sander Gigengack, Gustav E. Lienhard, and David E. James. 1991. “Immuno-Localization of the Insulin Regulatable Glucose Transporter in Brown Adipose Tissue of the Rat.” *The Journal of Cell Biology* 113 (1): 123–35. https://doi.org/10.1083/JCB.113.1.123.

Stenkula, Karin G., Vladimir A. Lizunov, Samuel W. Cushman, and Joshua Zimmerberg. 2010. “Insulin Controls the Spatial Distribution of GLUT4 on the Cell Surface through Regulation of Its Postfusion Dispersal.” *Cell Metabolism* 12 (3): 250–59. https://doi.org/10.1016/j.cmet.2010.08.005.

Stöckli, Jacqueline, Jonathan R. Davey, Cordula Hohnen-Behrens, Aimin Xu, David E. James, and Georg Ramm. 2008. “Regulation of Glucose Transporter 4 Translocation by the Rab Guanosine Triphosphatase-Activating Protein AS160/TBC1D4: Role of Phosphorylation and Membrane Association.” *Molecular Endocrinology* 22 (12): 2703–15. https://doi.org/10.1210/me.2008-0111.

Stoeber, Miriam, Ina Karen Stoeck, Christine HéCurrency Signnni, Christopher Karl Ernst Bleck, Giuseppe Balistreri, and Ari Helenius. 2012. “Oligomers of the ATPase EHD2 Confine Caveolae to the Plasma Membrane through Association with Actin.” *The EMBO Journal* 31 (10): 2350–64. https://doi.org/10.1038/EMBOJ.2012.98.

Strålfors, Peter. 2012. “Caveolins and Caveolae, Roles in Insulin Signalling and Diabetes.” *Advances in Experimental Medicine and Biology* 729: 111–26. https://doi.org/10.1007/978-1-4614-1222-9_8.

Struthers, Marion S., Scott G. Shanks, Chris MacDonald, Lindsay N. Carpp, Alicja M. Drozdowska, Dimitrios Kioumourtzoglou, Melonnie L.M. Furgason, Mary Munson, and Nia J. Bryant. 2009. “Functional Homology of Mammalian Syntaxin 16 and Yeast Tlg2p Reveals a Conserved Regulatory Mechanism.” *Journal of Cell Science* 122 (13): 2292–99. https://doi.org/10.1242/JCS.046441.

Südhof, Thomas C., and James E. Rothman. 2009. “Membrane Fusion: Grappling with SNARE and SM Proteins.” *Science*. NIH Public Access. https://doi.org/10.1126/science.1161748.

Sun, Xiao Jian, Paul Rothenberg, C. Ronald Kahn, Jonathan M. Backer, Eiichi Araki, Peter A. Wilden, Deborah A. Cahill, Barry J. Goldstein, and Morris F. White. 1991. “Structure of the Insulin Receptor Substrate IRS-1 Defines a Unique Signal Transduction Protein.” *Nature* 352 (6330): 73–76. https://doi.org/10.1038/352073a0.

Sun, Yi, Tim T. Chiu, Kevin P. Foley, Philip J. Bilan, and Amira Klip. 2014. “Myosin Va Mediates Rab8A-Regulated GLUT4 Vesicle Exocytosis in Insulin-Stimulated Muscle Cells.” *Molecular Biology of the Cell* 25 (7): 1159–70. https://doi.org/10.1091/mbc.E13-08-0493.

Tamori, Yoshikazu, Masatoshi Kawanishi, Toshiharu Niki, Hiroaki Shinoda, Satoshi Araki, Hideki Okazawa, and Masato Kasuga. 1998. “Inhibition of

Insulin-Induced GLUT4 Translocation by Munc18c through Interaction with Syntaxin4 in 3T3-L1 Adipocytes." *Journal of Biological Chemistry* 273 (31): 19740–46. https://doi.org/10.1074/jbc.273.31.19740.

Tamrakar, Akhilesh Kumar, Chandan K. Maurya, and Amit K. Rai. 2014. "PTP1B Inhibitors for Type 2 Diabetes Treatment: A Patent Review (2011 - 2014)." *Expert Opinion on Therapeutic Patents* 24 (10): 1101–15. https://doi.org/10.1517/13543776.2014.947268.

Tan, S.-X., Y. Ng, J. G. Burchfield, G. Ramm, D. G. Lambright, J. Stockli, and D. E. James. 2012. "The Rab GTPase-Activating Protein TBC1D4/AS160 Contains an Atypical Phosphotyrosine-Binding Domain That Interacts with Plasma Membrane Phospholipids To Facilitate GLUT4 Trafficking in Adipocytes." *Molecular and Cellular Biology* 32 (24): 4946–59. https://doi.org/10.1128/mcb.00761-12.

Tan, Shi Xiong, Kelsey H. Fisher-Wellman, Daniel J. Fazakerley, Yvonne Ng, Himani Pant, Jia Li, Christopher C. Meoli, Adelle C.F. Coster, Jacqueline Stöckli, and David E. James. 2015. "Selective Insulin Resistance in Adipocytes." *Journal of Biological Chemistry* 290 (18): 11337–48. https://doi.org/10.1074/jbc.M114.623686.

Thorn, Hans, Karin G. Stenkula, Margareta Karlsson, Unn Örtegren, Fredrik H. Nystrom, Johanna Gustavsson, and Peter Strålfors. 2003. "Cell Surface Orifices of Caveolae and Localization of Caveolin to the Necks of Caveolae in Adipocytes." *Molecular Biology of the Cell* 14 (10): 3967–76. https://doi.org/10.1091/mbc.E03-01-0050.

Tobi, Mohammed Nasser Rashid Al. 2018. "Consequences of Tyrosine Phosphorylation of Syntaxin4 and Munc18c on GLUT4 Trafficking." http://theses.gla.ac.uk/30757/.

Torrino, Stéphanie, Wei Shen, Cédric M. Blouin, Satish Kailasam Mani, Christine Viaris de Lesegno, Pierre Bost, Alexandre Grassart, et al. 2018. "EHD2 Is a Mechanotransducer Connecting Caveolae Dynamics with Gene Transcription." *The Journal of Cell Biology* 217 (12): 4092–4105. https://doi.org/10.1083/JCB.201801122.

Trávez, Andrés, Yoana Rabanal-Ruiz, Jaime López-Alcalá, Laura Molero-Murillo, Alberto Díaz-Ruiz, Rocío Guzmán-Ruiz, Victoria Catalán, et al. 2018. "The Caveolae-Associated Coiled-Coil Protein, NECC2, Regulates Insulin Signalling in Adipocytes." *Journal of Cellular and Molecular Medicine* 22 (11): 5648–61. https://doi.org/10.1111/jcmm.13840.

Trayhurn, Paul. 2013. "Hypoxia and Adipose Tissue Function and Dysfunction in Obesity." *Physiological Reviews* 93 (1): 1–21.

https://doi.org/10.1152/PHYSREV.00017.2012.

Varela-Guruceaga, Maider, Elise Belaidi, Lucie Lebeau, Ella Aka, Ramaroson Andriantsitohaina, Sophie Giorgetti-Peraldi, Claire Arnaud, and Soazig Le Lay. 2020. “Intermittent Hypoxia Mediates Caveolae Disassembly That Parallels Insulin Resistance Development.” *Frontiers in Physiology* 11 (November). https://doi.org/10.3389/fphys.2020.565486.

Varela-Guruceaga, Maider, F. I. Milagro, J. A. Martínez, and C. de Miguel. 2018. “Effect of Hypoxia on Caveolae-Related Protein Expression and Insulin Signaling in Adipocytes.” *Molecular and Cellular Endocrinology* 473 (September): 257–67. https://doi.org/10.1016/j.mce.2018.01.026.

Vazirani, Reema P., Akanksha Verma, L. Amanda Sadacca, Melanie S. Buckman, Belen Picatoste, Muheeb Beg, Christopher Torsitano, et al. 2016. “Disruption of Adipose Rab10-Dependent Insulin Signaling Causes Hepatic Insulin Resistance.” *Diabetes* 65 (6): 1577–89. https://doi.org/10.2337/db15-1128.

Venugopal, Joshi, Kazuhiko Hanashiro, Zhong Zhou Yang, and Yoshikuni Nagamine. 2004. “Identification and Modulation of a Caveolae-Dependent Signal Pathway That Regulates Plasminogen Activator Inhibitor-1 in Insulin-Resistant Adipocytes.” *Proceedings of the National Academy of Sciences of the United States of America* 101 (49): 17120–25. https://doi.org/10.1073/PNAS.0405278101.

Voldstedlund, Marianne, Jørgen Tranum-Jensen, and Jørgen Vinten. 1993. “Quantitation of Na+/K(+)-ATPase and Glucose Transporter Isoforms in Rat Adipocyte Plasma Membrane by Immunogold Labeling.” *The Journal of Membrane Biology* 136 (1): 63–73. https://doi.org/10.1007/BF00241490.

Wang, Hong, Paul F. Pilch, and Libin Liu. 2019. “Cavin-1/PTRF Mediates Insulin-Dependent Focal Adhesion Remodeling and Ameliorates High-Fat Diet-Induced Inflammatory Responses in Mice.” *The Journal of Biological Chemistry* 294 (27): 10544–52. https://doi.org/10.1074/JBC.RA119.008824.

Watson, Robert T., Satoshi Shigematsu, Shian Huey Chiang, Silvia Mora, Makoto Kanzaki, Ian G. Macara, Alan R. Saltiel, and Jeffrey E. Pessin. 2001. “Lipid Raft Microdomain Compartmentalization of TC10 Is Required for Insulin Signaling and GLUT4 Translocation.” *The Journal of Cell Biology* 154 (4): 829–40. https://doi.org/10.1083/JCB.200102078.

Weber, Thomas, Boris V. Zemelman, James A. McNew, Benedikt

Westermann, Michael Gmachl, Francesco Parlati, Thomas H. Söllner, and James E. Rothman. 1998. “SNAREpins: Minimal Machinery for Membrane Fusion.” *Cell* 92 (6): 759–72. https://doi.org/10.1016/S0092-8674(00)81404-X.

Widberg, Charlotte H., Nia J. Bryant, Milena Girotti, Shane Rea, and David E. James. 2003. “Tomosyn Interacts with the T-SNAREs Syntaxin4 and SNAP23 and Plays a Role in Insulin-Stimulated GLUT4 Translocation.” *The Journal of Biological Chemistry* 278 (37): 35093–101. https://doi.org/10.1074/JBC.M304261200.

Yamakawa, Daishi, Daisuke Katoh, Kousuke Kasahara, Takashi Shiromizu, Makoto Matsuyama, Chise Matsuda, Yumi Maeno, Masatoshi Watanabe, Yuhei Nishimura, and Masaki Inagaki. 2021. “Primary Cilia-Dependent Lipid Raft/Caveolin Dynamics Regulate Adipogenesis.” *Cell Reports* 34 (10). https://doi.org/10.1016/J.CELREP.2021.108817.

Yan, Wang, Zhang JinZhong, Chen Yu, Jiang Li, Ji Wei, and Xu Tao. 2009. “Characterization of GLUT4-Containing Vesicles in 3T3-L1 Adipocytes by Total Internal Reflection Fluorescence Microscopy.” *Science in China, Series C: Life Sciences* 52 (7): 665–71. https://doi.org/10.1007/s11427-009-0081-9.

Yang, Su Jung, Chen Yu Chen, Geen Dong Chang, Hui Chin Wen, Ching Yu Chen, Shi Chuan Chang, Jyh Fei Liao, and Chung Ho Chang. 2013. “Activation of Akt by Advanced Glycation End Products (AGEs): Involvement of IGF-1 Receptor and Caveolin-1.” *PloS One* 8 (3). https://doi.org/10.1371/JOURNAL.PONE.0058100.

Yeow, Ivana, Gillian Howard, Jessica Chadwick, Carolina Mendoza-Topaz, Carsten G. Hansen, Benjamin J. Nichols, and Elena Shvets. 2017. “EHD Proteins Cooperate to Generate Caveolar Clusters and to Maintain Caveolae during Repeated Mechanical Stress.” *Current Biology : CB* 27 (19): 2951-2962.e5. https://doi.org/10.1016/J.CUB.2017.07.047.

Yu, Haijia, Shailendra S. Rathore, Jamie A. Lopez, Eric M. Davis, David E. James, Jennifer L. Martin, and Jingshi Shen. 2013. “Comparative Studies of Munc18c and Munc18-1 Reveal Conserved and Divergent Mechanisms of Sec1/Munc18 Proteins.” *Proceedings of the National Academy of Sciences of the United States of America* 110 (35): E3271–80. https://doi.org/10.1073/PNAS.1311232110/SUPPL_FILE/PNAS.201311232SI.PDF.

Yu, Haijia, Shailendra S. Rathore, and Jingshi Shen. 2013. “Synip Arrests Soluble N-Ethylmaleimide-Sensitive Factor Attachment Protein Receptor

(SNARE)-Dependent Membrane Fusion as a Selective Target Membrane SNARE-Binding Inhibitor." *Journal of Biological Chemistry* 288 (26): 18885–93. https://doi.org/10.1074/JBC.M113.465450.

Yuan, Taichang, Shangyu Hong, Yao Yao, and Kan Liao. 2007. "Glut-4 Is Translocated to Both Caveolae and Non-Caveolar Lipid Rafts, but Is Partially Internalized through Caveolae in Insulin-Stimulated Adipocytes." *Cell Research* 17 (9): 772–82. https://doi.org/10.1038/cr.2007.73.

Zebisch, Katja, Valerie Voigt, Martin Wabitsch, and Matthias Brandsch. 2012. "Protocol for Effective Differentiation of 3T3-L1 Cells to Adipocytes." *Analytical Biochemistry* 425 (1): 88–90. https://doi.org/10.1016/J.AB.2012.03.005.

Zhao, Ping, Lu Yang, Jamie A. Lopez, Junmei Fan, James G. Burchfield, Li Bai, Wanjin Hong, Tao Xu, and David E. James. 2009. "Variations in the Requirement for V-SNAREs in GLUT4 Trafficking in Adipocytes." *Journal of Cell Science* 122 (19): 3472–80. https://doi.org/10.1242/JCS.047449.

Zierath, J. R., L. He, A. Gumà, E. Odegaard Wahlström, A. Klip, and H. Wallberg-Henriksson. 1996. "Insulin Action on Glucose Transport and Plasma Membrane GLUT4 Content in Skeletal Muscle from Patients with NIDDM." *Diabetologia* 39 (10): 1180–89. https://doi.org/10.1007/BF02658504.

Zmuda-Trzebiatowska, Emilia, Alina Oknianska, Vincent Manganiello, and Eva Degerman. 2006. "Role of PDE3B in Insulin-Induced Glucose Uptake, GLUT-4 Translocation and Lipogenesis in Primary Rat Adipocytes." *Cellular Signalling* 18 (3): 382–90. https://doi.org/10.1016/J.CELLSIG.2005.05.007.